

In compliance with the  
Canadian Privacy Legislation  
some supporting forms  
may have been removed from  
this dissertation.

While these forms may be included  
in the document page count,  
their removal does not represent  
any loss of content from the dissertation.



**University of Alberta**

**Blood Sample Preparation Using Microfluidic Platforms**

by

**Vasile Irimie Furdul**



A thesis submitted to the Faculty of Graduate Studies and Research in partial fulfillment of the requirements for the degree of **Doctor of Philosophy**

**Department of Chemistry**

Edmonton, Alberta

Fall 2003



National Library  
of Canada

Bibliothèque nationale  
du Canada

Acquisitions and  
Bibliographic Services

Acquisitons et  
services bibliographiques

395 Wellington Street  
Ottawa ON K1A 0N4  
Canada

395, rue Wellington  
Ottawa ON K1A 0N4  
Canada

*Your file* *Votre référence*

*ISBN: 0-612-87973-9*

*Our file* *Notre référence*

*ISBN: 0-612-87973-9*

The author has granted a non-exclusive licence allowing the National Library of Canada to reproduce, loan, distribute or sell copies of this thesis in microform, paper or electronic formats.

L'auteur a accordé une licence non exclusive permettant à la Bibliothèque nationale du Canada de reproduire, prêter, distribuer ou vendre des copies de cette thèse sous la forme de microfiche/film, de reproduction sur papier ou sur format électronique.

The author retains ownership of the copyright in this thesis. Neither the thesis nor substantial extracts from it may be printed or otherwise reproduced without the author's permission.

L'auteur conserve la propriété du droit d'auteur qui protège cette thèse. Ni la thèse ni des extraits substantiels de celle-ci ne doivent être imprimés ou autrement reproduits sans son autorisation.

# Canada

# University of Alberta

## Library Release Form

**Name of Author:** Vasile Irimie Furdui

**Title of Thesis:** Blood Sample Preparation Using Microfluidic Platforms

**Degree:** Doctor of Philosophy

**Year this Degree Granted:** 2003

Permission is hereby granted to the University of Alberta Library to reproduce single copies of this thesis and to lend or sell such copies for private, scholarly or scientific research purposes only.

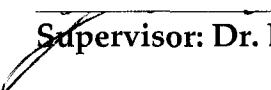
The author reserves all other publication and other rights in association with the copyright in the thesis, and except as herein before provided, neither the thesis nor any substantial portion thereof may be printed or otherwise reproduced in any material form whatever without the author's prior written permission.

Date: September 29, 2003

# University of Alberta

## Faculty of Graduate Studies and Research

The undersigned certify that they have read, and recommend to the Faculty of Graduate Studies and Research for acceptance, a thesis entitled "**Blood Sample Preparation Using Microfluidic Platforms**" submitted by **Vasile Irimie Furdui** in partial fulfillment of the requirements for the degree of **Doctor of Philosophy**.

  
Supervisor: Dr. D. Jed Harrison

  
Dr. Mark T. McDermott

  
Dr. John-Bruce D. Green

  
Dr. George Kotovych

  
Dr. Hanne L. Ostergaard

  
External Examiner: Dr. Chong H. Ahn  
University of Cincinnati

Date: September 29, 2003

*To my wife, Lucia, and our daughter, Andreea,  
for their constant support, love and inspiration.*

## Abstract

This thesis focuses on integrating rare cell capture from blood on a disposable sample-preparation device for a portable platform. Such a module is the interface between a macroscopic world sample and any polymerase chain reaction (PCR)-based microfluidic system. Immunomagnetic separation of T cells from human blood and Jurkat cells from reconstituted horse blood was performed and characterized. Although more dilute cells are ultimately contemplated, the T cells or Jurkat cells considered in this study offered a good initial model of rare cells in blood.

A PCR procedure was optimized and adapted for the characterization of the capture efficiencies obtained on the tested devices. The method uses direct PCR amplification of a T cell receptor  $\gamma$  gene junctional region. We described the use of paramagnetic beads for cell capture within microfluidic channels. After preliminary tests performed on a simple Y microfluidic device, eight different manifolds were designed and tested in an effort to reduce the analysis time, while maintaining the capture efficiency. A simple increase of the channel size for a quick processing of larger volumes of sample did not work for the immunomagnetic bead-bed method used in this study. It was necessary to split the flow into several smaller channels to get satisfactory capture efficiency.

We presented the first integration of micro-electrolysis pumps for the manipulation and initial processing of a blood sample. Jurkat cells were captured from a 7.5  $\mu\text{L}$  reconstituted horse blood sample using a pair of electrolysis chambers, which were designed to work in a stepwise fashion. First the blood sample was delivered when the pre-labeled cells were captured, and then a buffer was used to wash the captured cells.

Preliminary results obtained for the fabrication of polycarbonate devices were described. A master fabricated in silicon was etched using DRIE and used to electroform a nickel relief as a secondary master with the reverse features of the Si surface. The Ni master was used to stamp features into PC substrates by hot embossing. The resulting substrates had the same pattern as the original Si master. Substrates were thermally bonded under optimized bonding parameters to a coverplate using a hydraulic press.



## Acknowledgements

It is a pleasure to express my deep gratitude to my research supervisor, Professor D. Jed Harrison for his extensive guidance and support during my Ph.D. program at the University of Alberta. I am very thankful for his patience in reading my thesis and shaping it in its present form. I am also indebted for the scientific knowledge I have gathered from all the conferences I have attended thanks to him.

I would like to thank Dr. D. Jed Harrison's group members for their helpful discussions. Special thanks go to Dr. Hossein Salimi-Moosavi, Dr. Gregor Ocvirk, Dr. Fahima Ouchen and Dr. Guifeng Jiang for their advice related to my studies and Dr. James K. Kariuki and Dean Nair for their help in performing some parts of my studies. My sincere thanks go to Mrs. Arlene Figley for reading my thesis and making grammatical corrections.

I wish to express my gratitude to the members of my candidacy and defense committees in the persons of Dr. Mark McDermott, Dr. John-Bruce Green, Dr. Charles Lucy, Dr. George Kotovych, Dr. Hanne Ostergaard and Dr. Chong Ahn.

My appreciation also extends to Dr. Piotr Grodzinski and his group for permitting me to visit the Physical Sciences Research Laboratories from Motorola. Helpful discussions allowed me to develop a fabrication process for plastic microfluidic devices.

I extend my thanks to the technical support staff from the Chemistry Department, especially to Vincent Bizon, Dieter Starke and Hubert Hoffman from the Machine Shop, and Ed Feschuk, Kim Do and Allan Chilton from the Electronic Shop. I am grateful to Joanna Sadowska (Chemistry Department), Eva Pruski (Cross Cancer Institute) and Rod Szarka (Alberta Research Council) for their cell culture advice, and Dr. Ken Westra, Dione Chambers, Stephanie Bozic and Keith Franklin from our NanoFab facility for the micromachining training I received. Thanks go to Dr. Richard Smith for allowing me to perform my first experiments at Alberta Research Council and Dr. Linda Pilarski from Cross Cancer Institute for providing the blood samples used in this study.

I would like to thank the Defense Advanced Research Projects Agency, National Sciences and Engineering Research Council and University of Alberta for financial support of the studies presented in this thesis.

# Table of Contents

<b>Chapter 1: Introduction</b>	<b>1</b>
1.1 <b>Introduction</b> .....	1
1.1.1 Microfluidics and “Lab-on-a-Chip” .....	2
1.1.2 Blood Analysis in Microfluidics .....	3
1.1.2.1 On-Chip Blood Sample Preparation .....	3
1.1.2.2 On-Chip Blood Sample Preparation for PCR .....	6
1.1.2.2a Microfiltration .....	8
1.1.2.2b Dielectrophoresis .....	8
1.1.2.2c Multi-Chip Module System for Genetic Analysis .....	10
1.1.3 Motivation for This Study .....	13
1.2 <b>The Basics of Human Blood</b> .....	14
1.2.1 Human Blood Composition .....	14
1.2.2 Types of Blood Samples .....	15
1.2.3 T Cells .....	16
1.2.4 Methods for Cell Separation .....	17
1.2.4.1 General Methods .....	17
1.2.4.2 Specific Surface Methods .....	17
1.3 <b>The Basics of DNA</b> .....	19
1.3.1 T Cell Receptor Complex Genes .....	20
1.4 <b>Polymerase Chain Reaction</b> .....	21
1.4.1 Quantitative PCR .....	22
1.5 <b>Capillary Gel Electrophoresis</b> .....	23
1.5.1 Fundamentals of Capillary Electrophoresis .....	23
1.5.2 Capillary Gel Electrophoresis for DNA Separation .....	25
1.6 <b>Scope of the Thesis</b> .....	26
1.7 <b>References</b> .....	27

**Chapter 2: Optimization of an Off-Chip Procedure for Amplification and Detection of Genomic DNA** **35**

2.1	<b>Introduction</b> .....	35
2.2	<b>Experimental Section</b> .....	36
2.2.1	Reagents and Media .....	36
2.2.2	Cell Samples .....	37
2.2.3	Operation Procedure .....	37
2.2.3.1	Loading Protein A Paramagnetic Beads with Anti-CD3 .....	37
2.2.3.2	PCR Amplification of DNA Isolated from Blood and Jurkat Cell Samples ...	38
2.2.3.2.1	Method A .....	38
2.2.3.2.1a	Method A Used for Jurkat Cell Samples .....	38
2.2.3.2.1b	Method A Used for a Human Blood Sample .....	39
2.2.3.2.2	Method B .....	39
2.2.3.2.2a	Method B Used for Jurkat Cell Samples .....	40
2.2.3.2.2b	Method B Used for Jurkat Cell Samples Processed in the Presence of Protein A/Anti-human CD3 Paramagnetic Beads .....	41
2.2.3.2.2c	Method B Used for a Human Blood Sample .....	41
2.2.3.2.3	Method C .....	41
2.2.3.2.3a	Method C Used for Jurkat Cell Samples .....	42
2.2.3.3	Capillary Gel Electrophoresis of the PCR Product .....	43
2.3	<b>Results and Discussion</b> .....	43
2.3.1	PCR Analysis Following Method A .....	44
2.3.1.1	PCR Performed on Samples Containing Jurkat Cells .....	44
2.3.1.2	PCR Performed on Human Blood Samples .....	45
2.3.2	PCR Analysis Following Method B .....	48
2.3.2.1	PCR Performed on Samples Containing Jurkat Cells .....	48
2.3.2.2	PCR Performed on Jurkat Cell Samples in the Presence of Protein A/ Anti-Human CD3 Paramagnetic Beads .....	49
2.3.2.3	PCR Performed on Human Blood Samples .....	50
2.3.3	PCR Analysis Following Method C .....	52
2.3.3.1	PCR Performed on Samples Containing Jurkat Cells .....	52
2.4	<b>Conclusion</b> .....	53
2.5	<b>References</b> .....	54

<b>Chapter 3: Cell Separation Experiments on Different Devices</b>	<b>57</b>
3.1 <b>Introduction</b> .....	57
3.2 <b>Experimental Section</b> .....	59
3.2.1 Reagents and Media .....	59
3.2.2 Device Fabrication .....	60
3.2.3 Cell Samples .....	63
3.2.3.1 Blood Samples Used to Test the Y-intersection Device .....	63
3.2.3.2 Reconstituted Blood Samples Used to Test the FAT 3000 Device .....	64
3.2.3.2a Experiment 1 Performed on All Manifolds .....	64
3.2.3.2b Experiment 2 Performed on Manifolds 1, 3, 4 and 6 .....	64
3.2.4 Operating Procedure .....	67
3.2.4.1 Preconditioning of the Devices .....	67
3.2.4.1a Procedure for Y-intersection Device .....	67
3.2.4.1b Procedure for FAT 3000 Device .....	67
3.2.4.2 On-chip Cell Capture .....	68
3.2.4.2a Procedure for Y-intersection Device .....	68
3.2.4.2b Procedure for FAT 3000 Device .....	69
3.2.4.3 Off-chip Analysis of the Captured Cells .....	70
3.3 <b>Results and Discussion</b> .....	71
3.3.1 Jurkat Cell Capture on Glass Surface of a Y-intersection Device .....	72
3.3.2 T Cell Separation from Human Blood Performed on Y-intersection Device ...	73
3.3.3 Jurkat Cell Separation from Reconstituted Blood Performed on FAT 3000 Device .....	77
3.3.3.1 Experiment 1 Performed on All Eight Manifolds of the FAT 3000 Device ....	77
3.3.3.2 Experiment 2 Performed on Four Manifolds of the FAT 3000 Device .....	83
3.4 <b>Conclusions</b> .....	84
3.5 <b>References</b> .....	85

<b>Chapter 4: Microfabricated Electrolysis Pump System for Isolating Rare Cells in Blood</b>	<b>89</b>
4.1 <b>Introduction</b> .....	89
4.2 <b>Experimental Section</b> .....	90
4.2.1 Fabrication .....	90
4.2.2 Operation and Measurement Procedures .....	94
4.3 <b>Results and Discussion</b> .....	95
4.3.1 Design and Fabrication .....	95
4.3.2 Pump Performance .....	97
4.3.3 Rare Cell Capture System .....	100
4.4 <b>Conclusions</b> .....	102
4.5 <b>References</b> .....	103
<b>Chapter 5: Fabrication of Embossed Microfluidic Devices</b>	<b>104</b>
5.1 <b>Introduction</b> .....	104
5.2 <b>Fabrication</b> .....	109
5.2.1 Anisotropical Etching on Silicon Wafer .....	110
5.2.2 Master Fabrication by Ni Electroplating onto the Etched Silicon Wafer ...	110
5.2.3 Feature Embossing on Polycarbonate Surface .....	112
5.2.4 Bonding of Microfluidic Devices .....	113
5.3 <b>Results and Discussions</b> .....	115
5.3.1 Master Fabrication .....	115
5.3.2 Embossing on Polycarbonate Substrates .....	119
5.3.3 Thermal Bonding of Plastic Devices .....	124
5.4 <b>Conclusions</b> .....	127
5.5 <b>References</b> .....	128
<b>Chapter 6: Summary and Future Suggestions</b>	<b>132</b>
6.1 <b>References</b> .....	136

## List of Tables

<b>Table 3.1:</b>	Actual surface area of cross-sections in the FAT 3000 device .....	61
<b>Table 3.2:</b>	Stability of captured cells on glass surface as a function of flow rate used in a Y-channel with 0.0109 mm <sup>2</sup> cross sectional area .....	73
<b>Table 3.3:</b>	Efficiencies obtained on all channels of the FAT 3000 device, calculated using the peak heights obtained for the 300 bp PCR peak .....	79
<b>Table 5.1:</b>	Standard thermoplastic polymers used in microfabrication .....	105
<b>Table 5.2:</b>	Conditions used for bonding of 8×7 cm embossed substrates on a Carver hydraulic press .....	113
<b>Table 5.3:</b>	Characteristics of the PC bonding at 135 °C and 40 kN. Annealing was performed at 145 °C for 10 min .....	125

## List of Figures

<b>Figure 1.1:</b> The magnetic cell sorter system proposed by Blankenstein.....	4
<b>Figure 1.2:</b> H-Filter channel for diffusion-based separation of smaller from larger particles .....	5
<b>Figure 1.3:</b> Micronics hematology cartridge .....	5
<b>Figure 1.4:</b> Microfilter chambers used for cell separation .....	7
<b>Figure 1.5:</b> Dielectrophoretic enrichment of peripheral blood mononuclear cells .....	9
<b>Figure 1.6:</b> Fully integrated Multi-Chip Module (MCM) for DNA analysis .....	11
<b>Figure 1.7:</b> Characterization of the MCM system proposed by Motorola .....	12
<b>Figure 1.8:</b> Blood cell composition .....	14
<b>Figure 1.9:</b> Components of the T cell receptor: CD3 complex .....	16
<b>Figure 1.10:</b> Structure of a single DNA strand representing a tetranucleotide .....	19
<b>Figure 1.11:</b> Representation of a TCR $\gamma$ gene rearrangement .....	21
<b>Figure 1.12:</b> Schematic representations of a capillary zone electrophoresis system .....	23
<b>Figure 1.13:</b> Pictorial description of the size separation of DNA fragments by CGE .....	24
<b>Figure 2.1:</b> Annealing temperature program used in PCR for methods A, B and C .....	40
<b>Figure 2.2:</b> Electropherogram of the PCR product obtained following method A for PCR amplification .....	44
<b>Figure 2.3:</b> Electropherograms of the PCR product obtained from Jurkat cell samples using method A for PCR amplification. Separation was performed at 185 V/cm.....	45
<b>Figure 2.4:</b> Characterization of the PCR amplification with method A using DNA extracted from 0.5, 1, 2 and 4 $\mu$ L of blood. Separation was performed at 185 V/cm.....	46
<b>Figure 2.5:</b> Electropherogram of the PCR product obtained following method B for PCR amplification.....	47
<b>Figure 2.6:</b> Characterization of PCR amplification with method B using DNA extracted from 1, 14, 140 and 1400 Jurkat cells. Separation was performed at 370 V/cm.....	48
<b>Figure 2.7:</b> Characterization of the PCR amplification performed with method B in the presence and absence of paramagnetic beads .....	50
<b>Figure 2.8:</b> Characterization of the PCR amplification with method B using DNA extracted from 0.5, 1, 2 and 4 $\mu$ L of blood.....	51
<b>Figure 2.9:</b> Characterization of the peak height obtained by PCR amplification using method C; DNA was extracted from samples with 110, 220, 330, 660 and 1100 Jurkat cells....	52
<b>Figure 3.1:</b> Layout of the Y-intersection device .....	61
<b>Figure 3.2:</b> Layouts of the eight different manifold designs of the FAT 3000 device .....	62
<b>Figure 3.3:</b> Immunomagnetic separation of T cells using Y-intersection device .....	65
<b>Figure 3.4:</b> Immunomagnetic separation of T cells using FAT 3000 device .....	66
<b>Figure 3.5:</b> Images of captured T cells and Protein A/anti-human CD3 magnetic beads .....	71

<b>Figure 3.6:</b> Electropherogram of PCR product obtained following method A for PCR amplification. T cells were separated from 2 $\mu$ l of blood on a Y-device, followed by off-chip extraction of DNA.....	75
<b>Figure 3.7:</b> Electropherogram of 300 bp PCR product obtained using method B for PCR amplification. T cells were separated from 2 $\mu$ l of blood on a Y-device, followed by off-chip extraction of DNA.....	76
<b>Figure 3.8:</b> Correlation graph presenting peak height versus volume of blood used; DNA was extracted off-chip from 0.5, 1, 2 and 4 $\mu$ L of human blood and amplified by PCR following method B.....	77
<b>Figure 3.9:</b> Characterization of the PCR amplification with method C using as standards DNA extracted from different volumes of a reconstituted blood sample.....	78
<b>Figure 3.10:</b> Capture efficiency determined from simultaneous PCR analysis of samples captured in all eight manifolds of the FAT 3000 device.....	80
<b>Figure 3.11:</b> Cross-section profiles in the capture area of manifolds 1, 2, 3, 4 and 7 of the FAT 3000 device.....	81
<b>Figure 3.12:</b> Capture efficiency determined in different experiments for manifolds 1, 3, 4 and 6 of the FAT 3000 device.....	83
<b>Figure 3.13:</b> Capture efficiency determined for different samples processed in the same experiment on manifolds 3, 4 and 6 of the FAT 3000 device.....	84
<b>Figure 4.1:</b> Mask design for the Si die and the glass cover plate of the electrolysis pump system	91
<b>Figure 4.2:</b> Drawing of the Si die and the larger glass cover plate of the electrolysis pump system	92
<b>Figure 4.3:</b> Image of the integrated pump system device .....	92
<b>Figure 4.4:</b> Scheme for filling the various chambers within the integrated pump system device...	93
<b>Figure 4.5:</b> Detail of the layout of the chevron barrier .....	96
<b>Figure 4.6:</b> Flow rate as a function of applied current for a device filled with 0.5 M $\text{KNO}_3$ .....	97
<b>Figure 4.7:</b> Current leakage through one device .....	98
<b>Figure 4.8:</b> Flow rate as a function of applied potential comparing the pumping of reconstituted horse blood or phosphate buffered saline.....	99
<b>Figure 4.9:</b> Video frames showing the flows of blood and PBS pumped into the main channel...	101
<b>Figure 4.10:</b> Photomicrographs showing Jurkat cells trapped within the main flow channel .....	101
<b>Figure 5.1:</b> Schematic of the plastic device fabrication procedure employed in this study.....	109
<b>Figure 5.2:</b> Images of the Ni master fabricated by electrochemical deposition onto a Si wafer with features of the FAT 3000 device etched at 70 $\mu$ m.....	111
<b>Figure 5.3:</b> SEM images presenting the sidewall of a channel etched with DRIE on a Si substrate	114
<b>Figure 5.4:</b> SEM images presenting details of the features etched to a 70 $\mu$ m depth on silicon wafer, using the optimised conditions for the Bosch process.....	116
<b>Figure 5.5:</b> Images of the FAT 3000 device etched on silicon with depth details.....	117



<b>Figure 5.6:</b> Image of the Ni master after chemical cleaning and machining .....	119
<b>Figure 5.7:</b> SEM images presenting details of the same features of the FAT 3000 device, embossed on PC at 165 °C and 170 °C.....	120
<b>Figure 5.8:</b> SEM images presenting details of the same features of the FAT 3000 device, embossed on PC at 175 °C and 195 °C .....	121
<b>Figure 5.9:</b> Characterization of channel surface.....	122
<b>Figure 5.10:</b> SEM images presenting a defect on the right side of a 1500 µm wide feature embossed on PC at 165 °C, 170 °C and 175 °C.....	123
<b>Figure 5.11:</b> Schematic of the channel deformation observed after bonding.....	125
<b>Figure 5.12:</b> Depth obtained, substrate and coverplate deformation for different bonding times...	126
<b>Figure 6.1:</b> Proposed integrated system for rare cells separation from a blood sample, cells lysing and DNA capture.....	135

## List of Abbreviations

### Technical Words

$\eta$	Viscosity
$\mu_{ep}$	Electrophoretic Mobility
$\mu_{EOF}$	Electroosmotic Mobility
$\zeta$	Zeta potential
$\mu$ TAS	Micro-Total Analysis System
ATCC	American Type Culture Collection
bp	Base Pair
CD	Cluster of Designation
CE	Capillary Electrophoresis
CGE	Capillary Gel Electrophoresis
DARPA	Defense Advanced Research Project Agency
DEEMO	Dry Etching, Electroplating and Molding
DEP	Dielectrophoresis
diam	Diameter
DRIE	Deep Reactive Ion Etching
E	Electric Field
EDP	Ethylenediamine, Pyrocatechol
EOF	Electroosmotic Flow
FACS	Fluorescence Activated Cell Sorting
id	Internal Diameter
LIGA	Lithography Electroplating Molding (German)
LFDI	Laminar Fluid Diffusion Interface
MACS	Magnetic Activated Cell Sorting
MCM	Multi-Chip Module
MW	Molecular Weight
PBMNC	Peripheral Blood Mononuclear Cell(s)
PCR	Polymerase Chain Reaction
RBC	Red Blood Cell(s)
RPMI	Roswell Park Memorial Institute
RFU	Relative Fluorescence Unit(s)
RSD	Relative Standard Deviation
sccm	Standard Cubic Centimeters
SD	Standard Deviation

SEM	Scanning Electron Microscopy
TCR	T Cell Receptor
T <sub>g</sub>	Glass Transition Temperature
WBC	White Blood Cell(s)

## Chemicals

A	Adenine
BSA	Bovine Serum Albumine
C	Cytosine
DNA	Deoxyribonucleic Acid
G	Guanine
HEC	Hydroxyethylcellulose
HPMC	Hydroxypropylmethylcellulose
PBS	Phosphate Buffered Saline
PA6	Polyamide 6
PA66	Polyamide 66
PB	Polybutene
PC	Polycarbonate
PDMS	Polydimethylsiloxane
PE	Polyethylene
PET	Polyethylene-terephthalate
PETG	Polyethylenetetrathalate glycol
PI	Polyimide
PMMA	Polymethyl-methacrylate
PP	Polypropylene
PS	Polystyrene
PTFE	Polytetrafluoroethylene
PVC	Polyvinylchloride
RNA	Ribonucleic acid
T	Thymine
TBE	Tris-Boric acid-EDTA buffer
Tris	Tris-(hydroxymethyl)-aminomethane

## CHAPTER 1: Introduction

### 1.1 Introduction

Portability and automation were considered over the years a priority in designing analytical systems for clinical, ecological and industrial applications. Widmer proposed in 1983 the integration of sampling, transport, separation of individual components, detection/identification and data collection into a Total Analysis System (TAS), envisioning a significant reduction in total time and cost per analysis [1]. The idea of a Miniaturized (or Micro) Total Analysis Systems ( $\mu$ TAS), introduced in 1990 by Manz and Widmer [2] inspired a significant number of researchers to develop a variety of chemical, biological and environmental analysis systems. For more than a decade, planar microfluidic devices have constituted the platform for testing different  $\mu$ TAS concepts. Although the systems developed confirmed the usefulness of this technology, more effort is required for production of commercial, totally integrated systems. This thesis will explore some aspects of integrating sample preparation for genetic analysis. The ultimate goal of the studies presented here is the fabrication of a portable system for genetic analysis. This thesis presents the information required for designing a portable module able to separate and purify low concentration cells from undiluted blood sample and to deliver the cells of interest to a PCR module, for genetic analysis. An immunomagnetic method using a magnetically trapped bead bed is explored for capture and purification of low concentration cells from human blood. The integration of electrochemical pumps with the cell trapping system is investigated, intended for future incorporation in a portable device. Preliminary steps required for transferring the technology to cheap, disposable polymeric microfluidic devices are also investigated. T cells or spiked Jurkat cells were used as the initial model of rare cells in blood, although more dilute sample analyses are ultimately contemplated. This project was undertaken as part of a larger effort with Motorola and Arizona State University, who were to develop the PCR and PCR product detection modules.

The introductory chapter will first provide a brief review of relevant literature on microfluidic devices. Particular attention will be paid to previous applications to blood samples analyzed on  $\mu$ TAS devices. An introduction to blood samples and cell separation

will be presented, followed by an introduction to DNA and the polymerase chain reaction (PCR). The concept of capillary gel electrophoresis (CGE), the method used to analyze PCR products on many  $\mu$ TAS devices and also used in Chapters 2 and 3, will then be presented. Finally, an overview of this thesis work will be presented.

### 1.1.1 Microfluidics and “Lab-on-a-Chip”

Terry et al. first recognized the advantages of using microfabrication technologies for miniaturization of a chemical separation device and fabricated the first miniaturized gas chromatograph system on a 5 cm diameter silicon wafer [3]. This revolutionary approach remained untapped for more than a decade, until Manz et al. developed the first liquid-phase  $\mu$ TAS for performing liquid chromatography [4]. Unfortunately this planar microfluidic device was never tested. Less than two years later, Harrison and Manz presented a functioning capillary electrophoresis system with integrated sample injection on a planar microfluidic device [5, 6]. Such planar devices are also known as “chips”. The possibility of high resolution or faster analysis being performed using reduced volumes of liquids, and the possibility of mass fabrication at low costs were some of the major potential advantages of miniaturization. By integrating microstructures, detector systems, valveless switching of flow and electroosmotic pumping, the authors predicted the possibility of fabricating future complex miniaturized analytical systems called a “laboratory on a chip” [5, 7-9], and so simplifying automation of high throughput systems [10]. These early results attracted a large number of researchers to this multidisciplinary field, causing an exponential growth of  $\mu$ TAS-related developments and discoveries in the last decade. The significant number of reviews available offer a general picture of  $\mu$ TAS in general [11, 12] or focus specifically on some subject area, presenting genomic - proteomic [13-16], clinical and forensic [17, 18], biomedical - drug discovery [19] and cellomics [20] applications.

The first planar devices were micromachined using photolithography and chemical etching [21, 22] on materials with appropriate mechanical properties such as monocrystalline silicon [23] and glass [10, 24]. Based on the low cost and large range of material properties, polymers were considered for fabrication of microfluidic devices, aiming towards commercialization of mass fabricated disposable microfluidic devices.

The initial academic research entered the commercial world in the mid-1990s, when names like Aclara, Agilent, Asahi, Caliper, Cepheid, Gamera, Gyros, Hitachi, Micronics, Mitsubishi, Motorola, Nanogen, Orchid and Shimadzu became well known in the microfluidics field.

## **1.1.2 Blood Analysis in Microfluidics**

### **1.1.2.1 On-Chip Blood Sample Preparation**

Wilding et al. conducted an initial study to understand the fluid flow in microstructures, when pressure-driven flow was involved [25]. Complex fluids like whole blood, washed red blood cells (RBC) and white blood cells (WBC) were used. The pressure required to achieve a 250  $\mu\text{L}/\text{min}$  flow rate increased proportionally with the complexity and viscosity of the fluid, from a value of 75 kPa for distilled water to 250 kPa for whole blood. Because whole blood is primarily composed of RBC, which are highly flexible and smaller than WBC (2.6 to 5.4 times), a diluted blood sample required less driving force than a WBC preparation with the same cell concentration. The relative viscosity of serum, plasma, cell suspension and whole blood increased drastically as the flow rate was reduced, proving the non-Newtonian behavior, meaning that the fluid require a finite yield stress to start flowing. Tracey et al. performed blood cell deformability studies on RBC moving through an array of 90  $\mu\text{m}$  long flow channels with a width and depth of 4  $\mu\text{m}$  [26]. A clear, negative, linear correlation was obtained between cell volume and mean RBC velocity on a silicon micromachined hemacytometer with channel widths in a 3 to 4  $\mu\text{m}$  range. The isobaric conditions used for all measurements allowed observation of an increase of the mean velocity with increasing channel width [27]. A complex image acquisition and processing unit allowed scanning of each channel in each video frame for the presence and tracking of cells through subsequent frames until exiting. The cell volumes were determined using imaging methods, by calculating the integrated optical density of the haemoglobin-containing stroma of RBC.

The first study involving electroosmotic pumping of bacteria ( $10^8$  cells/mL) and canine erythrocytes (5 % hematocrit) was performed by Li and Harrison [28]. A linear velocity of 0.5 mm/s was achieved for yeast cells at a field of 160 V/cm. The study used

electric fields of less than 600 V/cm to avoid cell electroporation. Higher velocities can be obtained by increasing the electric field applied, but membrane can be permeated at fields higher than a threshold value (2 kV/cm for human erythrocytes) [29].

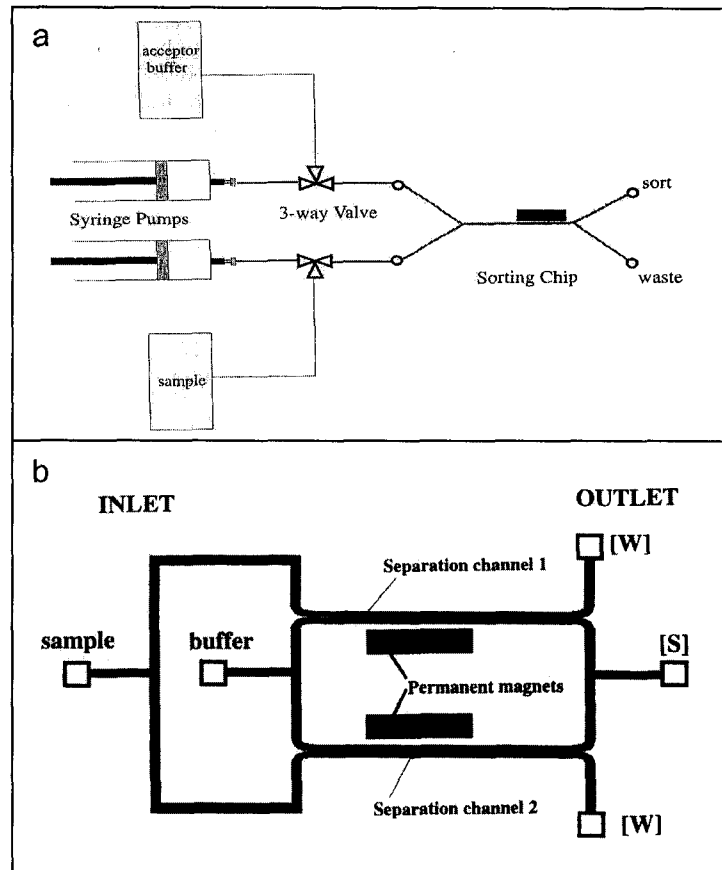


**Figure 1.1:** The magnetic cell sorter system proposed by Blankenstein. Figures adapted from reference 30.

Blankenstein reported the first application of magnetic cell sorting to a silicon microfabricated flow system [30]. Two syringe pumps were used to introduce the acceptor buffer and the sample into the sorting chip with the magnets (rare earth Samarium-Cobalt block magnet, rare earth Sr magnetic powder mixed with epoxy or electromagnet) were glued onto the chip (Figure 1.1a). Enrichment rates of more than 300 were reported for separating a mixture of magnetic Dynal particles (4.5  $\mu\text{m}$  diam) and fluorescent calibration beads (3.2  $\mu\text{m}$  diam). The system was tested for the sorting of human T lymphocytes (Jurkat cells) stained with the CD4 magnetic surface marker. The author also proposed a system for parallel magnetic sorting aimed at increasing the

separation speed (Figure 1.1b).

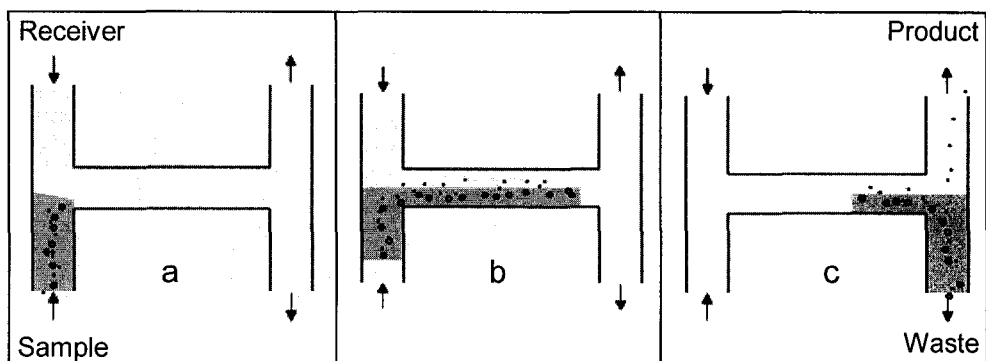


**Figure 1.2:** H-Filter channel for diffusion-based separation of smaller from larger particles ([http://www.micronics.net/technologies/h\\_filter.php](http://www.micronics.net/technologies/h_filter.php)).

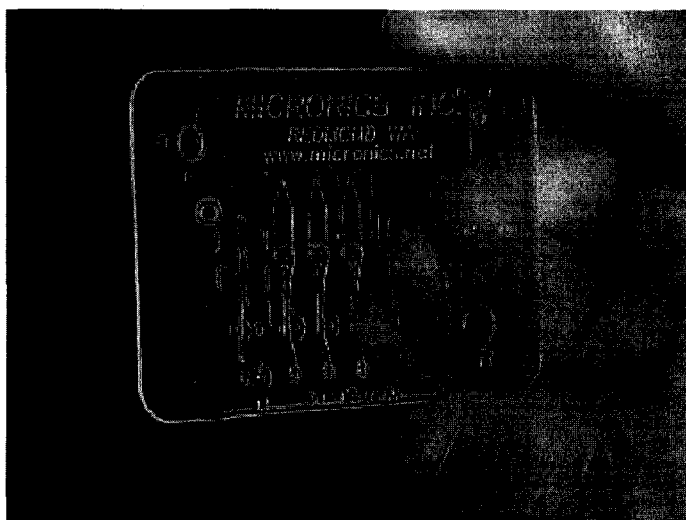


**Figure 1.3:** Micronics hematology cartridge. The device was designed for determination of red cells and platelet counts, hemoglobin concentration, white cell differential count and derived parameters. Figures adapted from reference 32.

In an effort to develop a small field-portable blood chemical analysis system, Yager et al. rejected the option of miniaturizing a centrifuge and adopted a simple system called an H-filter for continuous extraction from complex samples like blood [31]. To operate this filter, a blood sample and a receiver solvent, like water, are introduced as laminar streams (Figure 1.2a). Small components of the sample stream will diffuse into the



receiver stream [32]. Large particles like blood cells do not diffuse in the short time they are in contact with the receiver stream and remain on the same side of channel as the entry port (Figure 1.2b). The two parallel flows are then split into two separate reservoirs (product in receiver solvent and waste shown in Figure 1.2c). The content of the reservoirs can be further processed in integrated microfluidic structures like the disposable credit-card size cartridge presented in Figure 1.3. The H-filter, also called a Laminar Fluid Diffusion Interface (LFDI), was included by Weigl et al. in complex structures produced by Micronics for extraction of small proteins from whole blood samples and detection of various constituents in whole blood [31-34]. A recent collaboration between Micronics and Honeywell was undertaken for the development of a portable cytometer. A 1.4 kg prototype was tested with blood samples and the system is to be further downsized to 0.5 kg. The red blood cells from a drop of blood are lysed and the WBC analyzed on a scattering-based cytometer. The system would provide early detection of viral and bacterial infections based on quick measurement (30 s) of lymphocytes and neutrophil counts [35].

#### **1.1.2.2 On-Chip Blood Sample Preparation for PCR**

Inhibitors of nucleic acid amplification (section 1.4) present in blood have limited the number of on-chip methods used for PCR sample preparation of whole blood samples. Kellogg et al. proposed an integrated blood sample preparation for PCR without a cell enrichment step [36]. A blood sample was mixed (1:1) with 10 mM NaOH, the cells were lysed, the cell debris was washed away and PCR was performed on the DNA. The PCR amplification is affected by the presence of a large DNA background and would not work for rare target cells. Therefore a cell enrichment method must be considered. To date only microfiltration [37] and dielectrophoresis (DEP) [38, 39] were tested for integrating blood sample preparation with nucleic acid amplification reactions on microfabricated devices. These studies showed the complexity and challenge associated with attempting blood sample preparation for PCR. The microfiltration approach was prone to clogging the chip with a blood sample. The experiments performed with dielectrophoresis used only diluted or resuspended blood in a separation buffer with required conductivity. Blood sample preparation has thus remained a challenge on chip.

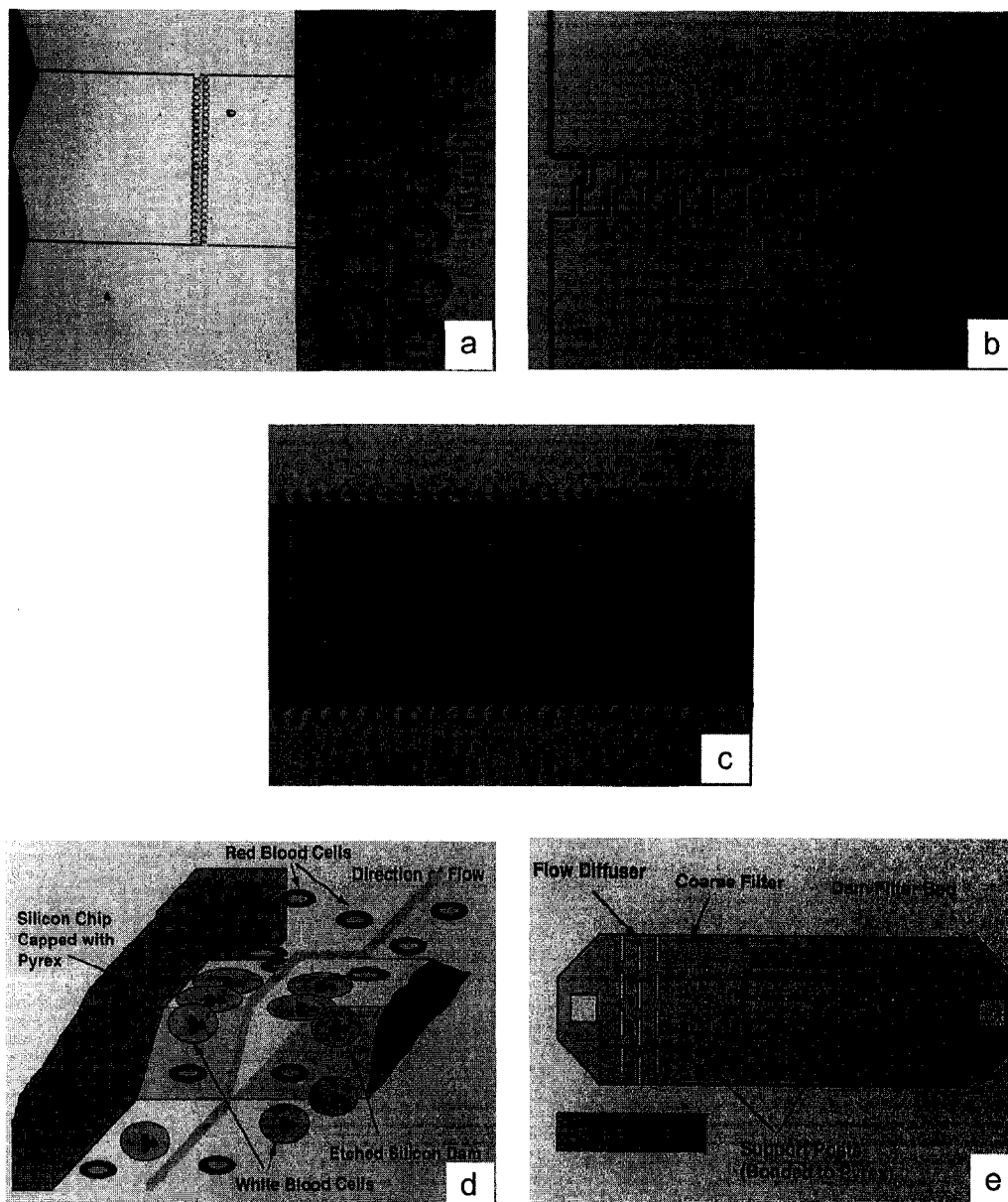


**Figure 1.4:** Microfilter chambers used for cell separation. Figures adapted from reference 37.

- a. Array of  $13 \times 20 \mu\text{m}$  microposts spaced  $7 \mu\text{m}$  apart on a  $500 \mu\text{m}$  wide,  $20 \mu\text{m}$  deep silicon channel;
- b. Array of complex microposts ( $73 \mu\text{m}$  wide, spaced  $30 \mu\text{m}$  apart) separated by tortuous channels on a  $500 \mu\text{m}$  wide,  $5.7 \mu\text{m}$  deep silicon channel;
- c. Comb-type filter formed by 120 posts ( $175 \times 18 \mu\text{m}$ ) separated by  $6 \mu\text{m}$  channels on a  $3 \text{ mm}$  wide,  $13 \mu\text{m}$  deep silicon channel;
- d. Schematic of weir-type filter;
- e. Design of a filter chip incorporating weir-type coil design filter bed.

### 1.1.2.2a Microfiltration

Wilding et al. used silicon-glass microfilter chambers to perform cell isolation. Silicon micropost-type (Figure 1.4 a-c) and weir-type (Figure 1.4d-e) microfilters were tested [37]. Samples of 3.5  $\mu\text{L}$  of whole human blood were pumped through the chips at a flow rate of 2.1  $\mu\text{L}/\text{min}$  by a syringe pump. After filtration of WBC, a phosphate saline buffer (PBS) wash solution was pumped at 130  $\mu\text{L}/\text{min}$  until the total removal of RBC was confirmed by microscope inspection of the chips. Capture efficiencies of 4 to 15 % were determined by counting the captured cells. The micropost structures shown in Figure 1.4a-b were effective in isolating nondeformable latex microspheres, but less effective for blood cells, which squeezed through the gaps. The comb-type filter (Figure 1.4c) was effective in separating blood cells, allowing the RBC to pass through the structure while WBC remained trapped in the filter. RBC easily passed through 3  $\mu\text{m}$  gaps, while larger WBC were stopped by gaps smaller than 7  $\mu\text{m}$ . After filtration with the more effective weir-type filter (Figure 1.4d-e), a PCR assay mixture was introduced into the channel, the WBC captured were thermally lysed and PCR amplification was performed on-chip. The silicon surface was covered with a thermally grown oxide layer to reduce the non-specific adsorption of PCR reagents and minimize the earlier observed inhibition [40]. The PCR product was analyzed off-chip by capillary gel electrophoresis. The authors do not comment on RBC contamination of the sample, but they did comment that the inhibition caused by the presence of RBC in PCR mixture was estimated at 36 % when 5,000 RBC were mixed with 10,000 WBC. Thus, they appear to conclude that they have enough separation.

The authors considered that the reduced capture efficiency of blood cells is caused by the cell deformability. Although the filtration mechanism was considered the cause of trapping WBC, the adhesion of cells on the filter surface may also be involved. The devices also would be prone to premature plugging of the filters, which could make them unreliable, especially for quantitative analysis.

### 1.1.2.2b Dielectrophoresis

The dielectric effect, an electrical polarization phenomenon, was well characterized by Pohl in 1978 [41]. Particles more polarizable than their surrounding media can be

retained at regions of high electric field strength (electrodes) by positive dielectrophoresis. Particles less polarizable than their surrounding media are repelled from regions of high electric field strength (electrodes) and can be collected in regions of low electric field strength by so called negative electrophoresis. Since the polarizability of a particle depends on their dielectric constant, conductivity and the frequency of the AC electric field applied, the transition from positive to negative DEP can be obtained by changing the frequency of the AC field. A crossover frequency is defined as the value at which transition from positive to negative DEP occurs. Based on measured dielectric characteristics, Yang et al. concluded that WBC subpopulations could be separated in a dielectrophoretic cell sorter [42].

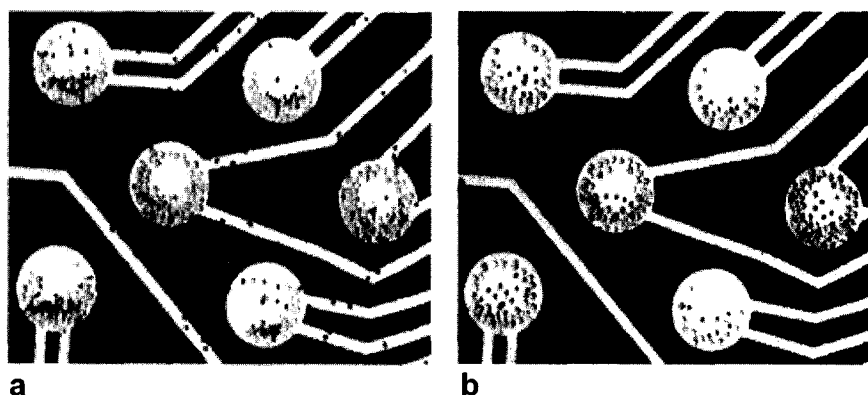


**Figure 1.5:** Dielectrophoretic enrichment of peripheral blood mononuclear cells from the mixture with red blood cells. Figures adapted from reference 39.

- a. Dielectrophoretic process when sample is still flowing over the chip;
- b. Final cell distribution.

A dielectrophoretic method for cell enrichment was considered at Nanogen for developing a future commercial genetic analysis system [38, 39]. *E. coli* were separated from a 1: 50 diluted blood sample in 0.05×TBE buffer containing the bacteria cells (ratio of 21:1 between *E. coli* and all other cells) [38]. Conductivity of the cell suspension was 315  $\mu\text{S}/\text{cm}$  and a sinusoidal signal of 10 V peak-to-peak at 10 kHz was used for separation. Cultured cervical carcinoma cells (*HeLa*) were also separated from peripheral blood cells using sinusoidal signal of 6 V peak-to-peak at 30 kHz [43]. The ratio between *HeLa* cells and all other cells in the suspension used cannot be calculated using the available information. A more recent study provides information about the capture efficiencies achieved with a microfabricated DEP chip [39]. Repetitive arrays of  $5 \times 5$

platinum electrodes (80  $\mu\text{m}$  diam) fabricated on silicon surface ( $5\times 5\text{ mm}^2$ ) were wire bonded to a printed circuit board. A polycarbonate flow cell with a cover slip was glued to the chip resulting in a 7.5  $\mu\text{L}$  sealed chamber. A 28 times enrichment was obtained for separating peripheral blood mononuclear cells (PBMNC) from an initial suspension containing  $1.6\times 10^7$  cells/mL (mixture of PBMNC and RBC). The captured cells were counted on each electrode (Figure 1.5) and the PBMNC to RBC ratio increased from 1:7 to 4:1. The cell suspension diluted in a sucrose-TBE buffer (suspension conductivity of 235  $\mu\text{S/cm}$ ) was continuously pumped at 30  $\mu\text{L/min}$  with a peristaltic pump as a sinusoidal signal of 6 V peak-to-peak at 200 kHz was applied at the electrodes. The separation was performed in 50 min, including 20 min of washing with the voltage on. A 30 times enrichment was also obtained from a 3500 times dilution of blood (WBC:RBC ratio of 1:1000,  $1.5\times 10^6$  cells/mL). So far the DEP chip was not able to separate and deliver a high purity collection of cells. Also, no separation from pure blood sample was reported, all cell suspensions used were either diluted or resuspended after centrifugation in a separation buffer which will provide the required solution conductivity for DEP. Finally, the length of time required is much greater than for conventional methods.

#### **1.1.2.2c Multi-Chip Module System for Genetic Analysis**

Collaboration between Motorola Microfluidics Laboratory (Phoenix, AZ, USA), Jed Harrison's group (University of Alberta, Canada) and Mark Hayes's group (Arizona State University, AZ, USA) was initiated in 2000 for developing a fully integrated system for genetic analysis. Such a system can potentially be used in a wide range of applications, including identification of a small number of specific bacteria or virus in a blood sample (infectious disease or biowarfare agents detection), fetal cells in maternal blood (genetic disease) and tumor cells in a background of normal cells (early cancer detection).

A fully integrated multi-chip module (MCM) microfluidic system which performs complete genetic analysis was developed by the Motorola team and presented at the  $\mu\text{TAS}$  2002 meeting by Liu et al. [44]. The device was based in part on work developed within this thesis. The large number of steps require a modular approach, instead of the well-known planar integration (Figure 1.6). The system incorporates micropumps, mixers

and microvalves, a target cell capture/PCR channel and a DNA array chip for detection. A piezoelectric disk attached to the reaction chamber acted as a bubble-induced acoustic mixer and allowed an enhanced mixing of the sample with the magnetic capture beads (Figure 1.7a). The convection generated significantly reduced the mixing time in a 50  $\mu\text{L}$  chamber from hours in the case of pure diffusion, to 6 seconds. Electrochemical pumps were used to deliver flows up to 1.2 mL/min (Figure 1.7b) for reagent transport.

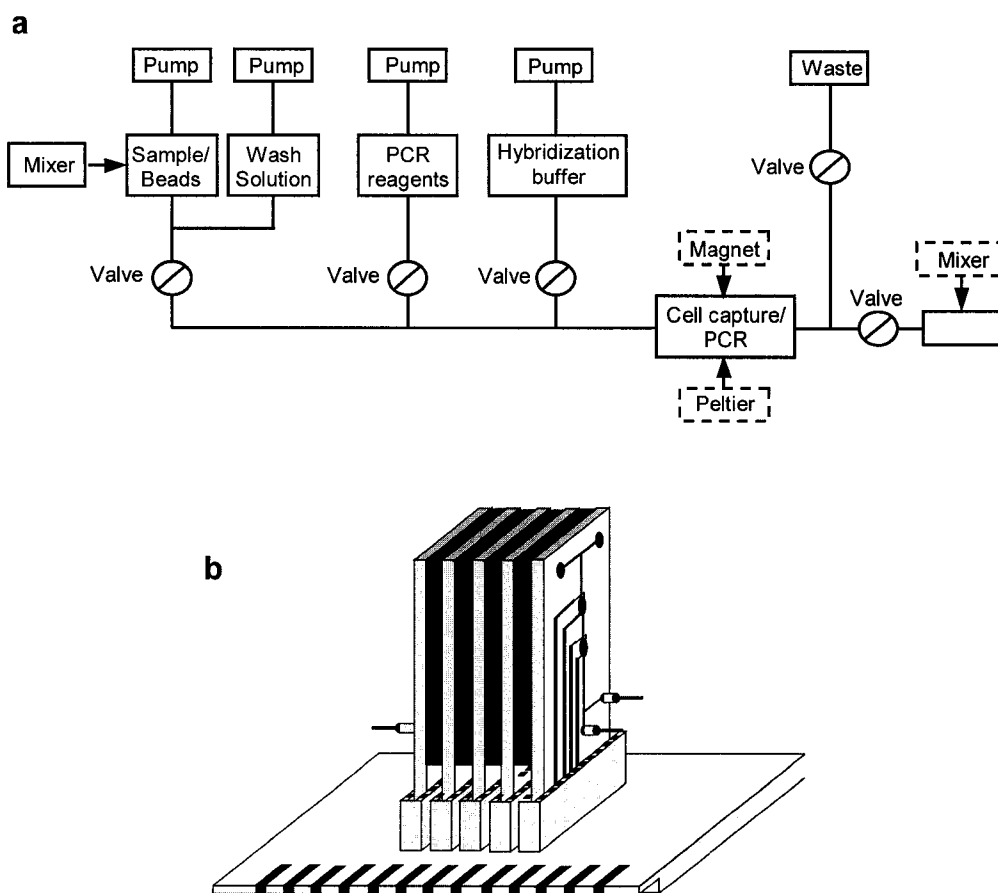


**Figure 1.6:** Fully integrated Multi-Chip Module (MCM) for DNA analysis. Figures adapted from reference 44.

- a. Description of the integrated system;
- b. Schematic of a MCM.

Although the results of such a system are impressive, the 2002 presentation focused on describing different types of single-use paraffin valves employed. The system was tested with a 1 mL sample, a relatively large volume for a microfluidic device. *E. coli*

cells were captured and concentrated in the channel by a magnet, followed by thermal lysis and PCR amplification. The authors claimed detection of 1000 *E. coli* cells captured from a 1 mL sample of unknown composition. Electrochemical detection was performed using a Motorola eSensor™ device.

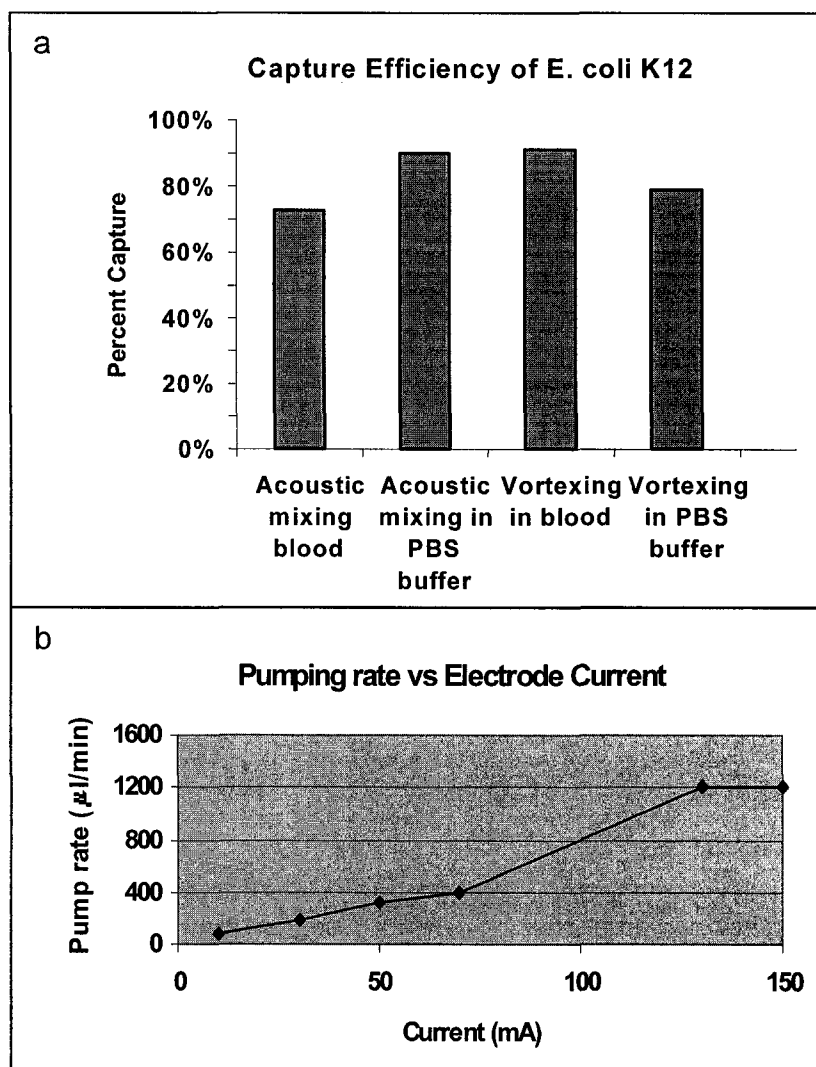


**Figure 1.7:** Characterization of the MCM system proposed by Motorola. Figures adapted from reference 44.

- Cell capture efficiency obtained with acoustic and vortex mixing;
- Characterization of the electrochemical pump used.

### 1.1.3 Motivation for This Study

The large number of studies performed on  $\mu$ TAS platforms for genetic analysis were focused on performing DNA sequencing [45-47], high throughput DNA sequencing [48-50], PCR [40, 51] or PCR followed by DNA sequencing [14, 52-56]. In all of these efforts the interfacing between the macroscopic world and microscopic environments is still considered a technical challenge [19].

For a microfluidic device the measurement is made in a very small volume. The consequence can be that sensitivity is not sufficient to measure low concentrations in small volumes. For example, 1 nL of a  $10^6$  cells/mL suspension contains only one cell. This issue was first mentioned by Manz [2] and explored for clinical samples by Petersen et al. [57]. Peterson used an assumption of a  $\mu$ TAS detection volume of 1 nL and concluded that many DNA assays would need to have a concentration of  $10^7$  copies/mL for such a volume to be analyzed. Some examples with the corresponding number of molecules or copies per mL are cancer cells in blood ( $\ll 10^4$  cells), asymptomatic HIV in blood ( $< 400$  copies), Gm- bacteremia in blood ( $< 10$  cells), biothreat agents in air ( $< 100$  copies) and food poisoning agents ( $< 10$  cell in 10 mL for *Salmonella sp.*, *E. coli O157:H7*) [57]. Based on these facts, Petersen et al. predicted the use of relatively large sample volumes, ranging from 0.1 mL to 10 mL, for diagnosis of infectious diseases, environmental pathogens, cancer analysis and other genetic analysis [57].

Integrating the sample preparation step into a microfluidic system, as presented in this thesis, would allow development of an integrated platform for rapid and complete genetic analysis of blood samples. The electrochemical pump approach considered here would also allow development of a portable device, powered by a small battery. The studies performed here would allow the design of an adequate sample preparation unit able to rapidly process undiluted blood samples (1-5 mL) and deliver suspensions of captured rare cells (less than 100 nL) for genetic analysis. This unit would be part of a portable, automated multi-chip module (MCM) microfluidic device able to detect biological warfare agents, which was considered for prototyping by Motorola (Microfluidics Laboratory), our co-contractor to DARPA (Defense Advanced Research Projects Agency) at the time of the study. Preliminary tests performed on an MCM unit prior to completion of this study were published earlier [44], as discussed above.



## 1.2 The Basics of Human Blood

### 1.2.1 Human Blood Composition

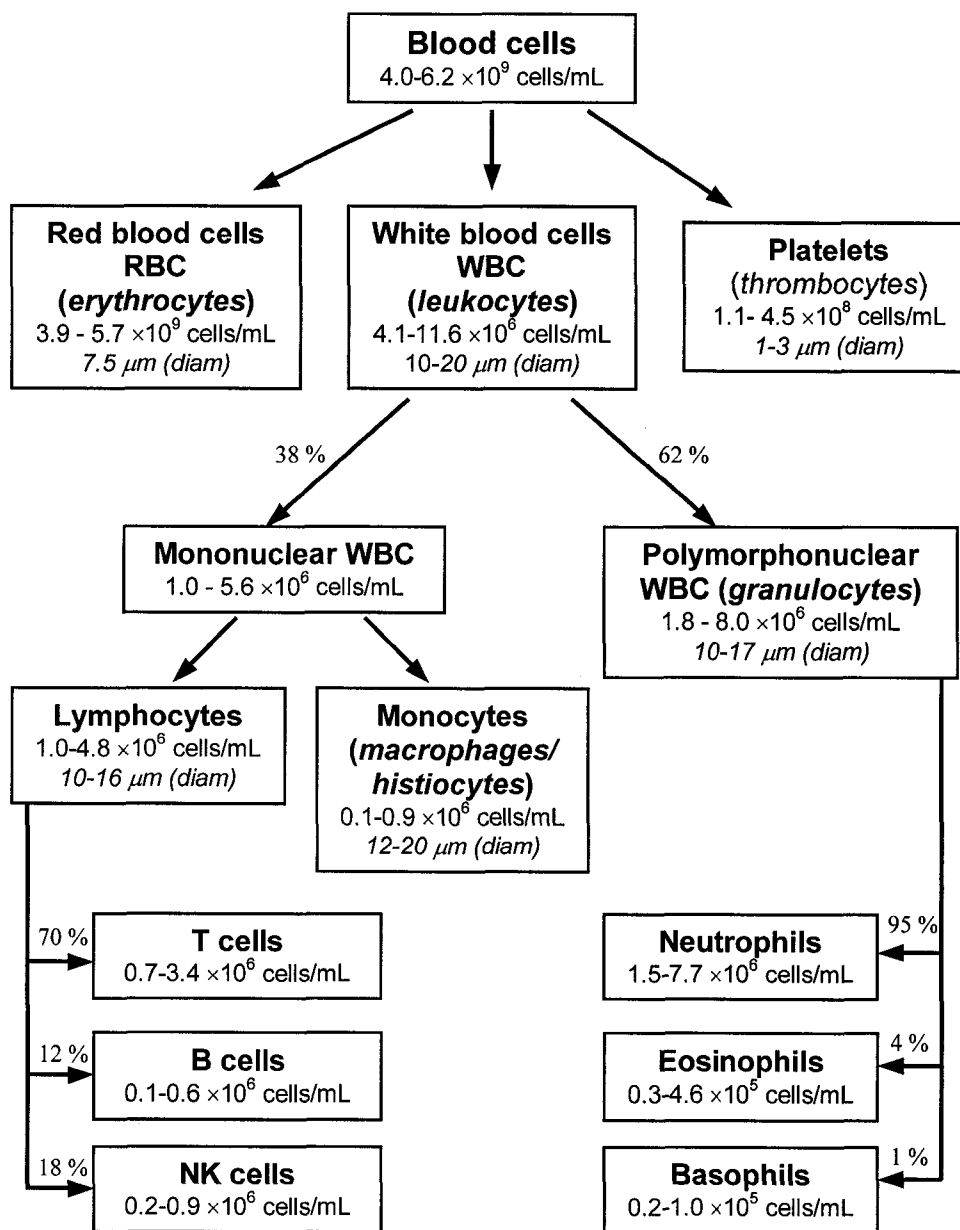


**Figure 1.8:** Blood cell composition. Cell concentrations, reported as the number in the volume of whole blood, were determined separately for every type of cell. Diameters given represent the long axis of spheroids, ellipsoids or rods.

Blood is mainly composed of cells (36 - 50 % of total volume) and a fluid component known as plasma. Composition and size details of the blood cell types are shown in Figure 1.8. The cell concentrations represent normal ranges in healthy adult male and female patients [58-61]. White blood cells (WBC), red blood cells (RBC) and platelets are the three major types of cells present in blood. In the neonatal period and occasionally in pregnancy, nucleated red blood cells (NRBC) are present in peripheral blood. The ratio of the volume of RBC to the volume of the whole blood is termed hematocrit. Mononuclear WBC are also referred to as peripheral blood mononuclear cells (PBMNC). Within the WBC family, the designation of B and T cells derives from their sites of maturation, bone marrow and thymus, respectively. Specific surface markers are characteristic for different types of cells such as RBC (AB and rhesus blood group antigens), T cells (CD2, CD3), B cells (CD19, CD20, CD22), natural killer NK cells (CD16, CD56), basophils (IgE receptor) and eosinophils (IgG receptor) [59].

### **1.2.2 Types of Blood Samples**

Depending on the collection procedure, blood samples can be classified as arterial, capillary and venous. Based on their different characteristics one has to decide which type is appropriate for a specific analytical determination. Arterial blood, the source of nutrients for all body tissues is the best sample to be used for evaluation of adequate delivery of necessary substances such as oxygen to the body tissue. Venous blood has lower concentrations of substances used in metabolism (oxygen, glucose) and higher concentrations of waste products (organic acids, ammonia, carbon dioxide). The differences between arterial and venous blood are inversely proportional to tissue perfusion and can be used in monitoring patients in shock by comparing the levels of blood-gases [62]. Capillary blood is generally closer in composition to arterial blood. However, differences in composition between these two types of blood exist, such as for patients in shock or in a fasting state [63].

A blood sample removed from the body starts to clot when a solid phase consisting of blood cells and fibrin separates from a liquid phase called 'serum'. Therefore anticoagulants, such as heparin, trisodium citrate and EDTA are usually mixed with blood specimens to prevent clotting. While heparin inhibits thrombin formation by

complexing with antithrombin III, trisodium citrate and EDTA chelate calcium, an essential ingredient for coagulation. Differences in blood composition can be induced by the addition of the anticoagulants, making their use in some subsequent analysis inappropriate [61]. Lithium or ammonium, the usual cations in heparin salts, can cause contamination of specimens used to determine these analytes. The chelation of divalent ions produced by EDTA can inactivate some enzymes, leading to changes in lipids, nucleic acids and peptide hormones [63]. Thus, the type of analysis to be performed on a sample must be considered when selecting reagents.

### 1.2.3 T Cells

The cell membrane of T cells (CD3+ cells) has an estimated 40,000 T cell receptors (TCR) expressed per cell [64]. The TCR has a complex heterodimeric structure (80-120 kDa), similar to an immunoglobulin, with constant and variable domains and a unique antigen-binding site [58, 65]. The TCR, a part of the CD3 complex, is shown in Figure 1.9. About 10 % of the TCR are expressed as  $\gamma\delta$  chains instead of  $\alpha\beta$  chains.

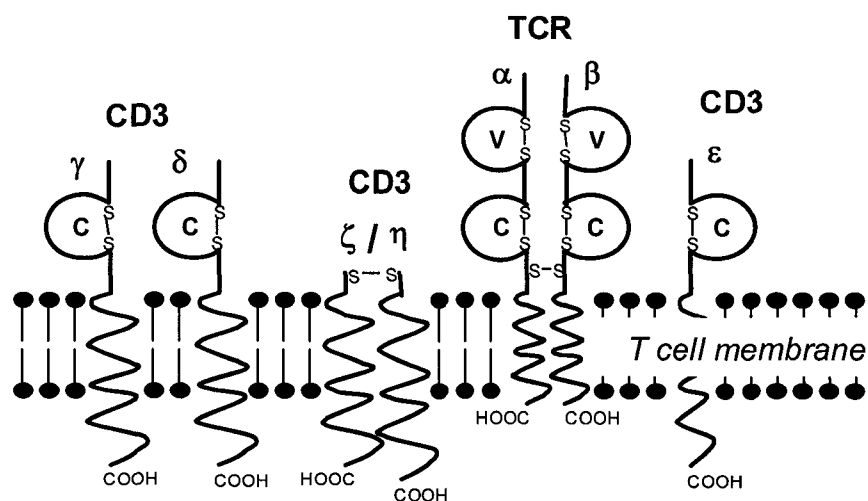


**Figure 1.9:** Components of the T cell receptor: CD3 complex. An  $\alpha\beta$  TCR complexed with the CD3  $\gamma$ ,  $\delta$ ,  $\epsilon$ ,  $\zeta$  and  $\eta$  chains in the membrane of a T cells is depicted. On some T cells the  $\alpha\beta$  chains are replaced by the  $\gamma\delta$  chains in TCR.

The TCR ( $\alpha\beta$  and  $\gamma\delta$ ) are characterized by a large diversity [66]. Based on their function, T cells can be subdivided into helper T lymphocytes (70 %; CD3+, CD4+) and cytotoxic T lymphocytes (30 %; CD3+, CD8+) [59]. A further discussion of the genetic material in T cells is presented in section 1.3.1 as it is relevant to their specific detection.

## **1.2.4 Methods for Cell Separation**

### **1.2.4.1 General Methods**

Separation of blood cells is usually done using two forms of density gradient centrifugation. In rate-zonal centrifugation the sample is layered on top of the gradient solution and centrifugal force is used to cause cells to move at different rates, depending on their density. Separation of more than two cell populations is possible, but because the density of the cells is greater than the density of the gradient, the method is time dependent. In isopycnic centrifugation the sample is mixed with the gradient solution and under centrifugal force the gradient redistributes and the cells band at their isopycnic positions. Cells cannot sediment further because of a denser medium below them and are separated on the basis of differences in density. The most commonly used materials to form density gradients are solutions of sucrose, synthetic sucrose-epichlorohydrin copolymer (MW 400,000, Ficoll, Pharmacia), suspensions of coated colloidal silica particles (Percoll, Pharmacia) and low molecular weight iodinated benzene compounds (Metrizamide and Nycodenz). Other methods are based on sedimentation at earth's gravity (unit gravity sedimentation), sedimentation in gravitational field with cell suspension introduced in counterflow (centrifugal elutriation), partition of cells based on different surface properties between aqueous two-phase mixtures, and differences in surface charge density of cells (electrophoresis) [67, 68]. Field flow fractionation, a concept developed by Giddings, includes different separation methods in which a transverse field is imposed on suspensions as it flows through a chamber [69, 70].

### **1.2.4.2 Specific Surface Methods**

Separation of cells with known differences in surface character can be done by specific and powerful methods. The most widely used molecules to mark cells are antibodies specific for a particular cell surface antigenic determinant, hormones or other

molecules that have corresponding cell surface receptors and lectins that bind to particular carbohydrate sequences on cell surfaces. In affinity chromatography, samples are passed through a column and cells with affinity for a bound ligand are captured in the column, before then being eluted. The types of ligand interaction used are the same as those used to mark cells. An alternative to direct coupling of antibody to the adsorbent is the use of Protein A, a protein from *Staphylococcus aureus*, which binds to the Fc region of IgG-type antibodies and to label the cells with a specific antibody. Bound cells can be eluted by competition with free IgG [67, 71]. A common problem with all of these techniques is the non-specific binding of cells to the column material.

Fluorescence activated cell sorting (FACS) introduced in the late 1960s by Herzenberg et al. [72] has proven to be a valuable technique and is widely used in commercial flow cytometers [73, 74]. Its success was also aided by the introduction of monoclonal antibodies [75], available as fluorescent labels to allow the optical identification of cell subpopulations for separation by sorting. Immunomagnetic cell separation, the method based on the capture of magnetically labeled cells in an external magnetic field, was made possible by loading monoclonal antibodies on synthetic paramagnetic microspheres [76]. The diameter of the magnetic labels used for magnetic activated cell sorting (MACS) varies from around 100 nm to 1-5  $\mu\text{m}$  [77]. The advantages of the 100 nm colloidal magnetic labels are that they offer better mass transport kinetics for labeling, react quickly with analytes and do not require frequent mixing because they remain suspended for extended periods. There are procedures developed for separation of fetal nucleated erythrocyte from maternal blood for noninvasive prenatal diagnosis [78, 79], separation of tumor cells [80-82] or cell subpopulations with viral content from human blood [83]. However, for all of the above references, an enrichment step, usually density gradient centrifugation, was required to remove the red blood cells, which otherwise may be captured in the high gradient magnetic field sorters often used, due to the paramagnetic property of RBC containing deoxyhaemoglobin [84].

### 1.3 The Basics of DNA

The deoxyribonucleic acid, best known as DNA, is a long, threadlike biological molecule responsible for carrying the information in all cellular life as well as in many viruses. It is composed of repeating units named nucleotides, each containing phosphate, sugar (deoxyribose) and one of the four bases (adenine A, guanine G, cytosine C and thymine T). A structure based classification divides the four bases into purines (A and G) and pyrimidines (C and T). By convention, a polynucleotide is written with its 5' end at the left and its 3' end to the right, with the phosphodiester bond linking neighboring ribose residues in the 5'-3' direction. The sequence from Figure 1.10 can be abbreviated as ATCG.

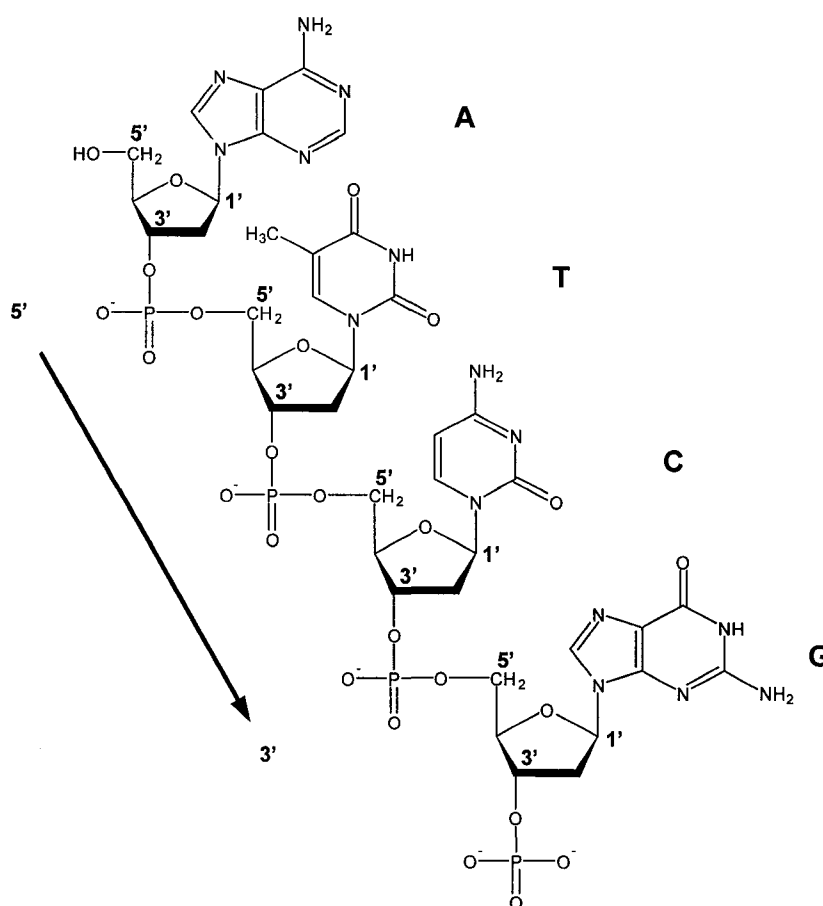


**Figure 1.10:** Structure of a single DNA strand representing a tetranucleotide. The sugar atom numbers are primed to distinguish them from the base atom numbers.

One of science's major intellectual achievements in the 20<sup>th</sup> century, with a strong impact on modern molecular biology was the elucidation of the DNA structure by Watson and Crick in 1953. This was based on X-ray studies and Chargaff's rules, which suggested the pairing of A-T residues and G-C residues, respectively. The two strands of DNA are held together by hydrogen bonds formed between the bases from opposite strands, A-T (2 hydrogen bonds) and G-C (3 hydrogen bonds), respectively. The stability of the double helix is attributed to multiple factors including hydrophobic interactions, exclusion of water molecules resulted from base stacking and also electrostatic interactions between the anionic phosphate backbone and paired cations [66].

Human genomic DNA is a collection of DNA molecules organized in 23 haploid chromosomes, containing  $2.9 \times 10^9$  base pairs (bp) with an end-to-end length of 99 cm for the stretched out native molecule. The dimensions of such a large molecule require extreme care in handling to prevent a possible mechanical damage caused by the hydrodynamic shearing forces (stirring, shaking, pipetting) generated during separation.

### 1.3.1 T Cell Receptor Complex Genes

The human T cell receptor (TCR) locus has been mapped to either chromosome 7 for TCR $\beta$  (7q35, 685 kb) and TCR $\gamma$  (7q15, 160 kb) or chromosome 14 for TCR $\alpha$  (14q11.2, >800 kb) and TCR $\delta$  (14q11.2, >195 kb). TCR $\gamma$  gene is the smallest of the four types of TCR genes. The genes encoding the other parts of the CD3/TCR complex are located at chromosome 1 (1q22-q23) for  $\zeta$  and  $\eta$  chains and chromosome 11 (11q23) for CD3 $\gamma$  (9 kb), CD3 $\delta$  (3.7 kb) and CD3 $\epsilon$  (13 kb) [65].

The large diversity of TCR expressed by T cells is obtained through somatic recombination of variable (V), joining (J), diversity (D) and constant-region (C) gene segments during the early stages of T cell development [64, 85]. An example of a TCR $\gamma$  gene rearrangement produced by joining V $\gamma$  gene segments to J $\gamma$  gene segments is presented in Figure 1.11. These rearrangements remain present during further maturation, in contrast to rearranged TCR $\delta$  genes, which are deleted on one or both alleles in mature T cells with TCR $\alpha\beta$  [86, 87]. The advantage of a relatively simple and limited combinatorial repertoire of the TCR $\gamma$  gene was exploited in PCR analysis [88, 89] and is

also considered for this work. Because the reorganization of the TCR $\gamma$  gene is specific to T cells, and is retained in the mature state, analysis of their genomic DNA specifically identifies T cells.

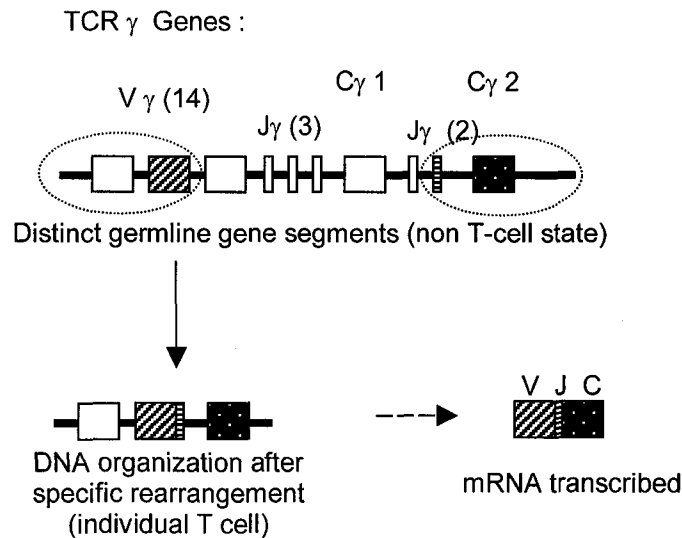


**Figure 1.11:** Representation of a TCR $\gamma$  gene rearrangement. The variable (V), joining (J) and constant-region (C) gene segments are represented.

#### 1.4 Polymerase Chain Reaction

Polymerase chain reaction (PCR), discovered by Erlich and Mullis in 1986 [90, 91], is a widely applied DNA amplification technique, with more than 150,000 publications searchable at PubMed (<http://www.ncbi.nlm.nih.gov>). PCR allows for the physical separation of any particular sequence of interest from its DNA context and provides in vitro amplification of this context, virtually without limit [92]. The technique is now so sensitive it was used to amplify genomic DNA [93-100], mRNA [101-106], bacterial DNA from single cells [107-110] or viral DNA from a single infected cell [111-113].

PCR is performed by incubating the samples at three temperatures corresponding to denaturation, annealing and extension. The double stranded DNA is denatured by briefly heating the sample to 90-95 °C, the primers are allowed to anneal to their complementary sequences by cooling to 40-60 °C, followed by heating at 72 °C when the polymerase starts extension of the annealed primers. Insufficient heating during the denaturation step can drastically reduce the efficiency of the amplification. Because of the very large excess of primers in the reaction mix, hybridization is almost instantaneous and a short



incubation is recommended to prevent the production of nonspecific products. If annealing and extension are performed at 72 °C, the specificity of the reaction may be improved in a simplified two-temperature cycle procedure [92, 114]. Under such high stringency conditions (higher annealing temperature), a better specificity is achieved as mispriming is reduced.

A large number of inhibitors are found in many types of specimens, so adequate methods for their removal must be adopted. Identified inhibitors in blood are blood anticoagulants (heparin [115, 116]), additives to blood culture media (sodium polyanetholsulphonate [117]), IgG from plasma [118], polypeptides (hemoglobin in erythrocytes and lactoferrin in leukocytes [119]) and particularly the heme [120]. Complex polysaccharides were also identified as PCR inhibitors in feces [121]. A method to remove polysaccharide inhibitors was proposed by Moreira using agarose-embedded DNA preparations [122]. The difference in size between the DNA macromolecules and these contaminants allows their effective removal from the agarose blocks by diffusion during the washing steps, whereas genomic DNA remains trapped within them. By sacrificing sensitivity, the effect of inhibitors can also be reduced if the sample is diluted [114].

#### **1.4.1 Quantitative PCR**

PCR was used previously in different quantitative approaches [123]. A general method considers a competitive PCR, where an internal control consisting of a known quantity of synthetic DNA is added to target DNA. Both the target and synthetic DNA have identical primer-binding sites and compete equally for the primers. The amplifications are performed using different dilutions of synthetic DNA [124-127]. A method to generate synthetic DNA was presented earlier by Perrin et al. [128]. In a simpler approach for quantitative PCR, amplifications are performed from serial dilutions of cells with known concentrations. The amplifications are then compared with the PCR performed on samples with unknown cell content [129, 130]. The advantage of this approach is that synthetic DNA is not necessary. Such PCR amplifications should be performed simultaneously to reduce variability in the amplification between samples. A version of this approach was used in this thesis research.

## 1.5 Capillary Gel Electrophoresis

### 1.5.1 Fundamentals of Capillary Electrophoresis

Capillary electrophoresis (CE) is a fast and efficient method to separate charged analytes, while using very small volumes of sample (1 – 50 nL). The relatively simple instrumentation of a CE system, shown in Figure 1.12a, is readily commercialized (e.g.

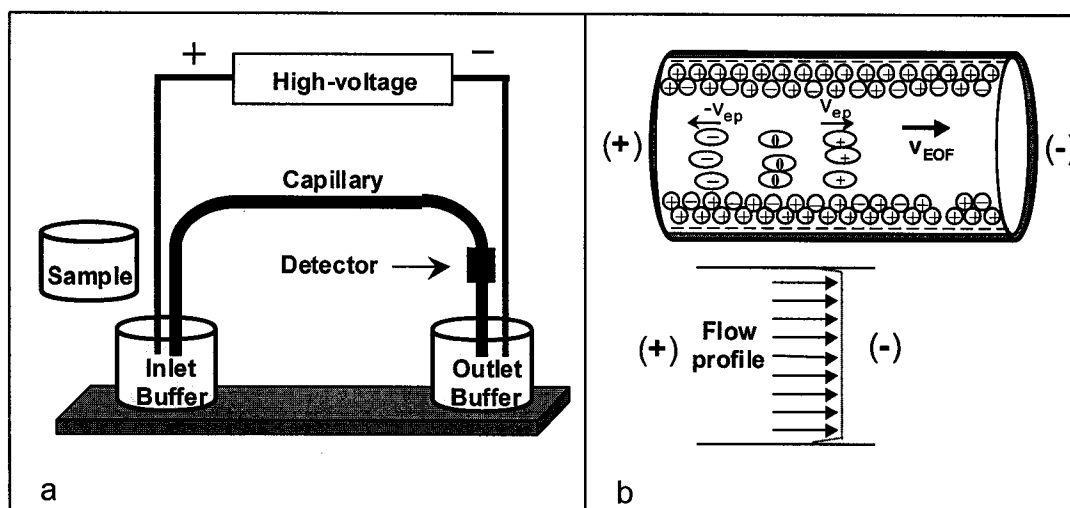


**Figure 1.12:** Schematic representations of a CE system (a) and of separation in capillary zone electrophoresis (b).

Beckman, Dionex, Bio-Rad, Agilent). Different modes of CE separation can be performed using a high voltage supply, a polyimide-coated fused silica capillary (25-75  $\mu\text{m}$  id), a detector and buffer/sample reservoirs [131, 132]. In the early 1980s, Jorgenson and Lukacs introduced the simplest mode of CE, capillary zone electrophoresis (CZE) for separation of amino acids and urine [133-135]. Differences in the electrophoretic mobilities of individual sample analytes are responsible for the separation and can be optimized by controlling voltage, composition of the separation buffer and surface coating. The electrophoretic mobility  $\mu_{ep}$  (units of  $\text{cm}^2/\text{V}\times\text{sec}$ ) as expressed in equation 1.1 is determined by the charge/size ratio of the analyte:

$$\mu_{ep} = \frac{q}{6\pi\eta r} = \frac{v_{ep}}{E} \quad (1.1)$$

where  $q$  is the effective charge of the sample analyte,  $r$  its hydrodynamic radius,  $\eta$  the viscosity of the separation media,  $v_{ep}$  the electrophoretic velocity and  $E$  the electric field determined by the ratio of the total voltage applied to the capillary length [131].

The silanol groups from the inner surface of the fused silica capillary are ionized in solution and the electrical double layer is formed in the presence of the buffer solution. Migration of the buffer solution through the capillary, known as the electroosmotic flow (EOF), is induced by the application of an external electric field (Figure 1.12b). The electroosmotic mobility  $\mu_{\text{EOF}}$  with the same units as  $\mu_{\text{ep}}$  ( $\text{cm}^2/\text{V}\times\text{sec}$ ) is characterized by equation 1.2:

$$\mu_{\text{EOF}} = \frac{\varepsilon \zeta}{4 \pi \eta} \quad (1.2)$$

where  $\zeta$  is the zeta potential defined as the potential at the plane of shear near the outer Helmholtz plane of the electrical double layer.  $\varepsilon$  and  $\eta$  are the dielectric constant and the viscosity of the separation media, respectively. The velocity  $v$  and migration time  $t$  for an analyte are given by:

$$v = \frac{(\mu_{\text{EOF}} + \mu_{\text{ep}})V}{L} \quad (1.3)$$

and

$$t = \frac{L L_d}{(\mu_{\text{EOF}} + \mu_{\text{ep}}) V} \quad (1.4)$$

where  $V$  is the voltage applied,  $L$  the length of the capillary and  $L_d$  the capillary length between the injector and detector.

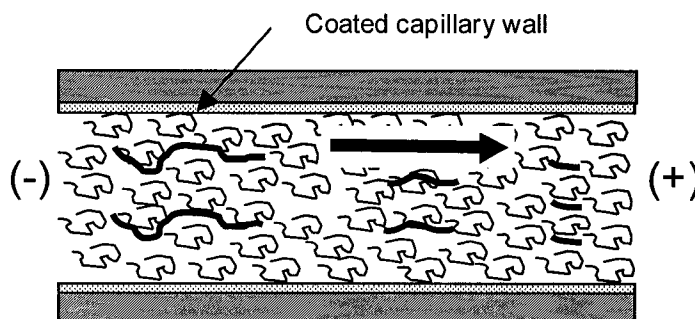


**Figure 1.13:** Pictorial description of the size separation of DNA fragments by CGE. After coating the capillary walls, the EOF is suppressed and negatively charged components (DNA fragments) migrate towards the anode. Smaller molecules migrate faster because of smaller friction with the gel.

### 1.5.2 Capillary Gel Electrophoresis for DNA Separation

DNA molecules cannot be separated by CZE because of the linear increase of charge with the length of the fragment. To perform CE separation of the polynucleotides, porous matrices comprised of hydrophilic polymer materials dissolved in a solvent (gels) are introduced into the capillary to form pores required for size separation (Figure 1.13). Two theories, the Ogston model and the reptation model have been proposed to explain the mechanism of gel electrophoresis [136]. The Ogston model considers the gel as a molecular sieve and predicts the decrease of the electrophoretic mobility as either the size of the analyte or the gel concentration is increased. However, the model fails to explain the difficult separation of large DNA molecules. The reptation model considers the high electric field influence on DNA molecules, when the molecules become rigid and rod-shaped. The model predicts that for small DNA molecules separated at low electric fields, the mobility is related to the DNA size. As the electric field increases, especially for large DNA molecules, the mobility becomes more related to the electric field and less dependent on size, making the separation of such molecules impossible.

The first CE separation of DNA fragments was performed by Cohen et al. with a cross-linked solution of polyacrylamide [137]. With a more efficient dissipation of Joule heat than slab gel electrophoresis, capillary gel electrophoresis (CGE) allowed application of higher field strengths and produced separation in shorter analysis times. The difficulty of producing good quality gel capillary columns and the limited number of separations achieved before gel breakdown were normally associated with the use of cross-linked gels. Following an earlier idea proposed by Bode [138, 139], the non-cross linked linear polymer solutions, known also as entangled polymers or physical gels, were introduced in CGE separations. A large number of polymers have been tested, including methylcellulose [140, 141], hydroxyethylcellulose (HEC) [142-144], hydroxypropylcellulose [141], hydroxypropylmethylcellulose (HPMC) [141, 145-148], linear polyacrylamide [144, 149, 150], linear poly(N-acryloylaminoethoxiethanol) [150], poly(vinylalcohol) [144] and liquefied agarose [151-153]. The cellulose polymers produce dynamic coating of the capillary [148] and allow reproducible separations with uncoated capillaries, since EOF is eliminated and the adsorption effects are minimized. Reverse polarity (i.e., cathode on the injection side) has to be considered for separation,

since EOF is eliminated.

Schwartz et al. found the peak/area precision to be concentration dependent. At DNA concentrations of 10-25  $\mu\text{g/mL}$  the peak height and peak area precision were 1 -7% (RSD) and 2 -9%, respectively. A significant deterioration was observed at a DNA concentration of 5  $\mu\text{g/mL}$ , when 12 -28% peak height and peak area precision were obtained. The electrophoretic mobility of the DNA fragments is decreased by the addition of intercalating agents such as ethidium bromide, mainly because of the positive charge of ethidium bromide and the increased molecular mass of the complex [146].

## 1.6 Scope of the Thesis

The present thesis work is centered on developing the building blocks of a disposable blood-sample-preparation device for rare cell capture that can be integrated on a portable platform. Such a module has to be incorporated by any PCR-based system that will be designed for clinical diagnostic field or blood-based biodetection.

In Chapter 2, we describe the optimization of a PCR-based procedure, which is able to determine and quantify the DNA content extracted from samples with unknown number of T cells. The study was justified by the need of a method to estimate the capture efficiency of the microfluidic devices tested in Chapter 3, as the use of a simpler cell counting method was impractical for the blood samples analyzed with the magnetic bead-bed approach. Conditions for PCR amplification and CGE product separation were optimized.

In Chapter 3, we first tested a simple Y microfluidic device for T cell capture from human blood. We describe the use of paramagnetic beads for cell capture within the microfluidic channels. Protein A/anti-human CD3 paramagnetic beads are introduced into the chip and captured in the magnetic field generated by an external magnet. Then the blood sample is introduced and T cells are captured as the other cells are collected at the outlet. The washed suspension of captured cells/beads is removed from the chip and a 42% capture efficiency was determined using the method presented in Chapter 2. The preliminary results provided guidance for designing and testing eight new devices which are able to process a sample ten times faster than was the initial design. A simple increase of the channel size for processing larger volumes of sample in a short time was not found

to be appropriate. An adequate stepwise flow bifurcation was required to allow larger volumes to be used. The capture efficiencies varied between 16 % and 37 %.

Chapter 4 describes the adaptation of electrolysis micropump to the manipulation and initial processing of a blood sample. A pair of electrolysis chambers was designed to work in a stepwise fashion to first deliver blood and then a buffer used to wash the captured cells.

In Chapter 5 we present the preliminary results obtained in fabrication of polycarbonate devices. The channels are etched anisotropically on a Si wafer by deep reactive ion etching and then Ni is electrochemically deposited to transfer the features onto a Ni master. The channels are embossed on a polycarbonate substrate using the Ni master and thermally bonded to a cover-plate to form microfluidic structures.

Chapter 6 focuses on future work and on overall conclusions from the thesis work. Based on the results reported in this thesis, a new design of an integrated system is proposed that will be able to deliver purified PCR-ready DNA of rare cells separated from a fresh blood sample.

## 1.7 References

- [1] Widmer, H. M. *Trends Anal Chem*, **1983**, *2*, R8-R10.
- [2] Manz, A.; Graber, N.; Widmer, H. M. *Sensors and Actuators B: Chemical*, **1990**, *1*, 244-248.
- [3] Terry, S. C.; Jerman, J. H.; Angell, J. B. *IEEE Transactions On Electron Devices*, **1979**, *ED-26*, 1880-1886.
- [4] Manz, A.; Miyahara, Y.; Miura, J.; Watanabe, Y.; Miyagi, H.; Sato, K. *Sensors and Actuators B: Chemical*, **1990**, *1*, 249-255.
- [5] Harrison, D. J.; Manz, A.; Fan, Z.; Ludi, H.; Widmer, H. M. *Anal Chem*, **1992**, *64*, 1926-1932.
- [6] Manz, A.; Harrison, D. J.; Verpoorte, E. M. J.; Fettinger, J. C.; Paulus, A.; Ludi, H.; Widmer, H. M. *J Chromatogr A*, **1992**, *593*, 253-258.
- [7] Manz, A.; Verpoorte, E.; Effenhauser, C. S.; Burggraf, N.; Raymond, D. E.; Harrison, D. J.; Widmer, H. M. *Journal of High Resolution Chromatography*, **1993**, *16*, 433-436.
- [8] Harrison, D. J.; Glavina, P. G.; Manz, A. *Sensors and Actuators B: Chemical*, **1993**, *10*, 107-116.

- [9] Harrison, D. J.; Fluri, K.; Seiler, K.; Fan, Z.; Effenhauser, C. S.; Manz, A. *Science*, **1993**, *261*, 895-897.
- [10] Manz, A.; Harrison, D. J.; Verpoorte, E.; Widmer, H. M. *Adv. Chromatogr.*, **1993**, *33*, 1-66.
- [11] Reyes, D. R.; Iossifidis, D.; Auroux, P. A.; Manz, A. *Anal Chem*, **2002**, *74*, 2623-2636.
- [12] Auroux, P. A.; Iossifidis, D.; Reyes, D. R.; Manz, A. *Anal Chem*, **2002**, *74*, 2637-2652.
- [13] Oleschuk, R. D.; Harrison, D. J. *Trends Anal Chem*, **2000**, *19*, 379-388.
- [14] Paegel, B. M.; Blazej, R. G.; Mathies, R. A. *Current Opinion in Biotechnology*, **2003**, *14*, 42-50.
- [15] Zhang, L.; Dang, F.; Baba, Y. *Journal of Pharmaceutical and Biomedical Analysis*, **2003**, *30*, 1645-1654.
- [16] Sanders, G. H. W.; Manz, A. *Trends Anal Chem*, **2000**, *19*, 364-378.
- [17] Tudos, A. J.; Besseling, G. A. J.; Schasfoort, R. B. M. *Lab on a Chip*, **2001**, *1*, 83-95.
- [18] Verpoorte, E. *Electrophoresis*, **2002**, *23*, 677-712.
- [19] Weigl, B. H.; Bardell, R. L.; Cabrera, C. R. *Advanced Drug Delivery Reviews*, **2003**, *55*, 349-377.
- [20] Andersson, H.; van den Berg, A. *Sensors and Actuators B: Chemical*, **2003**, *92*, 315-325.
- [21] Elwenspoek, M.; Jansen, H. V. *Silicon micromachining*, Cambridge University Press: Cambridge, England **1998**.
- [22] Rai-Choudhury, P. ed. *Handbook of microlithography, micromachining and microfabrication*, SPIE Optical Engineering Press: Bellingham, Wash., USA **1997**.
- [23] Petersen, K. E. *Proceedings of the IEEE*, **1982**, *70*, 420-457.
- [24] Manz, A.; Fettingner, J. C.; Verpoorte, E.; Ludi, H.; Widmer, H. M.; Harrison, D. J. *Trends Anal Chem*, **1991**, *10*, 144-149.
- [25] Wilding, P.; Pfahler, J.; Bau, H.; Zemel, J.; Kricka, L. *Clin Chem*, **1994**, *40*, 43-47.
- [26] Tracey, M. C.; Greenway, R. S.; Das, A.; Kaye, P. H.; Barnes, A. J. *IEEE Transactions On Bio-Medical Engineering*, **1995**, *42*, 751-761.
- [27] Sutton, N.; Tracey, M. C.; Johnston, I. D.; Greenway, R. S.; Rampling, M. W. *Microvascular Research*, **1997**, *53*, 272-281.
- [28] Li, P. C. H.; Harrison, D. J. *Anal Chem*, **1998**, *69*, 1564-1568.
- [29] Serpersu, H. E.; Kinoshita, K. J.; Tsong, T. Y. *Biochim Biophys Acta*, **1985**, *812*, 779-785.
- [30] Blankenstein, G. In *Scientific and Clinical Applications of Magnetic Carriers*, Urs Hafeli; Wolfgang Schutt; Joachim Teller; Maciej Zborowski, eds.; Plenum Press: New York, **1997**, pp. 233-245.

- [31] Yager, P.; Bell, D.; Brody, J. P.; Qin, D.; Cabrera, C. R.; Kamholz, A.; Weigl, B. H. In *Micro Total Analysis Systems 1998*; D. Jed Harrison; Albert van den Berg, eds.; Kluwer Academic Publishers: Banff, Canada, **1998**, pp. 207-212.
- [32] Weigl, B. H.; Bardell, R. L.; Kesler, N.; Morris, C. J. *Fresenius J Anal Chem*, **2001**, *371*, 97-105.
- [33] Brody, J. P.; Osborn, T. D.; Forster, F. K.; Yager, P. *Sensors and Actuators A: Physical*, **1996**, *54*, 704-708.
- [34] Jandik, P.; Weigl, B. H.; Kessler, N.; Cheng, J.; Morris, C. J.; Schulte, T.; Avdalovic, N. *J Chromatogr A*, **2002**, *954*, 33-40.
- [35] Cabuz, C.; Padmanabhan, A.; Fritz, B.; Cabuz, E.; Schwichtenberg, J.; Reutiman, P.; Demers, B.; Rezachek, T.; Satren, E.; Battrell, F. In *Micro Total Analysis Systems*; Yoshinobu Baba; Shuichi Shoji; Albert van den Berg, eds.; Kluwer Academic Publishers: Nara, Japan, **2002**; Vol. 2, pp. 646-648.
- [36] Kellogg, G. J.; Arnold, T. E.; Carvalho, B. L.; Duffy, D. C.; Sheppard, N. F. In *Micro Total Analysis Systems*; Albert van den Berg; W. Olthuis; Piet Bergveld, eds.; Kluwer Academic Publishers: Enschede, The Netherlands, **2000**, pp. 239-242.
- [37] Wilding, P.; Kricka, L. J.; Cheng, J.; Hvichia, G.; Shoffner, M. A.; Fortina, P. *Anal Biochem*, **1998**, *257*, 95-100.
- [38] Cheng, J.; Sheldon, E. L.; Wu, L.; Uribe, A.; Gerrue, L. O.; Carrino, J.; Heller, M. J.; O'Connell, J. P. *Nat Biotechnol*, **1998**, *16*, 541-546.
- [39] Huang, Y.; Ewalt, K. L.; Tirado, M.; Haigis, R.; Forster, A.; Ackley, D.; Heller, M. J.; O'Connell, J. P.; Krihak, M. *Anal Chem*, **2001**, *73*, 1549-1559.
- [40] Cheng, J.; Shoffner, M. A.; Hvichia, G. E.; Kricka, L. J.; Wilding, P. *Nucleic Acids Res*, **1996**, *24*, 380-385.
- [41] Pohl, H. A. *Dielectrophoresis: the behavior of neutral matter in nonuniform electric fields*, Cambridge University Press: New York **1978**.
- [42] Yang, J.; Huang, Y.; Wang, X.; Wang, X. B.; Becker, F. F.; Gascoyne, P. R. *Biophysical Journal*, **1999**, *76*, 3307-3314.
- [43] Cheng, J.; Sheldon, E. L.; Wu, L.; Heller, M. J.; O'Connell, J. P. *Anal Chem*, **1998**, *70*, 2321-2326.
- [44] Liu, R. H.; Bonanno, J.; Yang, J.; Ganser, D.; Lenigk, R.; Rhine, D.; Smekal, T.; Stevens, R.; Grodzinski, P. In *Micro Total Analysis Systems 2002*; Yoshinobu Baba; Shuichi Shoji; Albert van den Berg, eds.; Kluwer Academic Publ.: Nara, Japan, **2002**; Vol. 2, pp. 943-945.
- [45] Effenhauser, C. S.; Paulus, A.; Manz, A.; Widmer, H. M. *Anal Chem*, **1994**, *66*, 2949-2953.



- [46] Woolley, A. T.; Mathies, R. A. *Proc Natl Acad Sci U S A*, **1994**, *91*, 11348-11352.
- [47] Woolley, A. T.; Mathies, R. A. *Anal Chem*, **1995**, *67*, 3676-3680.
- [48] Paegel, B. M.; Emrich, C. A.; Wedemayer, G. J.; Scherer, J. R.; Mathies, R. A. *Proc Natl Acad Sci U S A*, **2002**, *99*, 574-579.
- [49] Emrich, C. A.; Medintz, I. L.; Tian, H.; Berti, L.; Mathies, R. A. In *Micro Total Analysis Systems 2001*; J. Michael Ramsey; Albert van den Berg, eds.; Kluwer Academic Publishers: Monterey, CA, USA, **2001**, pp. 13-15.
- [50] Simpson, P. C.; Roach, D.; Woolley, A. T.; Thorsen, T.; Johnston, R.; Sensabaugh, G. F.; Mathies, R. A. *Proc Natl Acad Sci U S A*, **1998**, *95*, 2256-2261.
- [51] Kopp, M. U.; Mello, A. J.; Manz, A. *Science*, **1998**, *280*, 1046-1048.
- [52] Khandurina, J.; McKnight, T. E.; Jacobson, S. C.; Waters, L. C.; Foote, R. S.; Ramsey, J. M. *Anal Chem*, **2000**, *72*, 2995-3000.
- [53] Lagally, E. T.; Medintz, I.; Mathies, R. A. *Anal Chem*, **2001**, *73*, 565-570.
- [54] Wooley, A. T.; Hadley, D.; Landre, P.; deMello, A. J.; Mathies, R. A.; Northrup, M. A. *Anal Chem*, **1996**, *68*, 4081-4086.
- [55] Waters, L. C.; Jacobson, S. C.; Kroutchinina, N.; Khandurina, J.; Foote, R. S.; Ramsey, J. M. *Anal Chem*, **1998**, *70*, 158-162.
- [56] Burns, M. A.; Johnson, B. N.; Brahmamandra, S. N.; Handique, K.; Webster, J. R.; Krishnan, M.; Sammarco, T. S.; Man, P. M.; Jones, D.; Heldsinger, D.; Mastrangelo, C. H.; Burke, D. T. *Science*, **1998**, *282*, 484-487.
- [57] Petersen, K. E.; McMillan, W. A.; Kovacs, G. T. A.; Northrup, M. A.; Christel, L. A.; Pourahmadi, F. *Biomedical Microdevices*, **1998**, *1*, 71-79.
- [58] Seymour, G. J.; Savage, N. W.; Walsh, L. J. *Immunology an introduction for the health sciences*, McGraw-Hill Book Company: Roseville, Australia **1995**.
- [59] Rowland-Jones, S. L.; McMichael, A. J. eds. *Lymphocytes*, Oxford University Press: New York, USA **2000**.
- [60] Bain, B. J. *Blood cells A practical guide*, Blackwell Science: Oxford **2002**.
- [61] McClatchey, K. D. ed. *Clinical laboratory medicine*, Williams & Wilkins: Baltimore, Maryland **1994**.
- [62] Adrogué, H. J.; Rashad, M. N.; Gorin, A. B.; Yacoub, J.; Madias, N. E. *N Engl J Med*, **1989**, *320*, 1312-1316.
- [63] Kaplan, L. A.; Pesce, A. J.; Kazmierczak, S. eds. *Clinical Chemistry; Theory, Analysis, Correlation*, Mosby: St. Louis, Missouri **2003**.
- [64] Davis, M. M. *Annu Rev Biochem*, **1990**, *59*, 475-496.

- [65] Barclay, A. N.; Brown, M. H.; Law, S. K. A.; McKnight, A. J.; Tomlinson, M. G.; van der Merwe, P. A. *The leucocyte antigen factsbook*, Academic Press: San Diego, USA **1997**.
- [66] Voet, D.; Voet, J. G. *Biochemistry*, John Wiley & Sons: New York **1995**.
- [67] Sharpe, P. T. *Methods of cell separation*, Elsevier Science Publishers: Amsterdam, The Netherlands **1988**.
- [68] Brauer, J. *J Chromatogr B*, **1999**, 722, 55-69.
- [69] Giddings, J. C.; Barman, B. N.; Liu, M.-K. In *Cell separation science and technology*, D. S. Kompala; P. Todd, eds.; American Chemical Society: Washington, **1991**; Vol. 464, pp. 128-144.
- [70] Giddings, J. C. *Science*, **1993**, 260, 1456-1465.
- [71] Shibusawa, Y. *J Chromatogr B*, **1999**, 722, 71-88.
- [72] Hulett, H. R.; Bonner, W. A.; Barrett, J.; Herzenberg, L. A. *Science*, **1969**, 166, 747-749.
- [73] Stewart, C. C.; Goolsby, C.; Shackney, S. E. *Hematol Oncol Clin North Am*, **2002**, 16, 477-495.
- [74] Herzenberg, L. A.; Parks, D.; Sahaf, B.; Perez, O.; Roederer, M.; Herzenberg, L. A. *Clin Chem*, **2002**, 48, 1819-1827.
- [75] Kohler, G.; Milstein, C. *Nature*, **1975**, 256, 495-497.
- [76] Rembaum, A.; Dreyer, W. J. *Science*, **1980**, 208, 364-368.
- [77] Safarik, I.; Safarikova, M. *J Chromatogr B Biomed Sci Appl*, **1999**, 722, 33-53.
- [78] Wang, J. Y.; Zhen, D. K.; Falco, V. M.; Farina, A.; Zheng, Y. L.; Delli-Bovi, L. C.; Bianchi, D. W. *Cytometry*, **2000**, 39, 224-230.
- [79] Bianchi, D. W.; Simpson, J. L.; Jackson, L. G.; Elias, S.; Holzgreve, W.; Evans, M. I.; Dukes, K. A.; Sullivan, L. M.; Klinger, K. W.; Bischoff, F. Z.; Hahn, S.; Johnson, K. L.; Lewis, D.; Wapner, R. J.; de la Cruz, F. *Prenat Diagn*, **2002**, 22, 609-615.
- [80] Georgieva, J.; Milling, A.; Orfanos, C. E.; Geilen, C. C. *Melanoma Res*, **2002**, 12, 309-317.
- [81] Engel, H.; Kleespies, C.; Friedrich, J.; Breidenbach, M.; Kallenborn, A.; Schondorf, T.; Kolhagen, H.; Mallmann, P. *Br J Cancer*, **1999**, 81, 1165-1173.
- [82] Martin, V. M.; Siewert, C.; Scharl, A.; Harms, T.; Heinze, R.; Ohl, S.; Radbruch, A.; Miltenyi, S.; Schmitz, J. *Exp Hematol*, **1998**, 26, 252-264.
- [83] Trippler, M.; Meyer zum Buschenfelde, K. H.; Gerken, G. *J Virol Methods*, **1999**, 78, 129-147.
- [84] Melville, D.; Paul, F.; Roath, S. *Nature*, **1975**, 255, 706.
- [85] Kronenberg, M.; Siu, G.; Hood, L. E.; Shastri, N. *Annu Rev Immunol*, **1986**, 4, 529-591.
- [86] Shutter, J.; Cain, J. A.; Ledbetter, S.; Rogers, M. D.; Hockett, R. D., Jr. *Mol Cell Biol*,

- 1995, 15, 7022-7031.
- [87] Moreau, E. J.; Langerak, A. W.; van Gastel-Mol, E. J.; Wolvers-Tettero, I. L.; Zhan, M.; Zhou, Q.; Koop, B. F.; van Dongen, J. J. *Leukemia*, **1999**, 13, 1620-1626.
- [88] Chhanabhai, M.; Adomat, S. A.; Gascoyne, R. D.; Horsman, D. E. *Am J Clin Pathol*, **1997**, 108, 295-301.
- [89] Kohler, S.; Jones, C. D.; Warnke, R. A.; Zehnder, J. L. *Am J Dermatopathol*, **2000**, 22, 321-327.
- [90] Saiki, R. K.; Bugawan, T. L.; Horn, G. T.; Mullis, K. B.; Erlich, H. A. *Nature*, **1986**, 324, 163-166.
- [91] Scharf, S. J.; Horn, G. T.; Erlich, H. A. *Science*, **1986**, 233, 1076-1078.
- [92] Erlich, H. A.; Gibbs, R.; Kazazian, H. H. *Polymerase chain reaction*, Cold Spring Harbor Laboratory Press: Cold Spring Harbor, N.Y. **1989**.
- [93] Hofbauer, M.; Wiesener, S.; Babbe, H.; Roers, A.; Wekerle, H.; Dornmair, K.; Hohlfeld, R.; Goebels, N. *Proc Natl Acad Sci U S A*, **2003**, 100, 4090-4095.
- [94] Ouhibi, N.; Olson, S.; Patton, P.; Wolf, D. *Curr Womens Health Rep*, **2001**, 1, 138-142.
- [95] Hahn, S.; Zhong, X. Y.; Troeger, C.; Burgemeister, R.; Gloning, K.; Holzgreve, W. *Cell Mol Life Sci*, **2000**, 57, 96-105.
- [96] Maryanski, J. L.; Attuil, V.; Bucher, P.; Walker, P. R. *Mol Immunol*, **1999**, 36, 745-753.
- [97] Kupper, M.; Loftin, U.; von Bonin, F.; Gause, A.; Pfreundschuh, M.; Daus, H.; Trumper, L. *Ann Oncol*, **1996**, 7, 35-39.
- [98] Brezinschek, H. P.; Brezinschek, R. I.; Lipsky, P. E. *J Immunol*, **1995**, 155, 190-202.
- [99] Holding, C.; Monk, M. *Lancet*, **1989**, 2, 532-535.
- [100] Kumar, R.; Barbacid, M. *Oncogene*, **1988**, 3, 647-651.
- [101] Hua, Y.; Crino, P. B. *Cereb Cortex*, **2003**, 13, 693-699.
- [102] Tanaka, Y.; Kato, S.; Tanaka, M.; Kuji, N.; Yoshimura, Y. *Biochem Biophys Res Commun*, **2003**, 304, 351-357.
- [103] Lindqvist, N.; Vidal-Sanz, M.; Hallbook, F. *Brain Res Brain Res Protoc*, **2002**, 10, 75-83.
- [104] Tommeras, K.; Bakke, I.; Sandvik, A. K.; Larsson, E.; Waldum, H. L. *Biochem Biophys Res Commun*, **2002**, 297, 335-340.
- [105] Razin, E.; Leslie, K. B.; Schrader, J. W. *J Immunol*, **1991**, 146, 981-987.
- [106] Brenner, C. A.; Tam, A. W.; Nelson, P. A.; Engleman, E. G.; Suzuki, N.; Fry, K. E.; Larrick, J. W. *Biotechniques*, **1989**, 7, 1096-1103.
- [107] Makino, S.; Cheun, H. I. *J Microbiol Methods*, **2003**, 53, 141-147.
- [108] Israel, D. A.; Salama, N.; Krishna, U.; Rieger, U. M.; Atherton, J. C.; Falkow, S.; Peek, R.

- M., Jr. *Proc Natl Acad Sci U S A*, **2001**, *98*, 14625-14630.
- [109] Steinman, C. R.; Muralidhar, B.; Nuovo, G. J.; Rumore, P. M.; Yu, D.; Mukai, M. *Anal Biochem*, **1997**, *244*, 328-339.
- [110] Toranzos, G. A.; Alvarez, A. J. *Can J Microbiol*, **1992**, *38*, 365-369.
- [111] Faumont, N.; Al Saati, T.; Brousset, P.; Offer, C.; Delsol, G.; Meggetto, F. *J Gen Virol*, **2001**, *82*, 1169-1174.
- [112] Haase, A. T.; Retzel, E. F.; Staskus, K. A. *Proc Natl Acad Sci U S A*, **1990**, *87*, 4971-4975.
- [113] Teramoto, N.; Tonoyama, Y.; Akagi, T.; Sarker, A. B.; Yoshino, T.; Yamadori, I.; Takahashi, K. *Acta Med Okayama*, **1994**, *48*, 189-193.
- [114] Singleton, P. *DNA methods in clinical microbiology*, Kluwer Academic Publishers: Dordrecht, The Netherlands **2000**.
- [115] Satsangi, J.; Jewell, D. P.; Welsh, K.; Bunce, M.; Bell, J. I. *Lancet*, **1994**, *343*, 1509-1510.
- [116] Wang, J.; Wang, T.; Sheu, J.; Lin, S.; Lin, J.; Chen, D. *J. Clin. Microbiol.*, **1992**, *30*, 750-753.
- [117] Fredricks, D. N.; Relman, D. A. *J. Clin. Microbiol.*, **1998**, *36*, 2810-2816.
- [118] Al-Soud, W. A.; Jonsson, L. J.; Radstrom, P. *J. Clin. Microbiol.*, **2000**, *38*, 345-350.
- [119] Al-Soud, W. A.; Radstrom, P. *J. Clin. Microbiol.*, **2001**, *39*, 485-493.
- [120] Akane, A.; Matsubara, K.; Nakamura, H.; Takahashi, S.; Kimura, K. *Forensic Sci.*, **1994**, *39*, 362-372.
- [121] Monteiro, L.; Bonnemaïson, D.; Vekris, A.; Petry, K.; Bonnet, J.; Vidal, R.; Cabrita, J.; Megraud, F. *J. Clin. Microbiol.*, **1997**, *35*, 995-998.
- [122] Moreira, D. *Nucl. Acids. Res.*, **1998**, *26*, 3309-3310.
- [123] Mullis, K. B.; Ferre, F.; Gibbs, R. A. eds. *The Polymerase Chain Reaction*, Birkhauser: Boston **1994**.
- [124] Stieger, M.; Demolliere, C.; Ahlborn-Laake, L.; Mous, J. *J Virol Methods*, **1991**, *34*, 149-160.
- [125] Sidhu, H.; Holmes, R. P.; Allison, M. J.; Peck, A. B. *J Clin Microbiol*, **1999**, *37*, 1503-1509.
- [126] Zhang, H.; Cooney, D. A.; Sreenath, A.; Zhan, Q.; Agbaria, R.; Stowe, E. E.; Fornace, A. J., Jr.; Johns, D. G. *Mol Pharmacol*, **1994**, *46*, 1063-1069.
- [127] Piatak, M., Jr.; Luk, K. C.; Williams, B.; Lifson, J. D. *Biotechniques*, **1993**, *14*, 70-81.
- [128] Perrin, S.; Gilliland, G. *Nucleic Acids Res*, **1990**, *18*, 7433-7438.
- [129] Schnittman, S. M.; Psallidopoulos, M. C.; Lane, H. C.; Thompson, L.; Baseler, M.; Massari, F.; Fox, C. H.; Salzman, N. P.; Fauci, A. S. *Science*, **1989**, *245*, 305-308.

- [130] Ferre, F.; Marchese, A.; Duffy, P. C.; Lewis, D. E.; Wallace, M. R.; Beecham, H. J.; Burnett, K. G.; Jensen, F. C.; Carlo, D. J. *AIDS Res Hum Retroviruses*, **1992**, *8*, 269-275.
- [131] Weinberger. *Practical capillary electrophoresis*, Academic Press: San Diego, CA, USA **1993**.
- [132] Heiger, D. *An introduction High performance capillary electrophoresis*, Agilent Technologies: Germany **2000**.
- [133] Jorgenson, J. W.; Lukacs, K. D. *Anal Chem*, **1981**, *53*, 1298-1302.
- [134] Jorgenson, J. W.; Lukacs, K. D. *Science*, **1983**, *222*, 266-272.
- [135] Jorgenson, J. W.; Lukacs, K. D. *Clin Chem*, **1981**, *27*, 1551-1553.
- [136] Landers, J. P. *Handbook of Capillary Electrophoresis*, CRC press: Boca Raton, USA **1997**.
- [137] Cohen, A. S.; Najarian, D. R.; Paulus, A.; Guttman, A.; Smith, J. A.; Karger, B. L. *Proc Natl Acad Sci U S A*, **1988**, *85*, 9660-9663.
- [138] Bode, H. J. *Anal Biochem*, **1977**, *83*, 204-210.
- [139] Bode, H. J. *Anal Biochem*, **1977**, *83*, 364-371.
- [140] Strege, M.; Lagu, A. *Anal Chem*, **1991**, *63*, 1233-1236.
- [141] Baba, Y.; Ishimaru, N.; Samata, K.; Tsuhako, M. *J Chromatogr A*, **1993**, *653*, 329-335.
- [142] Grossman, P. D.; Soane, D. S. *Biopolymers*, **1991**, *31*, 1221-1228.
- [143] Nathakarnkitkool, S.; Oefner, P. J.; Bartsch, G.; Chin, M. A.; Bonn, G. K. *Electrophoresis*, **1992**, *13*, 18-31.
- [144] Kleemiss, M. H.; Gilges, M.; Schomburg, G. *Electrophoresis*, **1993**, *14*, 515-522.
- [145] Hjerten, S.; Valtcheva, L.; Elenbring, K.; Eaker, D. *J. Liq. Chromatogr.*, **1989**, *12*, 2471-2499.
- [146] Schwartz, H. E.; Ulfelder, K.; Sunzeri, F. J.; Busch, M. P.; Brownlee, R. G. *J Chromatogr*, **1991**, *559*, 267-283.
- [147] Figeys, D.; Arriaga, E.; Renborg, A.; Dovichi, N. J. *J Chromatogr A*, **1994**, *669*, 205-216.
- [148] Heller, C. *J Chromatogr A*, **1995**, *698*, 19-31.
- [149] Carrilho, E.; Ruiz-Martinez, M. C.; Berka, J.; Smirnov, I.; Goetzinger, W.; Miller, A. W.; Brady, D.; Karger, B. L. *Anal Chem*, **1996**, *68*, 3305-3313.
- [150] Zhang, J.; Fang, Y.; Hou, J. Y.; Ren, H. J.; Jiang, R.; Roos, P.; Dovichi, N. J. *Anal Chem*, **1995**, *67*, 4589-4593.
- [151] Bocek, P.; Chrambach, A. *Electrophoresis*, **1991**, *12*, 1059-1061.
- [152] Bocek, P.; Chrambach, A. *Electrophoresis*, **1992**, *13*, 31-34.
- [153] Hjerten, S.; Srichaiyo, T.; Palm, A. *Biomed Chromatogr*, **1994**, *8*, 73-76.

## CHAPTER 2: Optimization of an Off-Chip Procedure for Amplification and Detection of Genomic DNA

### 2.1 Introduction

In this chapter we describe the optimization of a procedure for the determination and quantification of DNA extracted from T cells. T cells or Jurkat cells were used as the initial model of rare cells in blood, although more dilute sample analysis are ultimately contemplated. The method uses direct PCR amplification of a T cell receptor (TCR)  $\gamma$  gene junctional region and is to be used to determine the on-chip T cell capture efficiency of different microfluidic devices. The primers used in this study were designed and tested by Chhanabhai et al. [1]. Three different PCR procedures were tested, using either a classic or a hot-start PCR kit. The 300 bp PCR product was analyzed by capillary gel electrophoresis (CGE). The microchips are designed to capture T cells from blood samples using an immuno-magnetic capture procedure, wash and purify the cells, and then deliver them for subsequent PCR analysis.

The T cell content in human blood samples varies in healthy subjects, the ratio between T cells and all other blood cells being between 1:1500 and 1:8000 [2, 3]. The T cell content can be altered when a person is affected by diseases like multiple myeloma [4] or viruses [5]. Therefore a precise ratio between T cells and all other blood cells is hard to predict for an unknown blood sample, and measuring different cell ratios can provide useful diagnostic information.

A large number of studies have focussed on PCR analysis of the TCR genes within T cells, providing the necessary background information for our use of this analytical technique. One approach analyzed the expressed genes by isolating the RNA from T cell populations, followed by reverse transcription and PCR amplification (RT-PCR) of individual TCR genes [6-18]. A different approach used direct PCR amplification of TCR  $\gamma\delta$  gene junctional regions [19-29].

For both PCR analysis procedures gel electrophoresis was used to analyze the PCR products. To improve detectability of low-copy DNA samples by capillary gel electrophoresis, Chien and Burgi [30] employed injection of a short plug of water prior to sample introduction. The low-conductivity zone experienced high local field strength and

provided a longer path for injected sample components to migrate in the capillary, before being focussed at the water-buffer interface. A larger quantity of sample could be injected, while the resolution was not affected significantly. The water plug can be introduced either electrokinetically [30, 31] or hydrodynamically [32, 33]. This method was used in this project and successfully improved detectability of the PCR product amplified from the TCR $\gamma$  gene. An electrokinetic injection of deionized water was performed before the sample injection.

## 2.2 Experimental Section

### 2.2.1 Reagents and Media

The RPMI (Roswell Park Memorial Institute) 1640 culture media, antibiotic-antimycotic solution (10000 units/ml penicillin, 10 mg/ml streptomycin and 25  $\mu$ g/ml amphotericin B 25), L-glutamine, fetal bovine serum and hydroxy-propylmethylcellulose (HPMC, MW=86000) were obtained from Sigma-Aldrich (Oakville, ON, Canada). Dulbecco's phosphate buffered saline (PBS), PCR primers (V1, 5'-TACATCCACTGGTACCTACACCA-3', J1/2, 5'-CCCGTCTGACTACCTTGAAATGTTGTATTCTTC-3' [1]) and DNA marker ( $\Phi$ X174 RF DNA/*Hae* III fragments) were obtained from Invitrogen (Burlington, ON, Canada). The 2 M tris-(hydroxymethyl)-aminomethane (Tris) base solution, 0.5 M EDTA and boric acid for Tris-Boric acid-EDTA (TBE) running buffer and 50 $\times$  Tris-EDTA (TE) buffer, were purchased from Amersham Biosciences (Baie d'Urfé, QC, Canada). DNase/RNase-free distilled water from Invitrogen was used to prepare 0.5 $\times$  TBE (45 mM Tris-base, 45 mM boric acid, 1mM EDTA) running buffer for capillary gel electrophoresis (CGE) and 1 $\times$  TE (10 mM Tris-HCl, 1mM EDTA) buffer to dissolve the primers. Siliconized Eppendorf tubes (DNase/RNase-free), 0.2 mL PCR tubes and aerosol barrier filter tips (sterile, DNase/RNase-free) used were purchased from Rose Scientific (Edmonton, AB, Canada). Anti-human CD3 (clone HIT3a) was obtained from BD PharMingen Canada (Mississauga, ON), Protein A paramagnetic particles (1-2  $\mu$ m) from Polysciences (Warrington, PA, USA). The Dynabeads<sup>®</sup> DNA DIRECT<sup>™</sup> kit was purchased from Dynal Biotech (Lake Success, NY, USA), the GeneAmp<sup>®</sup> PCR Core Reagents (PCR kit I) from Applied Biosystems (Foster City, CA, USA) and Platinum<sup>®</sup> PCR SuperMix (PCR

kit II) from Invitrogen (Burlington, ON, Canada). Ethidium bromide homodimer, used to stain DNA, was obtained from Molecular Probes (Eugene, OR, USA) and Trypan Blue 0.4 % solution used to determine cell viability was purchased from Sigma-Aldrich.

### **2.2.2 Cell Samples**

Heparinized human blood samples (1 mL) were obtained from patients (anonymous) from the Cross Cancer Institute (Edmonton, Canada). Human blood samples were used on the day obtained, remaining portions were neutralized in a 0.6% bleach solution (5000 ppm free chlorine).

Jurkat cells (ATCC No. TIB-152, clone E6-1, T cell leukemia, human) were purchased from the American Type Culture Collection (ATCC) and maintained in RPMI 1640 supplemented with 10% fetal bovine serum, 1% L-glutamine 200 mM and 2% antibiotic antimycotic solution, stabilized in a humidified atmosphere with 8% CO<sub>2</sub> at 37°C provided by a NuAire US Autoflow (NU-4750) Automatic CO<sub>2</sub> water-jacketed incubator (Plymouth, MN, USA). Cells were counted with a hemacytometer (Sigma-Aldrich, Oakville, ON, Canada). Cell viability was determined by a dye exclusion test with Trypan Blue 0.4% solution. Cultures were maintained between  $1.0 \times 10^5$  and  $1.4 \times 10^6$  cells/mL, with 91% - 94% viable cells. As required for some determinations, serial dilutions in supplemented RPMI 1640 were performed. The SD and RSD values for cell concentration and number of cells used in different experiments were calculated assuming a  $\pm 0.1 \mu\text{L}$  error for every pipetting performed while diluting and sampling.

### **2.2.3 Operation Procedure**

#### **2.2.3.1 Loading Protein A Paramagnetic Beads with Anti-CD3**

Anti-human CD3 (BD PharMingen Canada, Mississauga, ON) was loaded onto 1-2  $\mu\text{m}$  diam paramagnetic beads by mixing 10  $\mu\text{L}$  of Protein A paramagnetic particle suspension (containing 133  $\mu\text{g}$  solids covered with 1  $\mu\text{g}$  Protein A) with 400  $\mu\text{L}$  of 20  $\mu\text{g}/\text{mL}$  anti-human CD3 in an Eppendorf tube for 10 min. Particles were pelleted with a magnetic particle concentrator MPC<sup>®</sup>-E-1 (Dynal Biotech), which contained a neodymium-iron-boron permanent disc magnet. After washing three times with 100  $\mu\text{L}$  PBS to remove the unbound anti-CD3, particles were resuspended in 10  $\mu\text{L}$  PBS.



## **2.2.3.2 PCR Amplification of DNA Isolated from Blood and Jurkat Cell Samples**

### **2.2.3.2.1 Method A**

Samples analyzed with method A were withdrawn from Jurkat cell suspensions and an undiluted human blood sample. Details about sample processing are provided in sections 2.2.3.2.1a and 2.2.3.2.1b. PCR amplifications were performed with PCR kit I for 35 cycles, using a constant annealing temperature of 55 °C. Each cycle consisted of denaturing at 94 °C for 1 min (5 min denaturing for the first cycle), annealing at 55 °C for 1 min and extension at 72 °C for 1 min (9 min for the last cycle).

#### **2.2.3.2.1a Method A Used for Jurkat Cell Samples**

Jurkat cell dilutions were prepared from a stock suspension with  $1.10 \times 10^6$  cells/mL (RSD=5.1%). Serially diluted suspensions contained  $2.20 \times 10^5$  cells/mL (RSD=5.1%),  $1.10 \times 10^5$  cells/mL (RSD=5.2%),  $2.20 \times 10^4$  cells/mL (RSD=5.1%),  $1.10 \times 10^4$  cells/mL (RSD=5.3%),  $2.20 \times 10^3$  cells/mL (RSD=5.2%) and  $1.10 \times 10^3$  cells/mL (RSD=5.4%). 10  $\mu$ L samples were withdrawn from every suspension. The samples contained respectively,  $11000 \pm 560$  (RSD= 5.1%),  $2200 \pm 110$  (RSD= 5.2%),  $1100 \pm 58$  (RSD= 5.3%),  $220 \pm 12$  (RSD= 5.3%),  $110 \pm 6$  (RSD= 5.4%),  $22 \pm 1$  (RSD= 5.4%) and  $11 \pm 1$  (RSD= 5.5%) Jurkat cells. DNA from undiluted blood samples (0.5  $\mu$ L to 4  $\mu$ L) and Jurkat cell suspensions (0.5  $\mu$ L to 10  $\mu$ L) was isolated using Dynabeads® DNA DIRECT™. Samples (0.5  $\mu$ L to 10  $\mu$ L) were mixed with 200  $\mu$ L of Dynabeads (superparamagnetic, monodisperse polymer particles) suspended in a lysing buffer, in 1.5 mL siliconized Eppendorf tubes. DNA released from the lysed cells was adsorbed on the surface of Dynabeads during a 5 min incubation. The supernatant, with residual contaminants and potential PCR inhibitors, was removed from the DNA/Dynabeads complex after 2 min in the magnetic particle concentrator. Three additional washings of the DNA/Dynabeads complex were performed, each one with 200  $\mu$ L of washing buffer provided by DYNAL. The complex was finally placed in 20  $\mu$ L resuspension buffer and processed with PCR kit I (Applied Biosystems, GeneAmp® PCR Core Reagents). PCR amplification was performed simultaneously for all samples in the presence of the Dynabeads. Each 20  $\mu$ L aliquot of DNA template (DNA/Dynabeads complex containing different amounts of DNA) was transferred using a micropipet into 0.2 mL PCR tubes, previously filled with

30  $\mu\text{L}$  of PCR mixture. The PCR mixture was prepared 10-30 min before performing the PCR, from the solutions provided with the PCR kit I (Applied Biosystems, GeneAmp<sup>®</sup> PCR Core Reagents), primer solutions (10 pmol/ $\mu\text{L}$  of V1 and J1/2) and DNase/RNase-free distilled water. Every 30  $\mu\text{L}$  of PCR mixture contained 2U AmpliTaq DNA polymerase, 10 pmol V1 primer, 10 pmol J1/2, 10 nmol dATP, 10 nmol dTTP, 10 nmol dCTP, 10 nmol dGTP, 75 nmol  $\text{MgCl}_2$ , 0.500  $\mu\text{mol}$  Tris-HCl and 2.500  $\mu\text{mol}$  KCl. The final concentrations in the 50  $\mu\text{L}$  PCR template were 2U AmpliTaq DNA polymerase, 0.20  $\mu\text{M}$  V1 primer, 0.20  $\mu\text{M}$  J1/2 primer, 0.20 mM dATP, 0.20 mM dTTP, 0.20 mM dCTP, 0.20 mM dGTP, 1.5 mM  $\text{MgCl}_2$ , 10 mM Tris-HCl and 50 mM KCl. The V-J junction of the T cell receptor (TCR)  $\gamma$  gene was amplified by PCR, using a Progene Techne thermal cycler (Mandel Scientific Company Ltd., Guelph, ON, Canada). A 300 bp product was obtained by following a published procedure, presented as method A [1] in the section above.

#### **2.2.3.2.1b Method A Used for a Human Blood Sample**

Samples withdrawn from the blood sample consisted of  $0.50 \pm 0.05$   $\mu\text{L}$  (RSD = 10%),  $1.00 \pm 0.05$   $\mu\text{L}$  (RSD = 5%),  $2.00 \pm 0.05$   $\mu\text{L}$  (RSD = 2.5%) and  $4.0 \pm 0.1$   $\mu\text{L}$  (RSD = 2.5%). The same procedure as described above for Jurkat cells (section 2.2.3.2.1a) was followed to lyse the cells, extract and purify the DNA. PCR amplification was performed simultaneously for all samples in the presence of Dynabeads. The DNA/Dynabeads complex placed in 20  $\mu\text{L}$  resuspension buffer was processed with PCR kit I (Applied Biosystems, GeneAmp<sup>®</sup> PCR Core Reagents) following the same steps as presented above for Jurkat cells (section 2.2.3.2.1a).

#### **2.2.3.2.2 Method B**

Samples analyzed with method B were withdrawn from an undiluted human blood sample and Jurkat cell suspensions. Details about sample processing are provided in sections 2.2.3.2.2a, 2.2.3.2.2b and 2.2.3.2.2c. A 300 bp product was obtained by following a published procedure presented here as method B [34]. PCR amplifications were performed with PCR kit I for 36 cycles, using annealing temperatures between 45°C and 65 °C as described below and presented in Figure 2.1. The first cycle consisted of

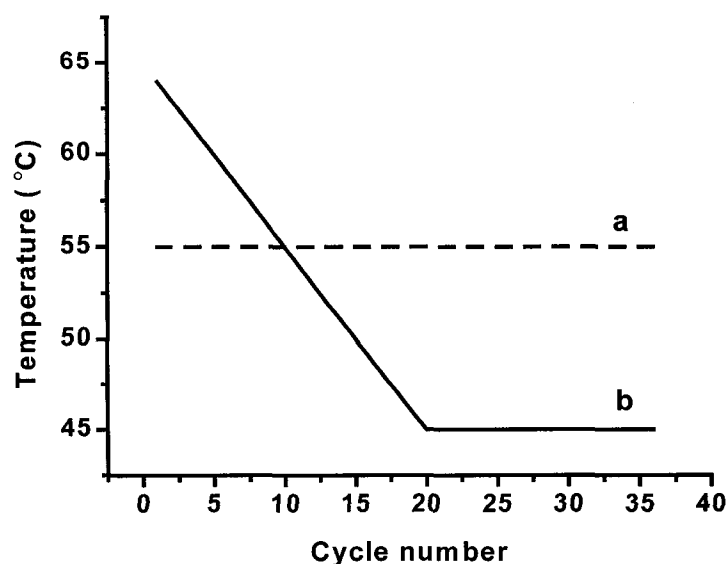


**Figure 2.1:** Annealing temperature program used in PCR for:  
 a. Methods A and C;  
 b. Method B.

denaturing at 95 °C for 10 min, annealing at 65 °C for 30 s and extension at 72 °C for 30s. The next 19 cycles consisted of denaturing at 95 °C for 40 s, annealing at 64 °C for 30 s with a decrease of 1 °C per cycle (45 °C for the 20<sup>th</sup> cycle) and extension at 72 °C for 30 s. The next 14 cycles consisted of denaturing at 95 °C for 40 s, annealing at 45 °C for 30 s and extension at 72 °C for 30 s. The last cycle consisted of denaturing at 95 °C for 40 s, annealing at 45 °C for 30 s and extension at 72 °C for 5 min. The Dynabeads were present during the PCR amplification performed on Jurkat samples described in section 2.2.3.2.2a, but not on the other samples described in sections 2.2.3.2.2b and 2.2.3.2.2c.

#### 2.2.3.2.2a Method B Used for Jurkat Cell Samples

A stock suspension of Jurkat cell containing  $1.40 \times 10^6$  cells/mL (RSD=8.6%) was used to prepare serially diluted suspensions with  $1.40 \times 10^5$  cells/mL (RSD=8.6%),  $1.40 \times 10^4$  cells/mL (RSD=8.7%),  $1.40 \times 10^3$  cells/mL (RSD=8.7%) and  $1.40 \times 10^2$  cells/mL (RSD=8.8%). 10  $\mu$ L samples were withdrawn from every suspension. The samples contained respectively,  $1400 \pm 120$  (RSD= 8.7%),  $140 \pm 12$  (RSD= 8.7%),  $14 \pm 1$  (RSD= 8.8%) and 1 (RSD=8.9%) Jurkat cells. The errors were calculated assuming a perfectly uniform concentration of cells in every suspension at the time of preparing dilutions and

sampling. PCR amplification was performed simultaneously for all samples in the presence of Dynabeads, as described in section 2.2.3.2.1a.

#### **2.2.3.2.2b Method B Used for Jurkat Cell Samples Processed in the Presence of Protein A/Anti-human CD3 Paramagnetic Beads**

Two 2  $\mu\text{L}$  samples containing  $1960 \pm 110$  Jurkat cells (RSD = 5.7%) were withdrawn from a stock suspension with  $1.00 \times 10^6$  cells/mL (RSD=5.1%). The two samples were treated in parallel in separate Eppendorf tubes, to which a 2  $\mu\text{L}$  suspension of Protein A/anti-human CD3 paramagnetic beads, 50  $\mu\text{L}$  of RPMI 1640 and 200  $\mu\text{L}$  of Dynabeads suspension were added. For one sample, DNA was released from the beads by incubating the suspension for 5 min at 65  $^{\circ}\text{C}$ , the beads were then quickly captured in the magnetic particle concentrator and the supernatant (20  $\mu\text{L}$ ) was transferred to a PCR tube. In the other sample the beads were not magnetically separated. PCR amplification was performed simultaneously for both samples, as described in section 2.2.3.2.1a.

#### **2.2.3.2.2c Method B Used for a Human Blood Sample**

Samples withdrawn from the blood sample consisted of  $0.50 \pm 0.05$   $\mu\text{L}$  (RSD = 10%),  $1.00 \pm 0.05$   $\mu\text{L}$  (RSD = 5%),  $2.00 \pm 0.05$   $\mu\text{L}$  (RSD = 2.5%) and  $4.0 \pm 0.1$   $\mu\text{L}$  (RSD = 2.5%). DNA was extracted using Dynabeads and PCR amplification was performed simultaneously for all samples. Samples were prepared following the same steps as presented above for Jurkat cells analyzed with method A (section 2.2.3.2.1a), but PCR amplification was performed after removing the Dynabeads from the mixture as described in the previous section (2.2.3.2.2b).

#### **2.2.3.2.3 Method C**

Method C differed from the previous two methods in using a hot-start PCR amplification. The Platinum<sup>®</sup> PCR SuperMix kit (Invitrogen) offered the advantage of an automatic hot start. Because of the specific binding with Platinum<sup>®</sup> *Taq* antibody, the recombinant *Taq* DNA polymerase was present in an inactive form and was reactivated at 94 $^{\circ}\text{C}$ , during the first denaturing step of the PCR amplification. Since all the PCR components were premixed, handling was simplified.

Samples analyzed with method C were withdrawn from Jurkat cell suspensions.

Details about sample processing are provided in section 2.2.3.2.3a. Dynabeads used for DNA capture were removed after releasing the DNA in the supernatant, as described in sections 2.2.3.2.2b and 2.2.3.2.2c for some samples processed with method B. Aliquots of 10  $\mu\text{L}$ , representing 50% of the volume of liquid containing the released DNA, were transferred with a micropipet to a 0.2 mL PCR tube. Every PCR tube was previously filled with 47  $\mu\text{L}$  PCR mixture obtained by adding 1  $\mu\text{L}$  of each primer solution (10 pmol/ $\mu\text{L}$ ) to 45  $\mu\text{L}$  of Platinum<sup>®</sup> PCR SuperMix. The final concentrations in the 57  $\mu\text{L}$  PCR template were 1U complexed recombinant *Taq* DNA polymerase with Platinum<sup>®</sup> *Taq* antibody, 0.18  $\mu\text{M}$  V1 primer, 0.18  $\mu\text{M}$  J1/2 primer, 0.17 mM dATP, 0.17 mM dTTP, 0.17 mM dCTP, 0.17 mM dGTP, 1.3 mM  $\text{MgCl}_2$ , 17 mM Tris-HCl and 43 mM KCl. Negative controls were amplified simultaneously with every experiment. Method C was obtained by modifying the previous two methods, following the specifications provided by Invitrogen for its automatic hot start kit (Platinum<sup>®</sup> PCR SuperMix). The temperature achieved in the thermal cycler was verified with an external thermocouple system. The temperature was measured inside of a PCR tube filled with 50  $\mu\text{L}$  of distilled water and placed in the thermal cycler. The times used in the program were corrected to maintain the temperatures for the optimal times recommended by Invitrogen. PCR amplifications were performed with PCR kit II for 36 cycles, using a constant annealing temperature of 55  $^{\circ}\text{C}$ . The first cycle consisted of denaturing at 94  $^{\circ}\text{C}$  for 5 min followed by annealing at 55  $^{\circ}\text{C}$  for 30 s and extension at 72  $^{\circ}\text{C}$  for 30 s. The next 35 cycles consisted of denaturing at 94  $^{\circ}\text{C}$  for 55 s followed by annealing at 55  $^{\circ}\text{C}$  for 50 s and extension at 72  $^{\circ}\text{C}$  for 40 s (5 min for the last cycle).

#### **2.2.3.2.3a Method C Used for Jurkat Cell Samples**

Samples analyzed with method C were withdrawn from a stock suspension of Jurkat cells with  $4.40 \times 10^5$  cells/mL (RSD=8.9%) and a 1:10 dilution (with RPMI) with  $4.40 \times 10^4$  cells/mL (RSD=8.9%). Aliquots of 2.5 and 1.5  $\mu\text{L}$  were withdrawn from the stock suspension and 7.5, 5.0 and 2.5  $\mu\text{L}$  from the diluted suspension. The samples contained respectively,  $1100 \pm 107$  (RSD= 9.7%),  $660 \pm 73$  (RSD= 11.1%),  $330 \pm 30$  (RSD= 9.0%),  $220 \pm 20$  (RSD= 9.1%) and  $110 \pm 11$  (RSD= 9.7%) Jurkat cells. DNA was extracted using Dynabeads. For samples processed with method C, the DNA was isolated

as described for method A (section 2.2.3.2.1a), then the DNA was released from Dynabeads by incubating the suspension for 5 min at 65 °C. As described in section 2.2.3.2.2b, the beads were quickly captured in the magnetic particle concentrator but only 10  $\mu$ L of supernatant, representing 50% of the volume available, was transferred to a PCR tube. PCR amplification was performed simultaneously for all samples.

### **2.2.3.3 Capillary Gel Electrophoresis of the PCR Product**

The 300 bp PCR product was analyzed by capillary gel electrophoresis (CGE), using a Beckman P/ACE 5010 equipped with a 488 nm laser module LIF detector, 580DF40 filter (Omega Optical, Brattleboro, VT, USA) and 488 nm notch filter. A 0.5 $\times$  TBE running buffer, containing 0.4% HPMC and 0.5  $\mu$ g/mL ethidium bromide was used to fill a 27 cm long, 50  $\mu$ m i.d. fused silica capillary and the vials used as inlet and outlet buffer reservoirs. To minimize run-to-run contamination, different vials were used for running the separation and for filling the capillary with gel. For samples analyzed with methods B and C, a 1 s hydrodynamic injection (0.5 psi; 1 psi = 6894.76 Pa) of pure water was performed prior to injecting the samples. This two-step injection procedure was reported to increase the precision of peak height simultaneously with sample loading due to enhancement of the local field strength [30-33]. The samples were injected at 5 kV for 5 s. To separate the PCR product, the Beckman P/ACE 5010 system was operated at 5 kV (185 V/cm) for samples analyzed with method A and at 10 kV (370 V/cm) for samples analyzed with methods B and C. The electropherograms were subsequently analyzed with the software provided by Beckman with the P/ACE 5010 capillary electrophoresis system.

## **2.3. Results and Discussion**

Three types of PCR amplification procedures were developed in an effort to optimize sensitivity. The first method (A) used a PCR kit from Applied Biosystems and employed a constant annealing temperature for 35 cycles of amplification. The 300 bp PCR product obtained was analyzed by CGE using an electric field of 185 V/cm. A better optimized method (B) used the same PCR kit as method A, but employed a ramped annealing temperature profile for 36 cycles of amplification, as shown in Figure 2.1. The

PCR product obtained was analyzed by CGE using an electric field of 370 V/cm. Method C was introduced after encountering significant problems with Method B (failure to amplify from 1000-4000 Jurkat cells). To quickly solve the problem the whole PCR kit was replaced. As later identified, the PCR failure was caused by a defective thermal cycler which did not achieve the programmed denaturing temperature, and also by using old primer solutions (more than the 6 month period recommended by the provider). Method C used an automatic hot start PCR kit from Invitrogen and used a constant annealing temperatures for 36 cycles of amplification. For the capillary gel electrophoresis procedure, a two-step injection procedure (pure water and sample), reported to enhance the sample loading capacity [30-33] was also used for methods B and C.

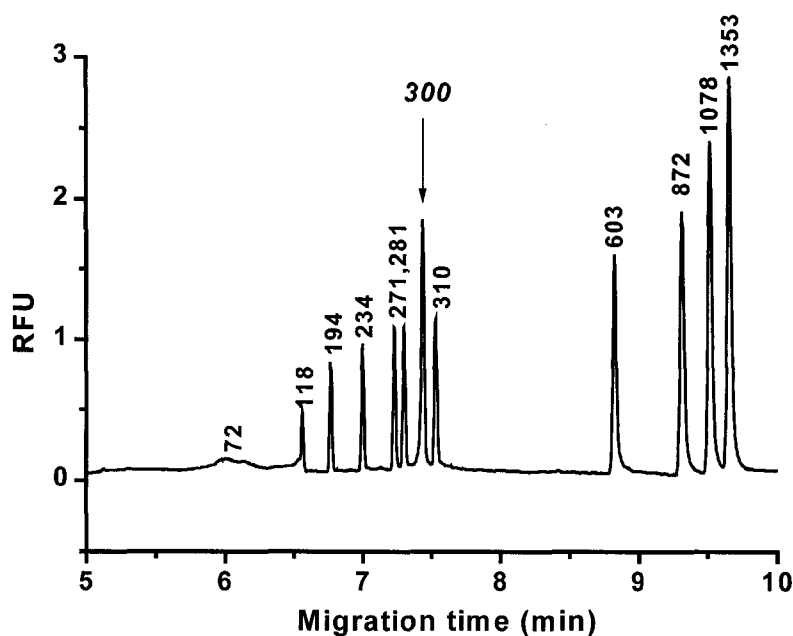


**Figure 2.2:** Electropherogram of the 300 bp PCR product obtained following method A for PCR amplification. DNA was extracted from 2200 Jurkat cells. The analyzed mixture consisted of 10  $\mu\text{L}$  of solution containing the PCR product and 5  $\mu\text{L}$  of 25  $\text{ng}/\mu\text{L}$  DNA ladder ( $\Phi\text{X174}$  RF DNA/Hae III fragments). Separation was performed at 185 V/cm.

### 2.3.1 PCR Analysis Following Method A

#### 2.3.1.1 PCR Performed on Samples Containing Jurkat Cells

Method A was tested by extracting the DNA from 2200 Jurkat cells, as described in section 2.2.3.2.1a. DNA was captured on Dynabeads, then a T cell receptor  $\gamma$  gene was amplified by PCR for 35 cycles and the product was analyzed by CGE using an electric field of 185 V/cm. Dynabeads were present during the amplification. The

electropherogram in Figure 2.2 presents the 300 bp peak obtained by injecting about 50 nL from 10  $\mu$ L of PCR product, mixed with 5  $\mu$ L of 25 ng/ $\mu$ L  $\Phi$ X174 RF DNA/*Hae* III fragments. As seen in Figure 2.3, the 300 bp DNA fragment was successfully amplified and identified when starting from 1100 Jurkat cells, but not from 220 cells or less.

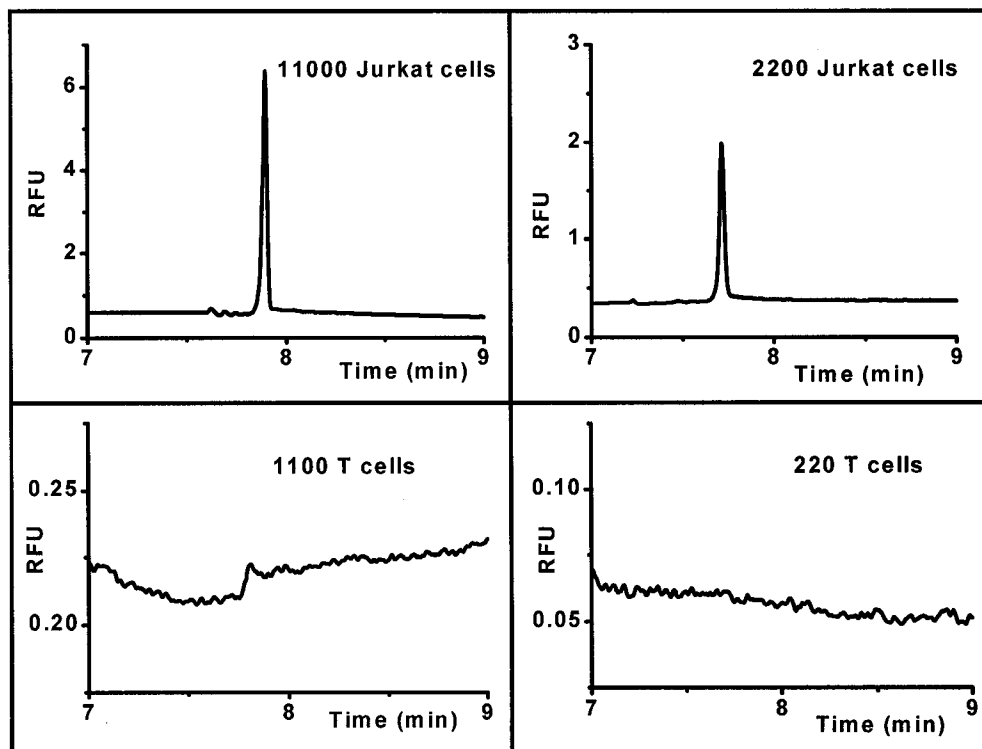


**Figure 2.3:** Electropherograms of the 300 bp PCR product obtained using method A for PCR amplification. DNA was extracted from samples containing the indicated numbers of Jurkat cells. Separation was performed at 185 V/cm.

### 2.3.1.2 PCR Performed on Human Blood Samples

DNA was isolated from a blood sample without separating the T cells. A T cell receptor  $\gamma$  gene was amplified by PCR for 35 cycles and the product was analyzed by CGE using an electric field of 185 V/cm. Dynabeads were present during the PCR amplification performed following method A. Figure 2.4a shows characterization of the PCR assay, using 0.5, 1.0, 2.0 and 4.0  $\mu$ L aliquots of human blood withdrawn from the same blood sample. Figure 2.4b presents a correlation graph of peak height of the 300 bp DNA fragment versus the volume of blood used, on a log-log scale. The average peak heights were determined from 3 to 4 electropherograms and gave RSD values between 5% and 12%.



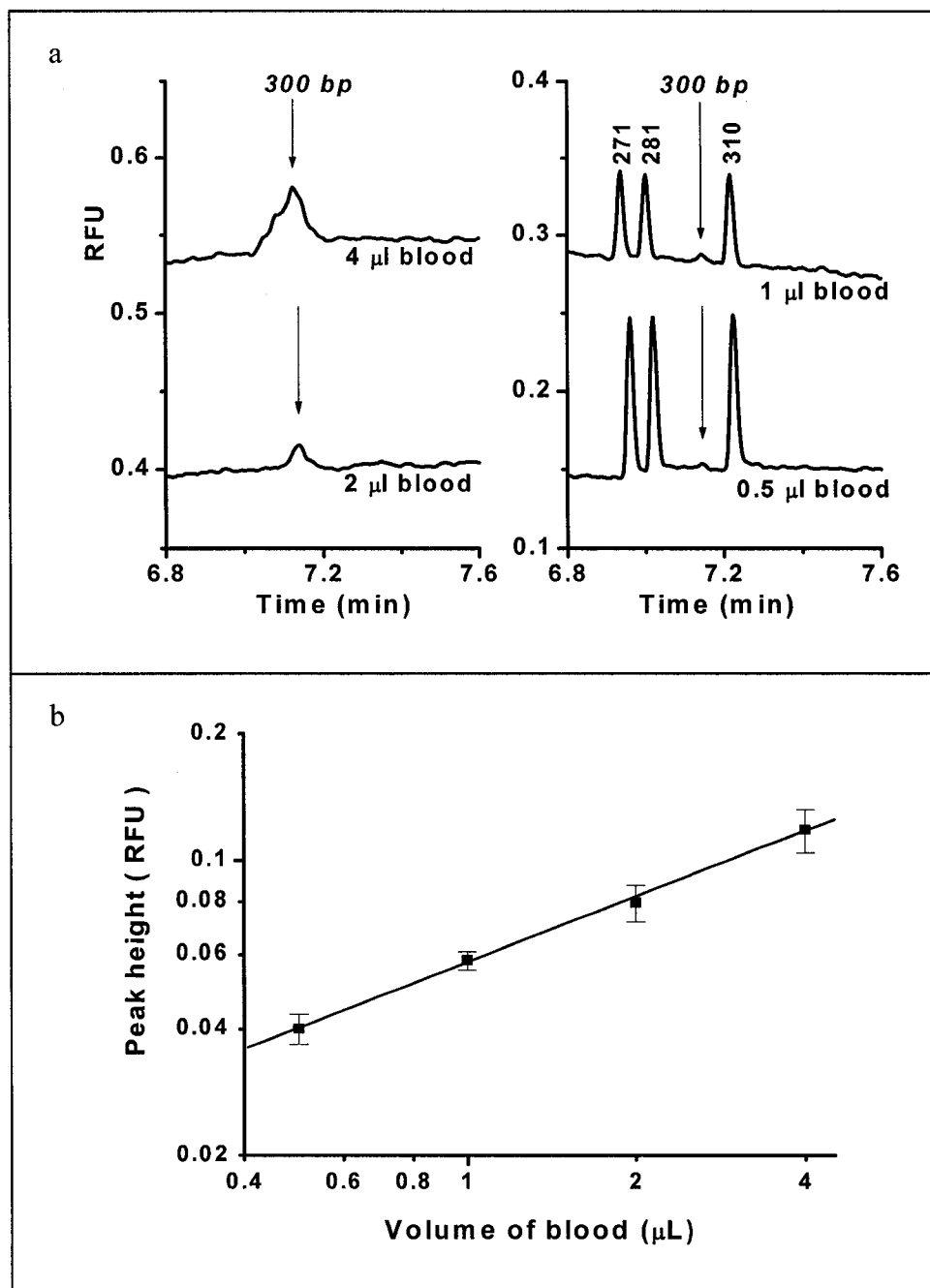


**Figure 2.4:** Characterization of the PCR amplification with method A using DNA extracted from 0.5, 1, 2 and 4  $\mu\text{L}$  of blood. Separation was performed at 185 V/cm.

- a. Electropherograms of the 300 bp product generated, with a  $\Phi\text{X174}$  RF DNA/Hae III fragments DNA ladder present in some of the samples;
- b. Peak height of the 300 bp product versus the volume of blood presented on a log-log scale.

Plotting the peak height versus the number of cells used might be more informative, but was less convenient because the number of T cells was not precisely known. A healthy patient would have an average of  $1.7 \times 10^3$  cells/ $\mu\text{L}$ . The T cell content could be altered in unhealthy subjects, but we had no information about our blood donors' health. Assuming an average T cell content of  $1.7 \times 10^3$  T cells/ $\mu\text{L}$ , the signal obtained from 0.5  $\mu\text{L}$  of blood corresponds to about 850 T cells.

Knowing the 300 bp peak height obtained using method A for PCR analysis, an unknown volume of a blood sample (limits between 0.4 and 5  $\mu\text{L}$ ) could be determined using a plot such as shown in Figure 2.4b as a calibration curve. (Of course, the actual T cell concentration in the blood standard would need to be determined independently, using a method such as flow cytometry) This procedure can allow us to determine the cell capture efficiency of a microfluidic device, by simultaneously performing PCR analysis on cells captured from a sample on a chip, and cells in different aliquot volumes of the same sample that are not subjected to the chip capture step. Efficiencies between 25% and 100% could be determined using a 2  $\mu\text{L}$  sample and a set of standards with volumes between 0.5 and 4  $\mu\text{L}$ .

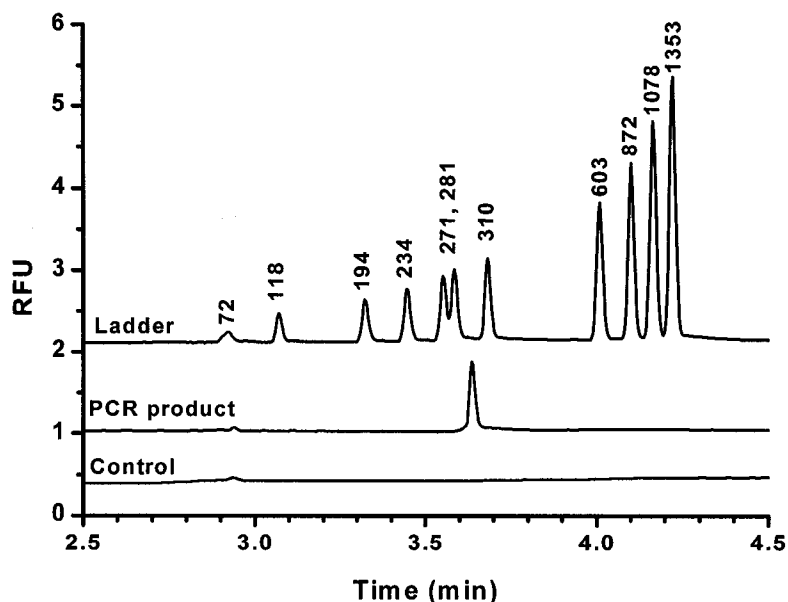


**Figure 2.5:** Electropherogram of the 300 bp PCR product obtained following method B for PCR amplification. DNA was extracted from 1400 Jurkat cells. The electropherograms obtained from an amplified negative control sample and a 25 ng/ $\mu\text{L}$  DNA ladder ( $\Phi\text{X174}$  RF DNA/Hae III fragments) are included. Separation was performed at 370 V/cm.

## 2.3.2 PCR Analysis Following Method B

### 2.3.2.1 PCR Performed on Samples Containing Jurkat Cells

Method B used the same PCR kit as method A (PCR kit I), but employed an annealing temperature ramp for the 36 cycles of amplification, in contrast to method A (Figure 2.1). Method B was tested by extracting the DNA from 1, 14, 140 and 1400 Jurkat cells.

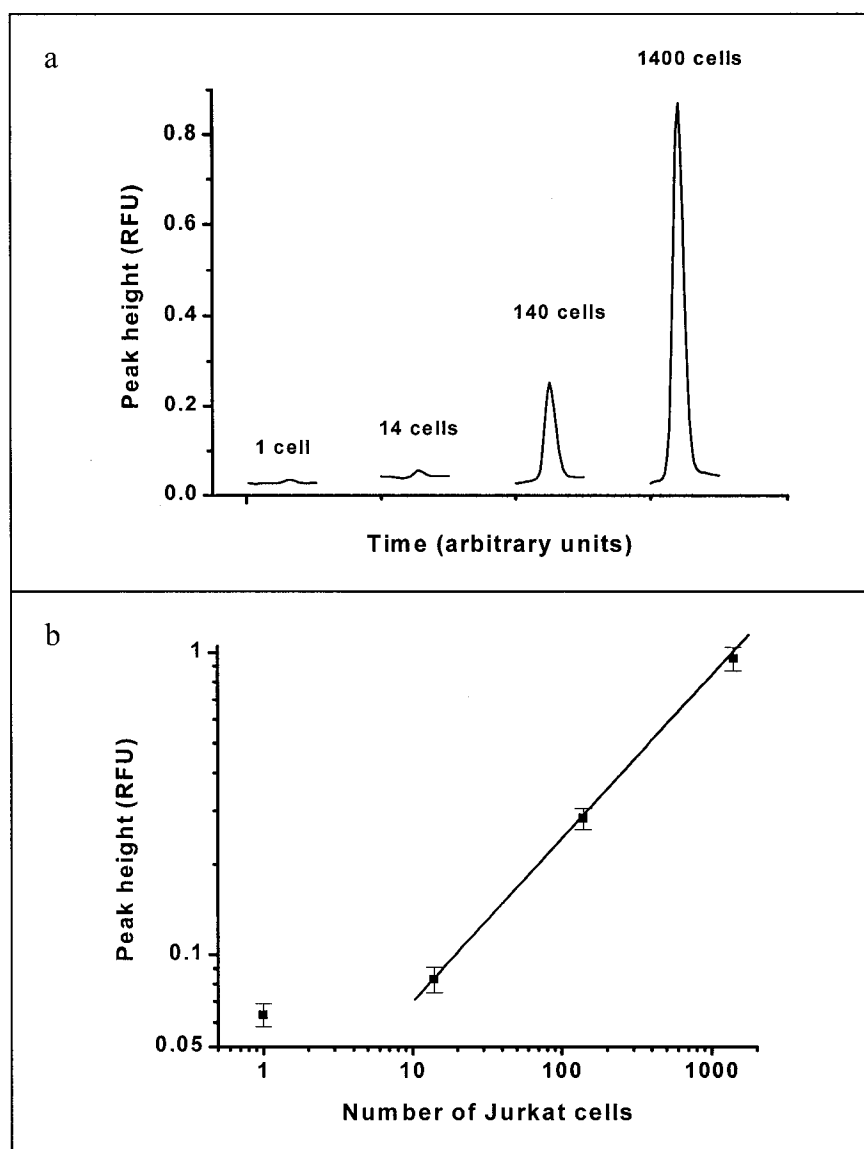


**Figure 2.6:** Characterization of PCR amplification with method B using DNA extracted from Jurkat cells. Separation was performed at 370 V/cm.

- The 300 bp peak obtained by PCR amplification of DNA extracted from 1, 14, 140 and 1400 Jurkat cells;
- Peak height of the 300 bp product versus the number of cells used, presented on a log-log scale. Linearity was observed when the product was obtained from 14 to 1400 cells. Error bars are the average % RSD for CGE measurements of 8 %.

DNA was captured on Dynabeads, a T-cell receptor  $\gamma$  gene was amplified by PCR for 36 cycles and the product was analyzed by CGE using an electric field of 370 V/cm. The electropherogram in Figure 2.5 shows the 300 bp peak obtained after processing the DNA from 1400 Jurkat cells. A DNA ladder was injected from a solution containing 25 ng/ $\mu$ L  $\Phi$ X174 RF DNA/*Hae* III fragments. As presented in Figure 2.6a, the 300 bp fragment was successfully amplified and identified even when PCR amplification was performed using a single Jurkat cell. Detection of peaks obtained from such a low number of cells can be explained by the high stringency conditions for PCR annealing steps provided by method B and the increased sample loading obtained in CGE separation with the two-step injection procedure. Figure 2.6b presents a correlation graph of peak height of the 300 bp DNA fragment versus the number of cells used on a log-log scale. As expected for a non-linear amplification technique, linearity between the peak height and the number of cells used was observed on a limited range of the log-log plot.

Knowing the value of peak height obtained following the experimental conditions of method B, the number of cells from an unknown sample (containing between 10 and 1500 cells) can be determined based on the plot from Figure 2.6b. This procedure can allow us to determine the cell capture efficiency performed on a microfluidic device. A set of samples with known, differing numbers of Jurkat cells (standards) is analyzed by PCR without using the chip capture step, along with samples that are subjected to the on-chip capture step. Efficiencies between 1% and 100% could be determined using a sample containing 1000 cells and a set of standards containing between 10 and 1000 cells.

### **2.3.2.2 PCR Performed on Jurkat Cell Samples in the Presence of Protein A/Anti-Human CD3 Paramagnetic Beads**

For the planned on-chip experiments, Protein A/anti-human CD3 coated paramagnetic beads were to be used to capture T cells from the samples. For the process of DNA capture and purification, the Protein A/anti-human CD3 beads would not be readily separated from the DNA capturing beads, due to their common paramagnetic properties. Thus, it was important to determine how the Protein A/anti-human CD3 paramagnetic beads would affect the PCR amplification.

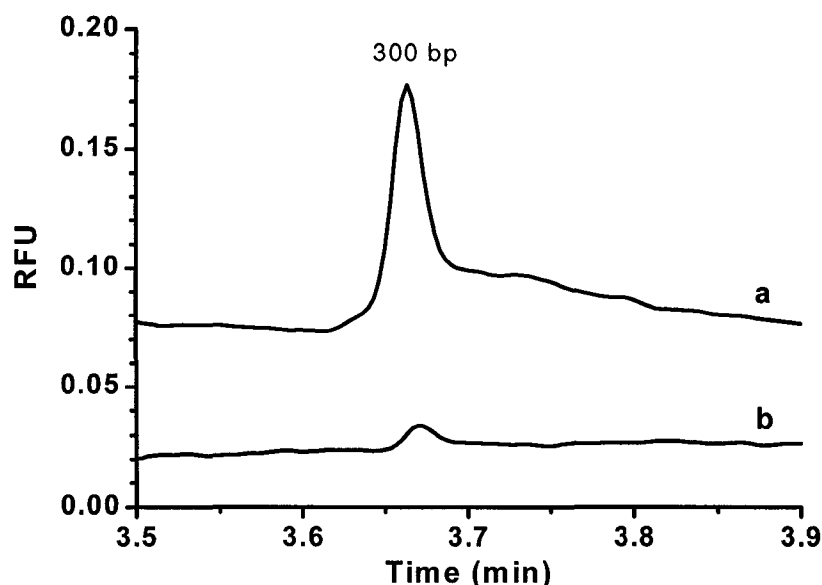


**Figure 2.7:** Characterization of the PCR amplification performed with method B in the presence and absence of paramagnetic beads. DNA was extracted from 1960 Jurkat cells for all samples. Protein A/anti-human CD3 magnetic beads and Dynabeads were (a) removed or (b) present during the PCR amplification. Separation was performed at 370 V/cm. Curve (b) is offset from curve (a) for clarity.

DNA was extracted from two different samples containing  $1960 \pm 110$  (RSD = 5.7%) Jurkat cells. As presented in Figure 2.7, a 3.5 times higher peak was obtained when the magnetic beads (Protein A and Dynabeads) were removed, indicating clearly their negative effect on amplification. The average peak heights were determined from 11 electropherograms and gave RSD values of 7.7% (with beads) and 9.2% (without beads). Since we were able to obtain a similar peak height in the presence of Dynabeads to that seen with all beads removed, the only beads producing inhibition appear to be the Protein A/anti-human CD3 coated paramagnetic beads. This experiment did not identify what produced inhibition, but it is clear that the highest signal would be obtained with the Protein A/anti-human CD3 beads removed.

### 2.3.2.3 PCR Performed on Human Blood Samples

Method B was tested using 0.5, 1.0, 2.0 and 4.0  $\mu\text{L}$  aliquots of human blood withdrawn from the same blood sample. DNA from all blood cells was captured on Dynabeads and the beads were removed before performing the PCR amplification. A T cell receptor  $\gamma$  gene was amplified by PCR (36 cycles) from the DNA eluted from

Dynabeads and the product was analyzed by CGE using an electric field of 370 V/cm. Figure 2.8 shows a correlation graph of peak height of the 300 bp DNA fragment versus the volume of blood used, on a log-log scale. To show the peak height enhancement obtained using this method, the results are plotted simultaneously with the data obtained using method A.

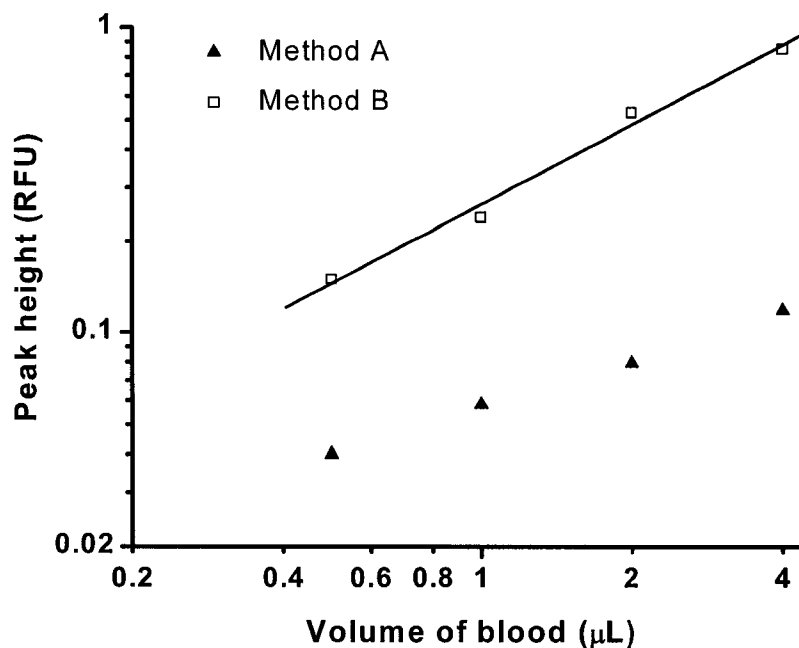


**Figure 2.8:** Characterization of the PCR amplification with method B using DNA extracted from 0.5, 1, 2 and 4  $\mu\text{L}$  of blood. A significant signal enhancement was observed in peak heights values compared to the corresponding values obtained with method A.

The peak heights obtained with method B were between 3.8 times higher for 0.5  $\mu\text{L}$  and 7.2 times higher for 4  $\mu\text{L}$  of blood, compared with the peak heights obtained following method A. The enhancement was obtained after adding an additional cycle to the PCR amplification and using an annealing temperature ramp for the first 20 cycles of amplification. Using an annealing temperature higher than 55  $^{\circ}\text{C}$  for the first 9 cycles (value used for method A) definitely minimized the effect of mismatching. Under such high stringency conditions for the first stages of amplification, partial hybridization at low levels of complementarity between primers and target was minimized and the 300 bp product was produced with a higher yield. The water plug introduced prior to sample injection allowed an increase in sample loading, also contributing to the peak height

enhancement observed [30]. The 2 times increased electric field (compared with method A) used for separation gave an increase in efficiency and resolution.

### 2.3.3 PCR Analysis Following Method C

#### 2.3.3.1 PCR Performed on Samples Containing Jurkat Cells

The hot start kit from Invitrogen was used after difficulties were encountered with the GeneAmp® PCR core reagents kit used in methods A and B. The reasons for the failure of that kit were not thoroughly explored, but two possible causes, independent of the PCR kit used, were later identified. The main cause was a defective thermal cycler, which didn't achieve the programmed denaturing temperature and halted the amplification process. Also, using old primer solutions (older than the 6 month shelf-life period recommended by the provider) probably affected the process. Method C was tested by extracting the DNA from 1100, 660, 330, 220 and 110 Jurkat cells. DNA was captured on Dynabeads and the beads were removed before performing the PCR amplification.

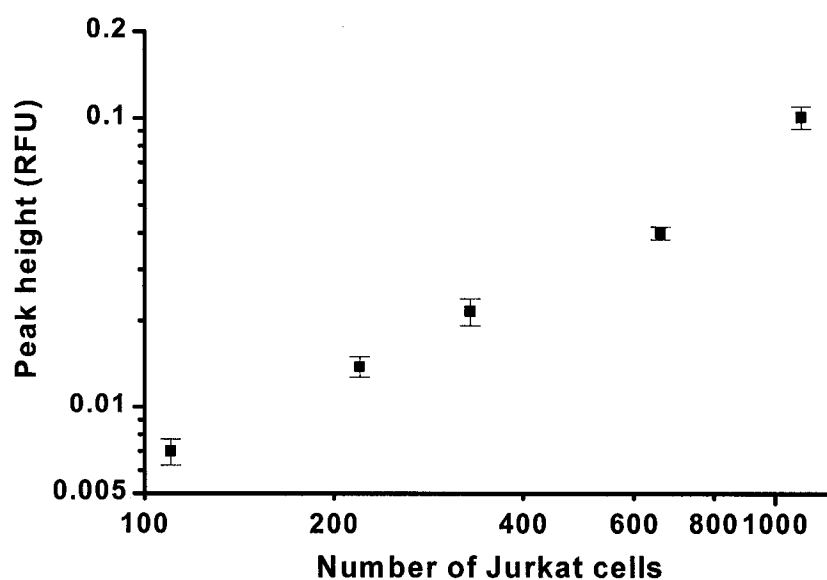


**Figure 2.9:** Characterization of the peak height obtained by PCR amplification using method C. DNA was extracted from samples containing 110, 220, 330, 660 and 1100 Jurkat cells.

A T cell receptor  $\gamma$  gene was amplified by PCR (36 cycles) from 50% of the DNA eluted from Dynabeads and the product was analyzed by CGE using an electric field of 370

V/cm. As presented in Figure 2.9, the 300 bp fragment was successfully amplified and identified from all samples. The average peak heights were determined from 3 to 5 electropherograms and gave RSD values between 4.5% and 12%.

The standard form of PCR used in methods A and B is susceptible to mispriming, especially before starting the PCR, when all the reactants were present at room temperature. The hot-start PCR promoted the specificity of amplification through minimized mispriming and enhanced the sensitivity of amplification through avoiding the non-specific amplification. The water plug introduced prior to sample injection allowed an increase in sample loading comparing with method A and determined also a peak height enhancement.

## 2.4 Conclusion

The experiments with method A were performed prior to fully optimizing the off-chip PCR procedure and the CGE separation. A minimum of about 800 T cells was required to characterize the amplified peak. Improvements in signal were associated with method B, for which a detection of as few as one Jurkat cell was demonstrated. Also the peak obtained from about 800 T cells was well defined and much easier to analyze than that obtained from method A. The optimized temperature cycling, with lower extension temperature in each subsequent cycle, clearly gave better sensitivity. Also the two-step injection procedure improved the sample loading and allowed detection from samples with low-copy DNA content.

PCR amplification was much more effective when the anti-CD3 coated paramagnetic beads were not present during the PCR stage. Because the amplification of only one Jurkat cell was successful even in the presence of Dynabeads, this suggests that it is the Protein A/anti-human CD3 paramagnetic beads that negatively affect the PCR process. While it is not necessary to remove the Dynabeads, it is not possible to selectively remove the anti CD3 beads after DNA capture on the Dynabeads. Removal before adding the Dynabeads would make quantitative DNA capture more difficult. However, for optimum sensitivity in future experiments, separation of beads from the PCR mixture would be required.

Method C used a hot-start PCR kit. Without varying the annealing temperature for



PCR, the 36 cycle amplification allowed identification and characterization of the 300 bp product obtained from as low as 110 Jurkat cells, even though only 50% of the volume with eluted DNA from Dynabeads was amplified. While greater sensitivity was achieved with method B, method C was sufficiently sensitive so that no further improvement was undertaken. The two-step injection procedure improved the sample loading and allowed detection from samples with low-copy DNA content.

While all three methods tested could be used to determine the efficiency of an on-chip capture of T cells, methods B and C offered better sensitivity. As will be described in Chapter 3, the magnetic beads containing captured cells can be removed from chip and then analyzed simultaneously with a set of standards with a known content of T cells.

## 2.5 References

- [1] Chhanabhai, M.; Adomat, S. A.; Gascoyne, R. D.; Horsman, D. E. *Am J Clin Pathol*, **1997**, *108*, 295-301.
- [2] Rowland-Jones, S. L.; McMichael, A. J. *Lymphocytes*, Oxford University Press: Oxford **2000**.
- [3] Bain, B. J. *Blood Cells A Practical Guide*, Blackwell Science Ltd.: London **2002**.
- [4] San Miguel, J. F.; Garcia-Sanz, R.; Gonzalez, M.; Orfao, A. *Baillieres Clin Haematol*, **1995**, *8*, 735-759.
- [5] Pignata, C.; Fiore, M.; de Filippo, S.; Cavalcanti, M.; Gaetaniello, L.; Scotese, I. *Pediatr Res*, **1998**, *43*, 77-83.
- [6] Turner, S. J.; Diaz, G.; Cross, R.; Doherty, P. C. *Immunity*, **2003**, *18*, 549-559.
- [7] Asnafi, V.; Radford-Weiss, I.; Dastugue, N.; Bayle, C.; Leboeuf, D.; Charrin, C.; Garand, R.; Lafage-Pochitaloff, M.; Delabesse, E.; Buzyn, A.; Troussard, X.; Macintyre, E. *Blood*, **2003**, *3*, 1000-1006.
- [8] Hawes, G. E.; Vietor, H. E.; Kanhai, H. H.; van den Elsen, P. J. *Int Immunol*, **1997**, *9*, 1103-1110.
- [9] Ahangari, G.; Halapi, E.; Tehrani, M. J.; Fransson, J.; Hammar, H.; Wigzell, H. *Scand J Immunol*, **1997**, *45*, 534-540.
- [10] Mato, T.; Masuko, K.; Misaki, Y.; Hirose, N.; Ito, K.; Takemoto, Y.; Izawa, K.; Yamamori, S.; Kato, T.; Nishioka, K.; Yamamoto, K. *Int Immunol*, **1997**, *9*, 547-554.

- [11] McVay, L. D.; Li, B.; Biancaniello, R.; Creighton, M. A.; Bachwich, D.; Lichtenstein, G.; Rombeau, J. L.; Carding, S. R. *Mol Med*, **1997**, *3*, 183-203.
- [12] Kashii, Y.; Shimizu, Y.; Nambu, S.; Minemura, M.; Okada, K.; Higuchi, K.; Watanabe, A. *J Hepatol*, **1997**, *26*, 462-470.
- [13] Manz, C. Y.; Dietrich, P. Y.; Schnuriger, V.; Nissen, C.; Wodnar-Filipowicz, A. *Blood Cells Mol Dis*, **1997**, *23*, 110-122.
- [14] Ahangari, G.; Berg, A.; Jeddi-Tehrani, M.; Halapi, E.; Hammar, H.; Wigzell, H. *Scand J Immunol*, **1996**, *44*, 330-334.
- [15] Chowers, Y.; Holtmeier, W.; Morzycka-Wroblewska, E.; Kagnoff, M. F. *J Immunol Methods*, **1995**, *179*, 261-263.
- [16] Hinz, T.; Wesch, D.; Friese, K.; Reckziegel, A.; Arden, B.; Kabelitz, D. *Eur J Immunol*, **1994**, *24*, 3044-3049.
- [17] Moonka, D.; Loh, E. Y. *J Immunol Methods*, **1994**, *169*, 41-51.
- [18] Duchmann, R.; Strober, W.; James, S. P. *DNA Cell Biol*, **1993**, *12*, 217-225.
- [19] Theodorou, I.; Delfau-Larue, M. H.; Bigorgne, C.; Lahet, C.; Cochet, G.; Bagot, M.; Wechsler, J.; Farcet, J. P. *Blood*, **1995**, *86*, 305-310.
- [20] Fodinger, M.; Buchmayer, H.; Schwarzinger, I.; Simonitsch, I.; Winkler, K.; Jager, U.; Knobler, R.; Mannhalter, C. *Br J Haematol*, **1996**, *94*, 136-139.
- [21] Andersen, W. K.; Li, N.; Bhawan, J. *J Cutan Pathol*, **1999**, *26*, 176-182.
- [22] Wood, G. S.; Uluer, A. Z. *Am J Dermatopathol*, **1999**, *21*, 547-551.
- [23] Nagasawa, T.; Nakatsuka, S.; Miwa, H.; Kanno, H.; Itami, S.; Yoshikawa, K.; Aozasa, K. *J Dermatol*, **2000**, *27*, 238-243.
- [24] Nyvold, C.; Madsen, H. O.; Ryder, L. P.; Seyfarth, J.; Engel, C. A.; Svejgaard, A.; Wesenberg, F.; Schmiegelow, K. *J Immunol Methods*, **2000**, *233*, 107-118.
- [25] Gebhard, S.; Benhattar, J.; Bricod, C.; Meuge-Moraw, C.; Delacretaz, F. *Histopathology*, **2001**, *38*, 37-44.
- [26] Germano, G.; Songia, S.; Biondi, A.; Basso, G. *Haematologica*, **2001**, *86*, 382-385.
- [27] Luo, V.; Lessin, S. R.; Wilson, R. B.; Rennert, H.; Tozer, C.; Benoit, B.; Leonard, D. G. *Mol Diagn*, **2001**, *6*, 169-179.
- [28] Zhu, D.; Kadin, M. E.; Samoszuk, M. *Am J Clin Pathol*, **2001**, *116*, 527-534.
- [29] Lukowsky, A. *Methods Mol Biol*, **2003**, *218*, 303-320.
- [30] Chien, R.-L.; Burgi, D. S. *J Chromatogr*, **1991**, *559*, 141-152.
- [31] Guttman, A.; Schwartz, H. E. *Anal Chem*, **1995**, *67*, 2279-2283.

- [32] Butler, J. M.; McCord, B. R.; Jung, J. M.; Wilson, M. R.; Budowle, B.; Allen, R. O. *J Chromatogr B Biomed Appl*, **1994**, *658*, 271-280.
- [33] Ulfelder, K. J.; Schwartz, H. E.; Hall, J. M.; Sunzeri, F. J. *Anal Biochem*, **1992**, *200*, 260-267.
- [34] Kohler, S.; Jones, C. D.; Warnke, R. A.; Zehnder, J. L. *Am J Dermatopathol*, **2000**, *22*, 321-327.

## CHAPTER 3: Cell Separation Experiments on Different Devices

### 3.1 Introduction

In this chapter we present a one-step immunomagnetic separation technique adapted to a simple Y-intersection microfluidic device. The target of our cell isolation and purification studies were T cells, based on their relatively low concentration in blood (about 1:10,000 cells). The methods developed in Chapter 2 for quantitative analysis of the captured T cells, which used PCR amplification, were employed. Method A was first employed, but did not allow a sensitive characterization of the PCR product peak. Method B was further optimized and allowed more sensitive characterization of genomic DNA. Method C utilized a hot-start PCR, and was used after the reagents for Method B became unreliable. The PCR components were stable as premixed and the annealing temperature was constant, unlike in method B, offering an easier approach to future on-chip integration of method C. T cells were successfully separated on-chip either from human blood or reconstituted blood samples and identified by PCR off-chip. A second-generation device, with larger channels for a rapid analysis of larger sample volumes was then designed and tested. A variety of flow path designs were fabricated and tested experimentally.

Clinical diagnostic PCR analyses require separation of specific cells from blood or other biological fluids, extraction of DNA or RNA, followed by amplification and identification of a DNA or RNA fragment. Since the heme in red blood cells is a well-known PCR inhibitor [1, 2], a separation is needed to remove those cells. Very sensitive assays would also benefit from sample enrichment in the target cells [3]. A variety of separation methods can be used for different applications. Specific cell surface recognition methods can be employed, including affinity chromatography, fluorescence and magnetic activated cell sorting (FACS, MACS). Centrifugation methods have been widely used for separation of large populations of cells, but are not very selective and are usually used only as a preliminary step of the separation. Miniaturization of this technique would be challenging, and perhaps ineffective, given the large volume of sample that must be processed. Cells are also separated based on the surface charge to size ratio using free-flow electrophoresis [4], but Joule heating of the media due to the

applied field limits the volume of sample and the solution conductivity which can be used.

Microfluidic devices are capable of performing sample preparation, chemical and biochemical reactions, separations and analysis. By using electric, magnetic or gravitational fields, cells can be separated by field-flow fractionation. Up to 80 % efficiency in cell separation was obtained by dielectrophoresis, when the target cells represented about 10% of the total number of cells [5]. Combined dielectrophoresis and gravitational field-flow fractionation were used by Gascoyne et al. to develop a system able to separate human peripheral blood white cells [6]. More recently, Gascoyne fabricated a magnetophoretic-dielectrophoretic-gravitational field-flow fractionator [7]. Flow cytometers can be used for cell sorting, and are frequently employed in conventional methods. Several groups have published their initial results in miniaturizing different versions of flow cytometers [8-14]. Microchip based flow cytometers performed sorting of different systems such as platelets/ RBC from diluted blood [8], lymphocytes/ neutrophils/monocytes from whole blood with lysed RBC [12] and *E. coli* cells expressing green fluorescent protein from a background of non-fluorescent *E. coli* cells [13]. Many flow cytometry systems are characterized by fairly large reagent consumption and require diluted samples. Some very new ones may begin to address these challenges.

To date only microfiltration [15] and dielectrophoresis [16, 17] were tested for integrating blood sample preparation with nucleic acid amplification reactions on microfabricated devices. A large number of chip based methods for genetic analysis have been reported, predominantly involving integration of the polymerase chain reaction (PCR) and separation of the PCR product [18-32]. As methods for performing RNA or DNA sample preparation [16, 33, 34], PCR [35-39] and hybridization on-chip [40, 41] have developed, it has become important to also integrate cell capture and concentration on-chip. The methods of microfiltration and dielectrophoresis have been suggested as a way to do the initial PCR sample preparation and so could be integrated. But the microfiltration approach was prone to clogging the chip with a blood sample. The experiments performed with dielectrophoresis used only diluted or resuspended blood in a separation buffer, which provided the specific conductivity required. Nevertheless, we can see that once all these processes are successfully coupled together, assay procedures

for PCR analysis will be simpler, the analysis time shorter, the reliability greater, and possibly a smaller amount of blood sample will be required.

The study presented in this chapter utilizes a hybrid affinity chromatography method that employs a paramagnetic bead-bed. T cells were used as the initial model of rare cells in blood, although more dilute sample analyses are ultimately contemplated. As shown in Chapter 2, T cells are readily analyzed directly in blood, without use of the chip. However, for more dilute target cells (1:1,000,000), the interference by background DNA becomes a greater problem, so that enrichment is beneficial. Protein A/anti-human CD3 paramagnetic beads are introduced into the chip and captured in the magnetic field generated by an external magnet. Then the blood sample is introduced and T cells are captured while the other cells are collected at the outlet. This system allows the capture of different types of cells from whole blood by simply changing the bounded antibody. After capture and washing, the cells could be removed from the chip or moved to a different module for subsequent analysis.

Paramagnetic beads were used successfully for dynamic DNA hybridization [40] and mRNA isolation [33] within a microfluidic device. An external magnet provided the magnetic field required for bead trapping. Recently a self-assembled magnetic bead bed was proposed for cell sorting [42] aiming to obtain a more controllable, compact magnetic bed. Ahn et al. demonstrated the use of integrated magnetic traps within a microfluidic device [43]. Their microfabricated versions of planar electromagnets [44, 45] allowed development of an integrated microfluidic system for performing magnetic bead-based immunoassay [46]. With minimal modifications, such a system could be adapted for a magnetic cell separation module, following the methods and procedures developed here.

## **3.2 Experimental Section**

### **3.2.1 Reagents and Media**

A large list of reagents was presented in chapter 2. Here we present items not included in section 2.2.1. Bovine serum albumin (BSA), used to block nonspecific adsorption on glass surfaces, was obtained from Sigma-Aldrich (Oakville, ON, Canada). 0211 glass was purchased from Corning (NY, USA) and HPR 504 positive photoresist

from Arch Chemicals (Norwalk, CT, USA). Microposit 354 developer was purchased from Shipley (Newton, MA, USA). The 6 mm diameter NdFeB permanent magnets used to create the magnetic field for paramagnetic bead trapping on-chip were purchased from Edmund Industrial Optics (Barrington, NJ, USA).

### 3.2.2 Device Fabrication

Based on device layouts designed with L-Edit software (Tanner Research, Pasadena, CA, USA), Adtek Photomask (Montreal, QC, Canada) fabricated the photomasks on 5" × 5" glass, with one side patterned with chromium to make opaque areas. After transferring the features from photomasks through a lithographic process, the channels were etched on substrates of 4" × 4" (540 μm thick) 0211 glass (Corning, NY, USA) at Micralyne, Edmonton, AB, Canada and at the University of Alberta Nanofab. Every glass substrate required a coating on one side with a Cr film 20 nm thick to form an adherent layer on glass, with a 100 nm thick Au film for protection (mask) against the glass etchant. The HPR 504 positive photoresist (Arch Chem., Norwalk, CT, USA) was deposited on the metal layers. After baking for 30 min at 120 °C, the substrate was exposed to UV light through a photomask in a contact mask aligner (ABM, San Jose, CA, USA) and the exposed photoresist was removed with Microposit 354 developer (Shipley, Newton, MA, USA), followed by baking the substrate for 30 min at 120 °C. The exposed Au and Cr were etched by using a 2.4 M KI, 0.8 M I<sub>2</sub> aqueous solution and a commercial Cr-etchant, respectively. The exposed glass was then etched by 49% HF/70% HNO<sub>3</sub>/H<sub>2</sub>O (20:14:66) at a rate of 1.6 μm/min. The unexposed photoresist and the Au and Cr metal layers were removed afterwards by using acetone, aqueous KI/I<sub>2</sub> solution and Cr-etchant, respectively. The final depths were measured with an Alphastep 200 profilometer (Tencor Instruments, KLA-Tencor Corp., San Jose, CA, USA). The microfluidic devices were completed by thermally bonding the substrates on 4" × 4" (540 μm thick) 0211 glass cover-plates. The access holes (1.5 mm) were previously drilled in the cover-plates using a jeweler's drill and diamond-coated drill bits (Lee Valley, Ottawa, ON, Canada). Reservoirs with a capacity of 50-100 μL were made from sectioned plastic pipet tips, which were centrally attached, with epoxy glue, on top of the inlet holes.

Two devices with different designs were used in this study. The Y-intersection device was designed previously by Hossein Salimi-Moosavi for other studies [33, 47]. Details of this device are presented in Figure 3.1. The Y-device consisted of two inlet ports from which reagents could be driven into a main channel. All structures were etched to 70  $\mu\text{m}$  depth, with a cross section in the capture area of  $2.17 \times 10^{-2} \text{ mm}^2$ , starting from a mask feature width of 200  $\mu\text{m}$ . Similar devices with 100  $\mu\text{m}$  wide photomask features were etched to 10, 30 and 50  $\mu\text{m}$  depths and were used for preliminary experiments of cell capture on the inner glass surface.

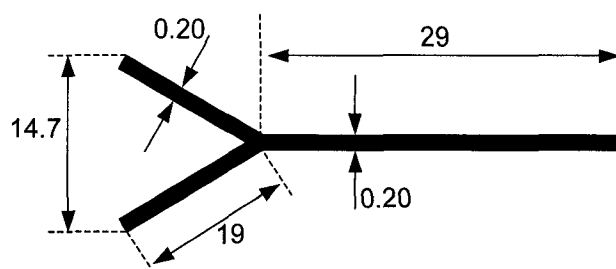


**Figure 3.1:** Layout of the Y-intersection device used for immunomagnetic separation of blood cells. Dimensions are indicated in mm and correspond to the photomask features. Channels were etched isotropically in 0.54 mm thick Corning 0211 glass.

The FAT 3000 device (Figure 3.2) was designed for this project, with eight different manifolds all having a total channel width of 3000  $\mu\text{m}$  on the photomask in the capture area. Every manifold consisted of an inlet port, a splitting scheme, followed by a capture area and a channel to connect at the outlet port. All structures were isotropically wet-etched in glass to a 50  $\mu\text{m}$  depth. The device was named FAT based on its features being much wider than our normal microfluidic devices. Based on the depth of 50  $\mu\text{m}$ , the total cross sectional area in the capture zone were calculated and are presented in Table 3.1. The percent variations were calculated with reference to manifold 4.

**Table 3.1:** Actual surface area of cross-sections in the FAT 3000 device.

Channel	1	2	3	4	5	6	7	8
Surface Area ( $\text{mm}^2$ )	0.181	0.197	0.181	0.154	0.158	0.166	0.181	0.166
Variation (%)	17.5	27.9	17.5	0	2.6	7.8	17.5	7.8



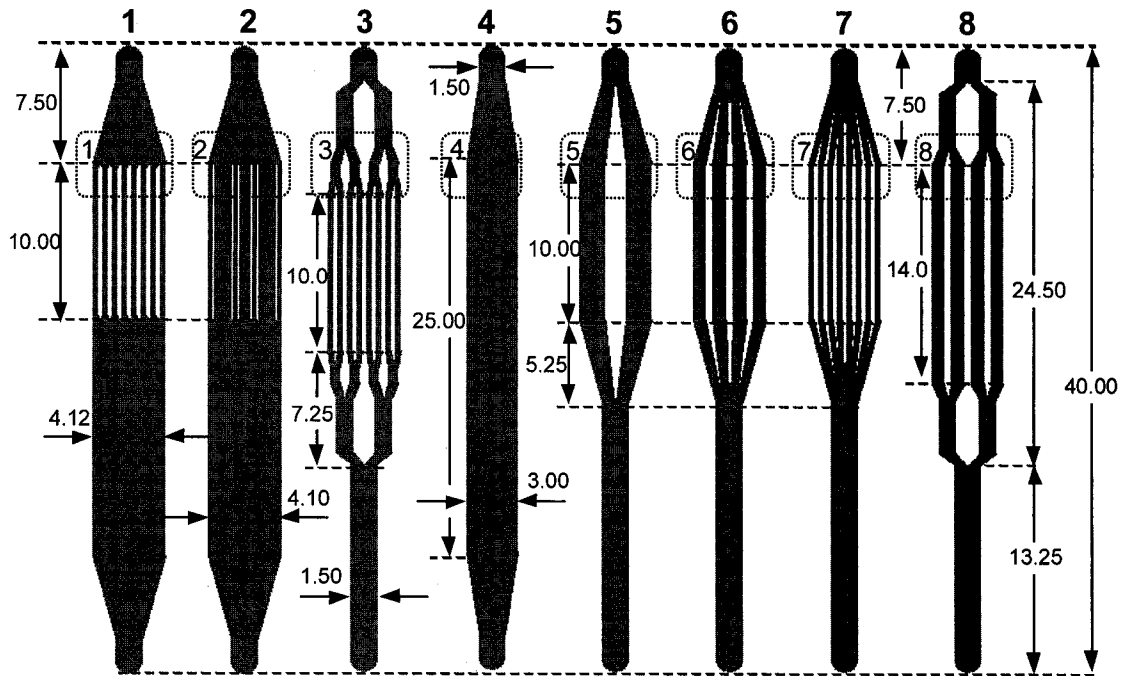


**Figure 3.2:** Layouts of the eight different manifold designs of the FAT 3000 device used for immunomagnetic separation of Jurkat cells. Dimensions are indicated in mm and correspond to the photomask features. Channels were etched isotropically in 0.54 mm thick Corning 0211 glass.

### 3.2.3 Cell Samples

Heparinized human blood samples (1 mL) were obtained from patients from the Cross Cancer Institute (Edmonton, Canada). Human blood samples were used on the same day as obtained and the remaining portions were neutralized in a 0.6% bleach solution (5000 ppm free chlorine).

Jurkat cells (ATCC No. TIB-152, clone E6-1, T cell leukemia, human) were purchased from the American Type Culture Collection (ATCC) and maintained in RPMI 1640 supplemented with 10% fetal bovine serum, 1 % L-glutamine 200 mM and 2 % antibiotic antimycotic solution, stabilized in a humidified atmosphere with 8 % CO<sub>2</sub> at 37°C provided by a NuAire US Autoflow (NU-4750) Automatic CO<sub>2</sub> water-jacketed incubator (Plymouth, MN, USA). Cells were counted with a hemacytometer (Sigma-Aldrich, Oakville, ON, Canada). Cell viability was determined by a dye exclusion test with Trypan Blue 0.4 % solution. Cultures were maintained between  $1.0 \times 10^5$  and  $1.4 \times 10^6$  cells/mL, with 91 % - 94 % viable cells. As required for some determinations, serial dilutions in supplemented RPMI 1640 were performed. The SD and RSD values for cell concentration and the number of cells used in different experiments were calculated assuming a  $\pm 0.1 \mu\text{L}$  error for every pipetting step performed for diluting and sampling volumes larger than 2  $\mu\text{L}$  and  $\pm 0.05 \mu\text{L}$  for sampling volumes smaller or equal to 2  $\mu\text{L}$ .

Concentrated horse red blood cells ( $1 \times 10^{10}$  -  $2 \times 10^{10}$  cells/mL, HemoStat Labs, Dixon, CA, USA), free of white blood cells, were mixed with  $1 \times 10^5$  -  $1 \times 10^6$  Jurkat cells/mL suspended in supplemented RPMI 1640 to obtain reconstituted blood samples with 10,000 horse red blood cells for every human T cell. Horse red blood cells are similar in size to human red blood cells (6-8  $\mu\text{m}$ ). While the horse red blood cells /Jurkat cells mixture offered similar physical properties to human blood samples, the mixture used allowed a quick and precise preparation of reconstituted blood samples with a well controlled number of T cells.

#### 3.2.3.1 Blood Samples Used to Test the Y-intersection Device

Aliquots of  $2.00 \pm 0.05 \mu\text{L}$  (RSD = 2.5%) human blood were analyzed on-chip. A set of standards consisting of  $0.50 \pm 0.05 \mu\text{L}$  (RSD = 10%),  $1.00 \pm 0.05 \mu\text{L}$  (RSD = 5%),

$2.00 \pm 0.05 \mu\text{L}$  (RSD = 2.5%) and  $4.0 \pm 0.1 \mu\text{L}$  (RSD = 2.5%) of blood, withdrawn from the same stock blood sample analyzed on-chip, was analyzed simultaneously. These blood samples were treated as described in Sec 2.2.3.2.1b (method A) or 2.2.3.2.2c (method B).

### **3.2.3.2 Reconstituted Blood Samples Used to Test the FAT 3000 Device**

Sample aliquots were withdrawn from reconstituted blood consisting of Jurkat cells and horse red blood cells (1:9300 and 1:10000 ratio) suspended in a mixture of supplemented RPMI 1640 media and horse plasma.

#### **3.2.3.2a Experiment 1 Performed on All Manifolds**

The stock solution of reconstituted blood contained  $5.35 \times 10^5$  Jurkat cells/mL (RSD= 9.3%) and  $5.0 \times 10^9$  horse red blood cells/mL (1: 9300 ratio of Jurkat cells to horse red blood cells in 1:1 supplemented RPMI 1640 media to horse plasma). Samples of  $2 \mu\text{L}$  ( $1070 \pm 104$  Jurkat cells, RSD=9.7%) reconstituted blood were analyzed on every channel, as described in section 3.2.4.2b. The set of standards with  $107 \pm 11$  (RSD= 10.6%),  $214 \pm 21$  (RSD= 9.7%),  $321 \pm 30$  (RSD= 9.5%),  $428 \pm 40$  (RSD= 9.4%) and  $1070 \pm 100$  (RSD= 9.4%) Jurkat cells were withdrawn from a 1:10 dilution of the stock suspension in supplemented RPMI 1640.

#### **3.2.3.2b Experiment 2 Performed on Manifolds 1, 3, 4 and 6**

The stock solution of reconstituted blood contained  $8.9 \times 10^5$  Jurkat cells/mL (RSD= 4.3%) and  $8.9 \times 10^9$  horse red blood cells/mL (1: 10000 ratio of Jurkat cells to horse red blood cells in 1.25:1 supplemented RPMI 1640 media to horse plasma). Samples of  $1 \mu\text{L}$  ( $890 \pm 59$  Jurkat cells, RSD= 6.6%) reconstituted blood were analyzed on channels 1, 3, 4 and 6, as described in section 3.2.4.2b. Standards with  $134 \pm 8$  (RSD= 5.6%),  $445 \pm 22$  (RSD= 4.9%) and  $890 \pm 41$  (RSD= 4.6%) Jurkat cells were withdrawn from a 1:10 dilution in supplemented RPMI 1640 and a standard with  $1780 \pm 87$  (RSD= 4.9%) was withdrawn from the stock cell suspension.

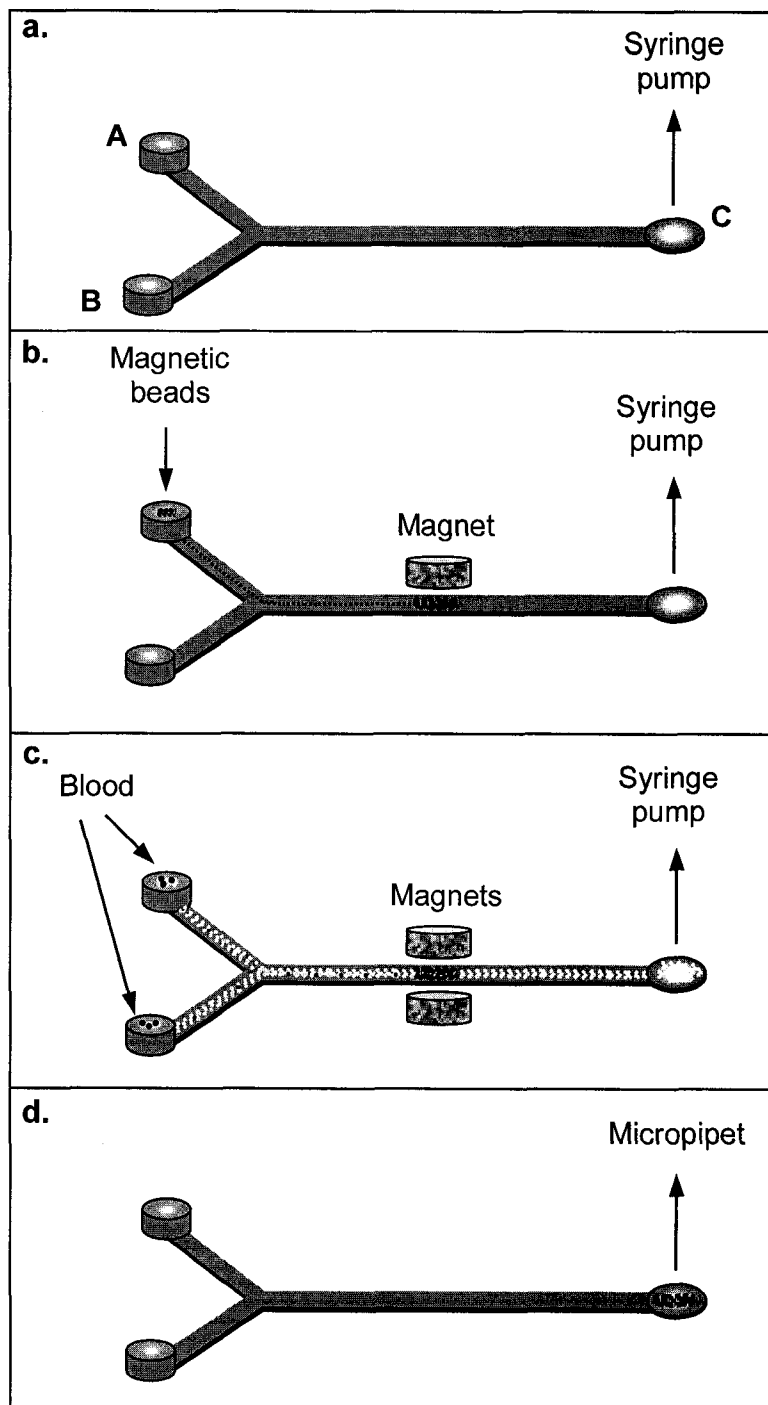


**Figure 3.3:** Immunomagnetic separation of T cells using Y-intersection device:

- The device was connected to a syringe pump using tubing;
- Protein A/anti-human CD3 magnetic beads were introduced from one reservoir into the channel and captured with one magnet placed on top of the device;
- Blood samples were introduced from both channels, T cells were captured with two magnets and washed with RPMI 1640;
- Captured cells and magnetic beads were removed from the outlet with a micropipet.

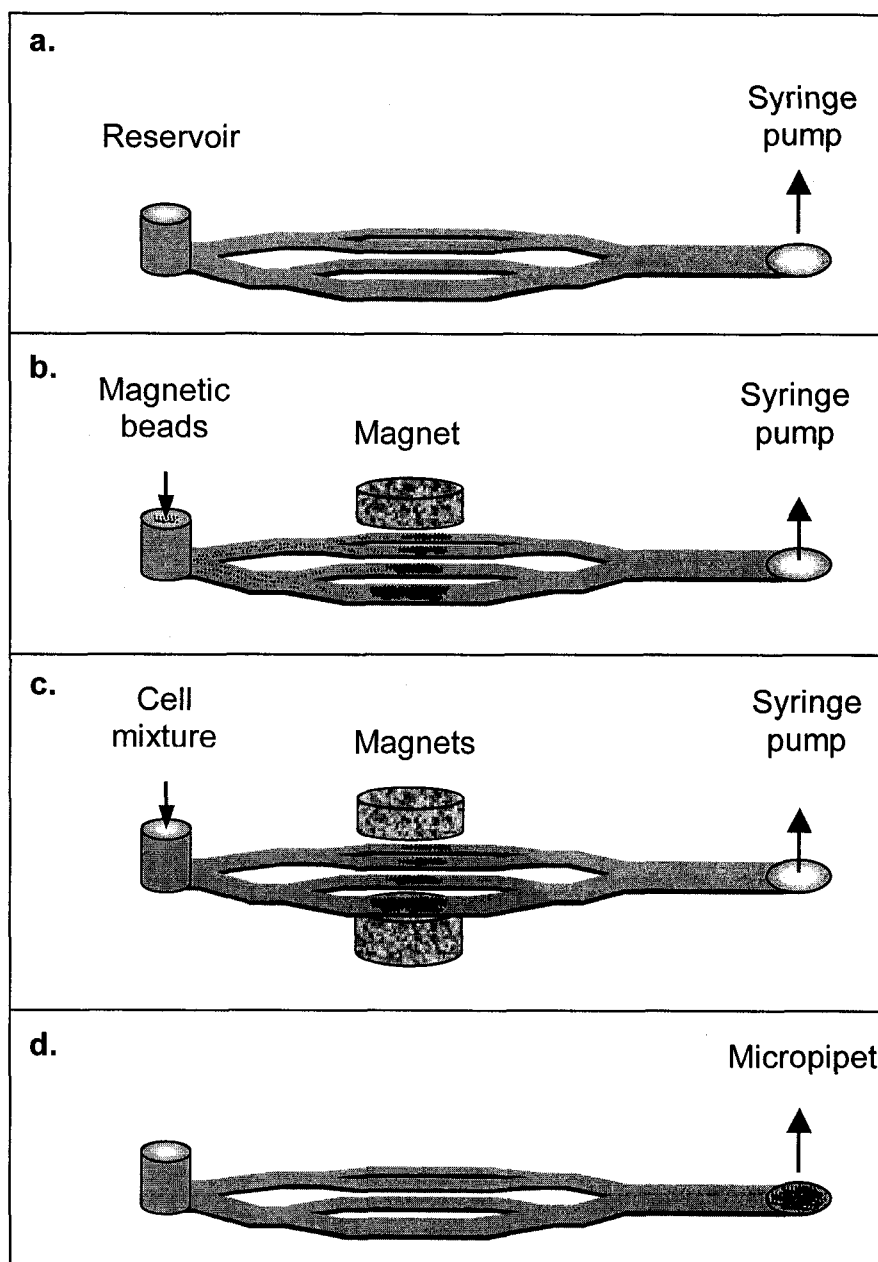


**Figure 3.4:** Immunomagnetic separation of T cells using FAT 3000 device:

- The device was connected to a syringe pump using tubing;
- Protein A/anti-human CD3 magnetic beads were introduced from the reservoir into the channel and captured with one magnet placed on top of the device;
- Cell mixtures were introduced, Jurkat cells were captured with two magnets and washed with RPMI 1640;
- Captured Jurkat cells and magnetic beads were removed from the outlet using a micropipet.

### **3.2.4 Operating Procedure**

#### **3.2.4.1 Preconditioning of the Devices**

The channels required a preconditioning treatment to block possible non-specific adsorption of cells on the glass surface. The channels were conditioned with BSA and filled with PBS. A PHD 70-2001 syringe pump (Harvard Apparatus, Saint-Laurent, QC, Canada) with a 100  $\mu\text{L}$  SGE gas-tight syringe (Supelco, Sigma-Aldrich Canada, Oakville, ON) was used in the withdrawal mode (i.e. suction) to pump the liquids through the channels at constant flow rates.

##### **3.2.4.1a Procedure for Y-intersection Device**

The Y-intersection device was preconditioned using 70 % ethanol (technical grade) loaded into each reservoir, A and B (Figure 3.3a). Vacuum was applied at port C using the syringe pump fixed at 50  $\mu\text{L}/\text{min}$  (withdraw mode) for 1 min and then 1  $\mu\text{L}/\text{min}$  for 10 min. The remaining liquid was removed from reservoirs using a vacuum line. The reservoirs were rinsed three times with 1 % BSA solution in PBS and then filled with the same solution. Vacuum was applied again at port C by setting the syringe pump at 1  $\mu\text{L}/\text{min}$  for 1 min and then at 0.25  $\mu\text{L}/\text{min}$  for the next 30 min. The remaining liquid was removed from reservoirs using a vacuum line. The reservoirs were first rinsed three times with PBS and then filled with the same solution. The excess of BSA from inside the channel was removed with the syringe pump fixed at 1  $\mu\text{L}/\text{min}$  for 1 min and at 0.25  $\mu\text{L}/\text{min}$  for the next 10 min.

##### **3.2.4.1b Procedure for FAT 3000 Device**

The eight different manifolds of the FAT 3000 device were conditioned similarly to the Y-device, one manifold at a time. A syringe pump was connected to the outlet of one channel and 70 % ethanol was loaded in the reservoir (Figure 3.4a). Vacuum was applied at the outlet, using the syringe pump fixed at 50  $\mu\text{L}/\text{min}$  (withdrawal mode) for 30 s and then 10  $\mu\text{L}/\text{min}$  for 5 min. The reservoir was refilled as required. After stopping the syringe pump, the reservoir was emptied using a vacuum line, rinsed three times with 1 % BSA solution in PBS and then filled with the same BSA solution. Vacuum was applied again at the outlet by setting the syringe pump at 10  $\mu\text{L}/\text{min}$  for 1 min and then at 2.5

$\mu\text{L}/\text{min}$  for the next 5 min. The remaining liquid was removed from reservoirs using a vacuum line. The reservoir was first rinsed three times with PBS and then filled with the same solution. The excess of BSA inside the channel was removed with the syringe pump set at  $10 \mu\text{L}/\text{min}$  for 1 min and at  $2.5 \mu\text{L}/\text{min}$  for the next 10 min.

### **3.2.4.2 On-chip Cell Capture**

Devices were clamped on a chip holder mounted on an X-Y translation stage and the channels were observed through a microscope mounted over top of the device. The microscope was fixed on a Z translation stage to allow focusing on the channel with a  $25\times$  objective (Leitz Wetzlar, Germany). Images were captured using a color video camera (TK-1280U, JVC, Japan) and recorded with a VCR. In order to perform on-chip cell capture experiments with all tested devices, Protein A/anti-human CD3 paramagnetic particles were introduced first into the channel and captured magnetically in the capture area. The method used to capture anti-human CD3 on Protein A paramagnetic beads was described in section 2.2.3.1. Human blood or reconstituted horse blood samples were introduced into the channels of the Y-intersection and FAT 3000 devices, when T cells or Jurkat cells, respectively, were captured.

#### **3.2.4.2a Procedure for Y-intersection Device**

The operating procedure is illustrated in Figure 3.3. Each reservoir was filled with  $40 \mu\text{L}$  of PBS and a magnet was placed on top of the capture channel. With the pump set at  $50 \mu\text{L}/\text{min}$  (withdrawal mode), a  $2 \mu\text{L}$  suspension of Protein A/anti-human CD3 paramagnetic particles was slowly introduced with a micropipet into the bottom of reservoir A. The beads were quickly transported inside the channel and captured at the magnet (Figure 3.3b). After stopping the syringe pump, the reservoir was emptied using a vacuum line, rinsed three times with PBS and refilled with PBS. To mobilize any beads that had stopped in the channel before reaching the magnetic field zone, the syringe pump was started again at  $50 \mu\text{L}/\text{min}$  until the portion of channel outside the magnetic zone, checked through the microscope, was confirmed to be free of beads. The reservoirs were then refilled as required. After stopping the pump, PBS in the reservoirs was removed using a vacuum line. The reservoirs were filled with supplemented RPMI 1640 (RPMI

1640 mixed with 10% fetal bovine serum, 1% L-glutamine 200 mM and 2% antibiotic antimycotic solution) and the syringe pump was started at 100  $\mu\text{L}/\text{min}$  and after 30 sec changed to 1  $\mu\text{L}/\text{min}$ . A second magnet was then placed under the device, paired with the first magnet. A 2  $\mu\text{L}$  human blood sample was slowly layered down at the bottom of both reservoirs A and B. The syringe pump was used in the withdrawal mode for 30 min at 0.25  $\mu\text{L}/\text{min}$  to completely introduce the blood sample (Figure 3.3c). After stopping the syringe pump, reservoirs A and B were emptied using a micropipet, rinsed three times with PBS, refilled with 50  $\mu\text{L}$  PBS and then the syringe pump was used again in withdraw mode for at least 20 min at 1  $\mu\text{L}/\text{min}$ . The syringe pump was stopped, the connection to the syringe pump was removed and the magnets were removed from the channel. The paramagnetic beads with captured cells were moved slowly toward port C (Figure 3.3d), transferred into a pipette tip and used for further off-chip analysis. The beads were mobilized by filling the two reservoirs with PBS and, also, if necessary, by slowly moving one magnet underneath the channel, towards the outlet. The Y-intersection device was reused after cleaning the channel with 0.6 % bleach solution, deionized water and 70 % ethanol.

#### **3.2.4.2b Procedure for FAT 3000 Device**

The operating procedure is shown in Figure 3.4. The reservoir was filled with 40  $\mu\text{L}$  of PBS and a magnet was placed on top of the capture channel. With the pump set at 50  $\mu\text{L}/\text{min}$  (withdrawal mode), a 5  $\mu\text{L}$  suspension of Protein A/anti-human CD3 paramagnetic particles was slowly introduced with a micropipet at the bottom of the inlet reservoir. The beads were quickly transported inside the manifold and captured under the magnet (Figure 3.4b). After stopping the syringe pump, the reservoir was emptied using a vacuum line, rinsed three times with PBS and refilled with PBS. To mobilize any beads stopped inside the channels before reaching the magnetic field zone, the syringe pump was started at 50  $\mu\text{L}/\text{min}$  until the portion of channel outside the magnet area, checked through the microscope, was confirmed to be free of beads. The reservoirs were refilled as required and after stopping the pump, any PBS remaining in the reservoirs was removed using a vacuum line. The reservoirs were filled with supplemented RPMI 1640 and the syringe pump was started at 100  $\mu\text{L}/\text{min}$  and after 30 sec changed to 3  $\mu\text{L}/\text{min}$ . A



second magnet was placed under the device, paired with the first magnet. Reconstituted blood samples of 1-2  $\mu\text{L}$  were slowly layered down at the bottom of the inlet reservoir. The syringe pump was used in the withdrawal mode for 3 min at 3  $\mu\text{L}/\text{min}$  to completely introduce the blood sample (Figure 3.4c). After stopping the syringe pump, the reservoir was emptied using a micropipet, rinsed three times with PBS, refilled with 50  $\mu\text{L}$  PBS and then the syringe pump was used again in withdraw mode for 20 min at 10  $\mu\text{L}/\text{min}$ . The syringe pump was stopped, the connection from the syringe pump was removed and the magnets were removed from the manifold. The paramagnetic beads with captured cells were slowly moved toward the outlet (Figure 3.4d), loaded in a pipette tip and used for further off-chip analysis. The beads were mobilized by filling the reservoir with PBS and, also, if necessary, by slowly moving one magnet underneath the channels, towards the outlet. The steps described here were repeated for every tested manifold of the device. All manifolds of the FAT 3000 device were reused after cleaning them with 0.6 % bleach solution, deionized water and 70 % ethanol.

#### **3.2.4.3 Off-chip Analysis of the Captured Cells**

DNA from the cells captured on-chip on Protein A/anti-human CD3 beads was isolated using the Dynabeads® DNA DIRECT™ kit. The paramagnetic beads with captured cells were mixed with 200  $\mu\text{L}$  of Dynabeads suspended in a lysing buffer, inside of 1.5 mL siliconized Eppendorf tubes. Simultaneously, DNA was extracted using the DNA DIRECT™ kit from different aliquot volumes taken from the same blood sample used for the on-chip capture. The standard samples contained between 10% and 200% of the T cells analyzed on-chip, providing a set of standards. DNA released from the lysed cells was processed as described in section 2.2.3.2. The V-J junction of the T cell receptor (TCR)  $\gamma$  gene was amplified by PCR, following the procedures presented in section 2.2.3.2. Methods A and B were used for samples analyzed on the Y intersection device (section 3.3.2) and method C was used for samples analyzed on the FAT 3000 device (section 3.3.3). PCR was performed in the absence of the paramagnetic beads (Dynabeads and Protein A) for all samples, except the blood sample analyzed on the Y intersection device with method A. PCR was done for all samples at the same time, to reduce differences in amplification from run to run. The 300 bp PCR product obtained

after amplification of DNA extracted from the on-chip captured cells was analyzed along with the blood sample set of standards by capillary gel electrophoresis (CGE). A Beckman P/ACE 5010 instrument equipped with a 488 nm laser module LIF detector was used. A physical gel containing 0.4% HPMC and 0.5  $\mu\text{g}/\text{mL}$  ethidium bromide in 0.5 $\times$  TBE running buffer was used with a 27 cm long, 50  $\mu\text{m}$  i.d. fused silica capillary. Details about operation of the CE were provided in section 2.2.3.4.

### 3.3. Results and Discussion

The first goal was to show magnetic bead beds could be used on-chip to capture cells using an antibody, and that the captured cells could then be delivered off-chip for subsequent analysis. Initial studies used a Y-channel device with relatively small volumes. A second design was then tested to evaluate the best geometry for increased fluid flow rates and more rapid sample workup. One of the PCR techniques described in Chapter 2 was used to analyze the captured cells.

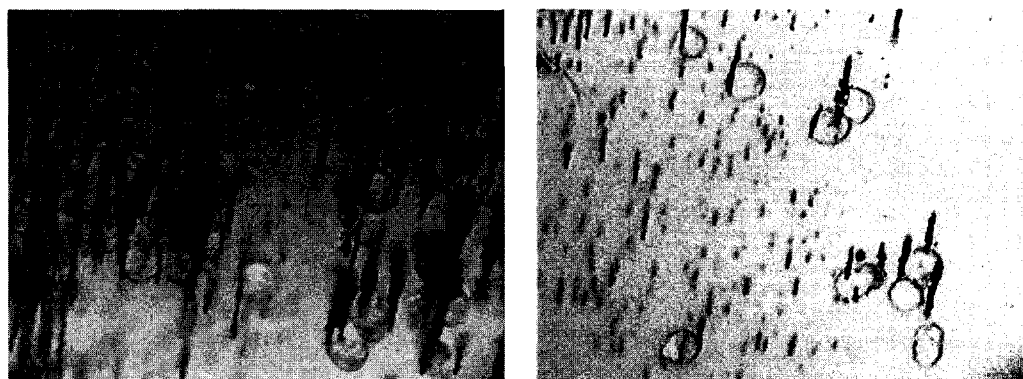


**Figure 3.5:** T cells and Protein A/anti-human CD3 magnetic beads captured in magnetic field, showing two regions of the chip with different densities of beads. Beads show up as dark streaks. Imaging was performed after cell capture and moving of the two magnets from the channel zone.

Anti-CD3 coated magnetic beads were introduced first and trapped with a magnet, then cells were added and sucked downstream with a syringe pump. Figure 3.5 presents images of the human T cells captured from blood on Protein A/ anti-human CD3 beads. The magnetically captured cells were washed free of other human blood cells with PBS. The images were captured in the vicinity of the magnets, the image with the higher

density of beads being obtained in a closer position to the magnets. The beads were then collected in a reservoir and removed from the chip for analysis. In order to determine the effectiveness of on-chip cell capture, the cells were lysed, the DNA was captured on Dynabeads and a T-cell specific receptor  $\gamma$  gene was amplified by PCR (300 bp). CGE of the product along with a set of standards was performed using a Beckman P/ACE 5000 with 0.4 % HPMC gel and ethidium bromide stain.

### 3.3.1 Jurkat Cell Capture on Glass Surface of a Y-intersection Device

The capture of T cells directly onto flow channel surfaces was explored. Due to the polar nature of the glass surface, proteins can adsorb on it. However, surface preparation was important in maximizing the amount of protein adsorbed. Good results were obtained by using concentrated nitric acid for 1 h (stopped flow), 2 M sulfuric acid for 20 min and 1 M sodium hydroxide for 1 h. Protein A adsorbed on the glass surface was then able to bind IgG. The best result was obtained by using 20  $\mu\text{g}/\text{mL}$  Protein A for 1 h (stopped flow), followed by 20  $\mu\text{g}/\text{mL}$  anti-human CD3 for 30 min and then 1% BSA for 30 min to block non-specific adsorption. This gave a glass surface that could capture T-cells. However, the reproducibility of cell capture was poor.

In an effort to increase cell capture efficiency two devices with etch depths of 30 and 10  $\mu\text{m}$ , respectively, were tested. The 30  $\mu\text{m}$  deep device was easy to operate with Jurkat cell suspensions ( $10^6$  cells /mL), but when blood samples were introduced, the device was easily plugged. The 10  $\mu\text{m}$  deep device worked for Jurkat cell suspensions, but did not allow blood sample flow due to excessive plugging.

Stability of captured T cells on a glass surface as a function of flow rate was investigated in a Y-intersection channel etched at 50  $\mu\text{m}$  depth from a 100  $\mu\text{m}$  wide feature on the photomask (0.0109  $\text{mm}^2$  actual cross-sectional area). T cells were captured from a pure T cell suspension of  $1 \times 10^5$  cells /mL. A flow rate of 1.25  $\mu\text{L}/\text{min}$  was maintained for 5 min and cells were counted on a  $200 \times 300 \mu\text{m}$  surface. The flow rate was decreased to 0.5  $\mu\text{L}/\text{min}$  and maintained constant for 30 s, then increased and maintained constant for 30 s at specified values (Table 3.2) and cells were counted on the same surface from corresponding captured images. It is clear that the effectiveness of capture is a strong function of the final flow rate, decreasing as the shear force increases.

As a result, the volume flow rates that may be achieved are lower than might be required for rapid analysis. In contrast, a bead bed should give more effective capture at similar flow rates, although the kinetics of T cell binding to anti-CD3 from the beads may limit the usable flow rate.

**Table 3.2:** Stability of captured cells on glass surface as a function of flow rate used in a Y-channel with 0.0109 mm<sup>2</sup> cross sectional area.

Number of captured cells	Final flow rate* (μL/min)	Calculated linear velocity (mm/sec)	Fraction of captured cells (%)
196	0.5	0.8	100
149	1.25	1.9	76
52	5	7.6	27
46	10	15.3	23
24	20	30.6	12
6	50	76.5	3
0	125	191.1	0

\* sample flow at 1.25 μL/min for 5 min, 0.5 μL/min for 30 s, then at specified rate for 30 s.

### 3.3.2 T Cell Separation from Human Blood Performed on Y-intersection Device

The performance of the Y-device for cell capture was tested using two PCR methods, A and B, described in sections 2.2.3.2.3 and 2.2.3.2.4.

In a first approach we considered the introduction of Protein A paramagnetic beads into the channel, followed by on-chip capture of anti-human CD3. However, we observed under the microscope that some Protein A beads remained attached on the glass surface inside the channel, and these were removed only after washing the channels with 70 % HNO<sub>3</sub> for more than 30 min at a flow rate of 200 μL/min. Such conditions are too harsh for proteins on the bead surface. A first solution was to introduce the beads at a higher flow rate. When a pair of magnets was used, the bead capture efficiency was estimated visually at much less than 50 % for a flow rate of 100 μL/min (linear velocity of 77 mm/s). The bead capture efficiency was drastically improved by placing only one magnet on top of the device. No significant bead loss was observed even at a flow rate of 200 μL/min (linear velocity of 154 mm/s). This result can be explained considering the

different distribution of beads in the channel, when only one magnet was used. The beads captured in the upper part of the channel (stronger magnetic field) allowed the liquid to flow around the bead bed. In contrast, when a pair of magnets was used, the extended bead bed occupied a large fraction of the channel. Based on a small available cross-section area, the liquid achieved higher linear velocity in the bed zone and dragged a large fraction of beads towards the outlet. We also found that the Protein A beads, pre-coated with anti-human CD3, showed a much lower tendency to stick on the glass surface. They were quantitatively transported to the capture area and then to the outlet reservoir. In conclusion, for all on-chip experiments, the Protein A beads were first coated with anti-human CD3, introduced into the channel at a flow rate of 50  $\mu\text{L}/\text{min}$  (linear velocity of 38 mm/s) and captured using only one magnet. Although higher velocities can be used, 50  $\mu\text{L}/\text{min}$  allowed beads introduction in less than 30 s.

The optimal flow rate for cell capture was determined by introducing samples of 1  $\mu\text{L}$  Jurkat cell suspension ( $6.0 \times 10^5$  cells/mL, 93 % viability) from each reservoir A and B. As observed through the microscope, the cells were easily captured when flow rates of 0.1 – 1  $\mu\text{L}/\text{min}$  were used. As the flow rate was increased above 1  $\mu\text{L}/\text{min}$  some cells started to wash away, the short time of contact with the beads, or the higher shear rate not allowing them to be trapped. The fraction of captured cells continued to decrease as the flow rate was further increased. However, a precise quantification was not possible because the large number of opaque beads masked the captured cells, making cell counting impossible. Based on these experiments performed with a Jurkat cell suspension, the flow rate used for T cell capture from blood was established at 0.25  $\mu\text{L}/\text{min}$ , about four times lower than the maximal value usable for the relatively dilute Jurkat cell suspension that was tested. For easy comparison, this flow rate was employed for all experiments performed on the Y-device. The value corresponded to an estimated linear velocity of 190  $\mu\text{m}/\text{s}$  for cells inside the channel.

A 2  $\mu\text{L}$  human blood sample was introduced into both inlets of the Y-device, following formation of the bead bed, and cells were captured as described in section 3.2.3.1. Cells collected from the device were then analyzed by PCR. DNA from the cells was captured on Dynabeads and analyzed along with a set of standards. The standards were prepared off-chip using different volumes of the same blood sample (volumes

representing between 25% and 200% of the sample volume analyzed on-chip). This is a relative standard, as it is the same blood sample used for sample and standards. This set of standards provides a measure of the PCR performance as a function of the total number of T cells in a given blood aliquot. It also allows a comparison of the signal obtained from cells captured on-chip with those analyzed directly in the blood, providing a measure of the chip capture efficiency. A T cell receptor  $\gamma$  gene was amplified simultaneously from sample and standards using PCR (35 cycles, method A) and the product was then analyzed by CGE, using an electric field of 185 V/cm. The peak obtained using method A to amplify the chip-captured sample is presented in the electropherogram in Figure 3.6.

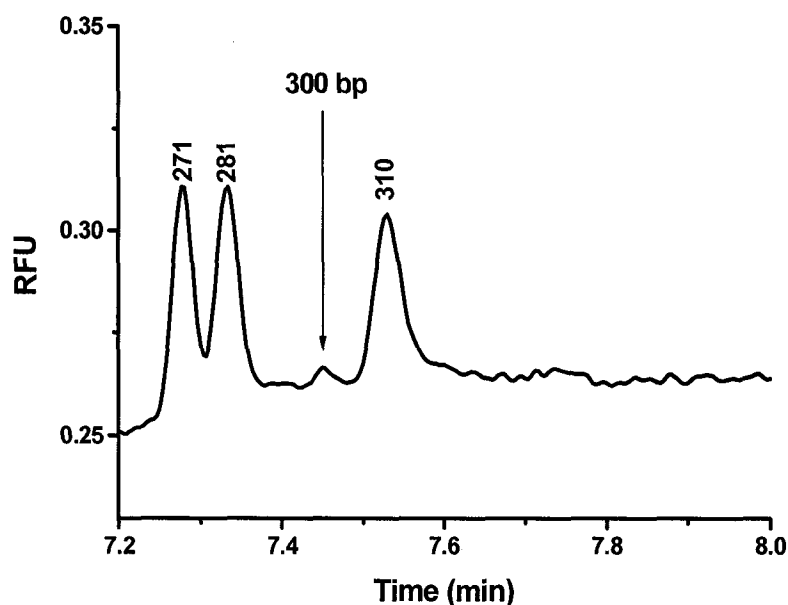


**Figure 3.6:** Electropherogram of 300 bp PCR product obtained following method A for PCR amplification. Cell separation from 2  $\mu$ l of blood was performed on a Y-device (70  $\mu$ m depth), followed by off-chip extraction of DNA. DNA ladder ( $\Phi$ X 174 RF DNA/Hae III fragments) was used and CGE separation was performed at 185 V/cm.

Figure 2.4a showed characterization of the PCR assay, using various quantities of whole blood, containing between 25% and 200% of the T cells analyzed on-chip. Comparison between the peak height obtained from sample analyzed on-chip (Figure 3.6) and blood sample standards (Figure 2.4a) indicated the sample captured on-chip had a T cell content similar to that of 0.5 to 1  $\mu$ l volume of blood. Since 2  $\mu$ l of blood were actually introduced on-chip, this study indicated the T cell capture efficiency on-chip was

between 25 and 50 %. However, the values are only estimates, since a matrix effect could be involved in the values obtained. The Protein A beads, present only in the sample analyzed on-chip, were not removed prior to performing PCR amplification, and these beads do reduce PCR efficiency as discussed in Chapter 2. The beads were removed in subsequent experiments.

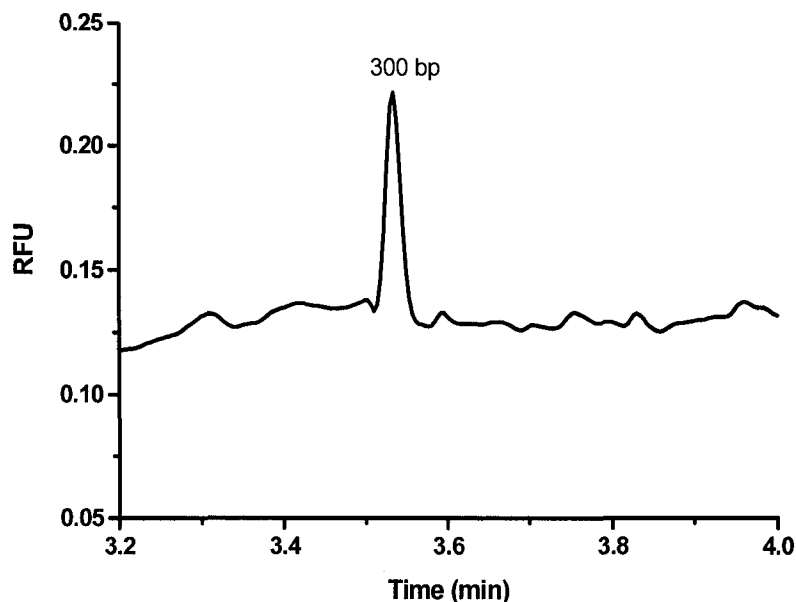


**Figure 3.7:** Electropherogram of 300 bp PCR product obtained using method B for PCR amplification. Cell separation from 2  $\mu$ l of blood was performed on a Y-device (70  $\mu$ m depth), followed by off-chip extraction of DNA. CGE separation was performed at 370 V/cm.

The study described above was performed prior to fully optimizing the off-chip PCR procedure. It was repeated using the optimized method B, with a 2  $\mu$ L human blood sample, containing about 3400 T cells. The peak obtained using method B is presented in the electropherogram (370 V/cm) in Figure 3.7. The peak height was  $0.2266 \pm 0.019$  RFU. The log-log correlation graph of peak height versus the volume of blood used is shown in Figure 3.8. Peak height values used in the calculations are an average of three or four electropherograms. The equation obtained from the standard curve was:

$$\text{Log [Peak height (RFU)]} = -0.577 + 0.868 \log [\text{Volume of blood } (\mu\text{L})] \quad (3.1)$$

Significant improvements in signal were associated with the optimized method B. Based on equation 3.1, the on-chip cell capture corresponded to 0.835  $\mu$ L of blood. However, because 2  $\mu$ L of blood were actually introduced into the chip, the capture

efficiency was apparently  $42 \pm 4 \%$ . The 4 times increase in peak height obtained with method B (compared with method A) from the 0.5  $\mu\text{L}$  blood standard suggests that the 2  $\mu\text{L}$  blood sample analyzed on-chip can be reduced to 0.5  $\mu\text{L}$  for these analyses.

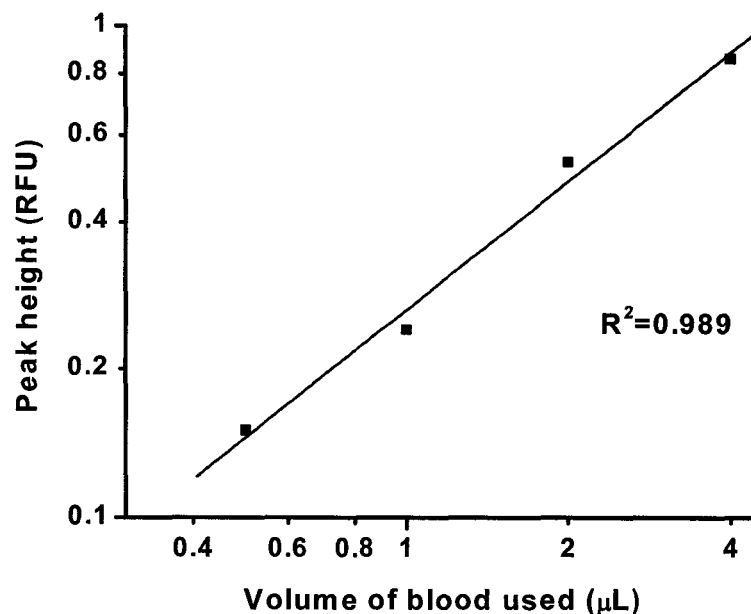


**Figure 3.8:** Correlation graph presenting peak height versus volume of blood used on a log-log plot. DNA was extracted off-chip from 0.5, 1, 2 and 4  $\mu\text{L}$  of human blood and amplified by PCR following method B. CGE separation was performed at 370 V/cm.

### 3.3.3 Jurkat Cell Separation from Reconstituted Blood Performed on FAT 3000 Device

#### 3.3.3.1 Experiment 1 Performed on All Eight Manifolds of the FAT 3000 Device

The capture efficiency of the FAT 3000 device was also tested using method C (section 2.2.3.4) for PCR amplification and reconstituted horse blood samples, with well defined T-cell content. Samples of 2  $\mu\text{L}$  (containing 1070 Jurkat cells) were withdrawn from reconstituted blood ( $5.4 \times 10^5$  Jurkat cells/mL and  $5.0 \times 10^9$  horse red blood cells/mL, 1: 9300 ratio) and introduced into each channel at calculated linear velocities between 250 and 320  $\mu\text{m/s}$ . These velocities can be contrasted with 190  $\mu\text{m/s}$  calculated for Y-intersection device. After collection of the captured cells, their DNA was captured on Dynabeads. The chip-isolated samples were analyzed along with a set of horse blood standards, as described in section 3.2.3.2. Standards contained between 10% and 100% of



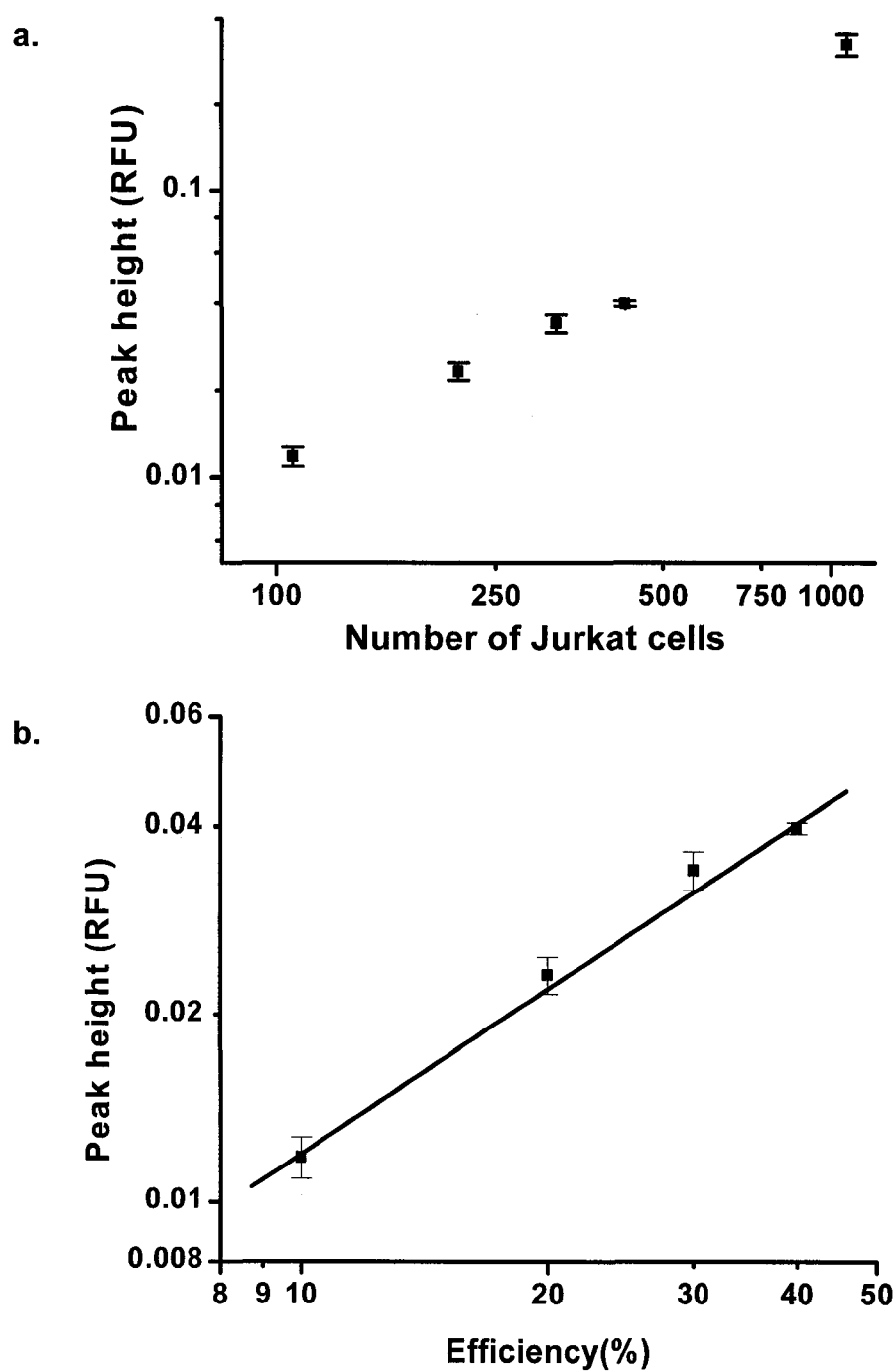


**Figure 3.9:** Characterization of the PCR amplification with method C using as standards DNA extracted from different volumes of a reconstituted blood sample. Separation was performed at 370 V/cm.

- Peak height versus the number of Jurkat cells used (107, 214, 321, 428 and 1070) presented on a log-log plot;
- Peak height versus capture efficiency plot derived from the linear part of graph (a).

the T cells analyzed on-chip and were prepared from the same cell suspension. A T cell receptor  $\gamma$  gene was amplified simultaneously from sample and standards using PCR (36 cycles) and the product was then analyzed by CGE, using an electric field of 370 V/cm (method C). The peak for the product was observed at about 3.6 min. Peak height values used in calculations are an average value of three or four electropherograms. The correlation graph of peak height versus the volume of blood used is shown in Figure 3.9a. The plot in figure 3.9b is derived from the linear part of the graph from Figure 3.9a (100 - 500 cells). The x-axis is expressed as 100 times the ratio of the number of cells in the standard to 1070 cells (the number in the 2  $\mu$ L samples). Plotting signal for each standard versus the ratio provides a calibration curve for the sample runs that can be used to determine the efficiency of cell capture on-chip. The equation for this line was:

$$\text{Log [Peak height (RFU)]} = -2.802 + 0.879 \text{ Log [Efficiency(\%)]} \quad (3.2)$$

Table 3.3 presents the PCR product signal intensity obtained after separation of cells in the different channel designs of the FAT 3000 device and the efficiencies calculated using equation 3.2. The comparison of results shown in Figure 3.10 illustrates that channels 3 and 8 gave the highest efficiency.

**Table 3.3:** Efficiencies obtained on all channels of the FAT 3000 device, calculated using the peak heights obtained for the 300 bp PCR peak:

Manifold	Peak height (RFU)	Efficiency (%)	Cross sectional area (mm <sup>2</sup> )	No. of channels (*n-simultaneous) (** n/2-bifurcations)
1	0.02279 $\pm$ 0.00289	21 $\pm$ 3	0.181	8 *
2	0.01712 $\pm$ 0.00203	15 $\pm$ 2	0.197	12 *
3	0.03739 $\pm$ 0.00362	37 $\pm$ 4	0.181	8 **
4	0.01821 $\pm$ 0.00071	16 $\pm$ 1	0.154	—
5	0.02759 $\pm$ 0.00333	26 $\pm$ 4	0.158	2 **
6	0.02535 $\pm$ 0.00193	24 $\pm$ 2	0.166	4 *
7	0.01973 $\pm$ 0.00151	18 $\pm$ 2	0.181	8 *
8	0.03507 $\pm$ 0.00540	34 $\pm$ 6	0.166	4 **

\* n-simultaneous refers to n-times splitting of channel at one point

\*\* n/2-bifurcations refers to repeated bifurcation of channels to produce n splittings

Cross sectional area is the area of the multiple channels after isotropic etching.

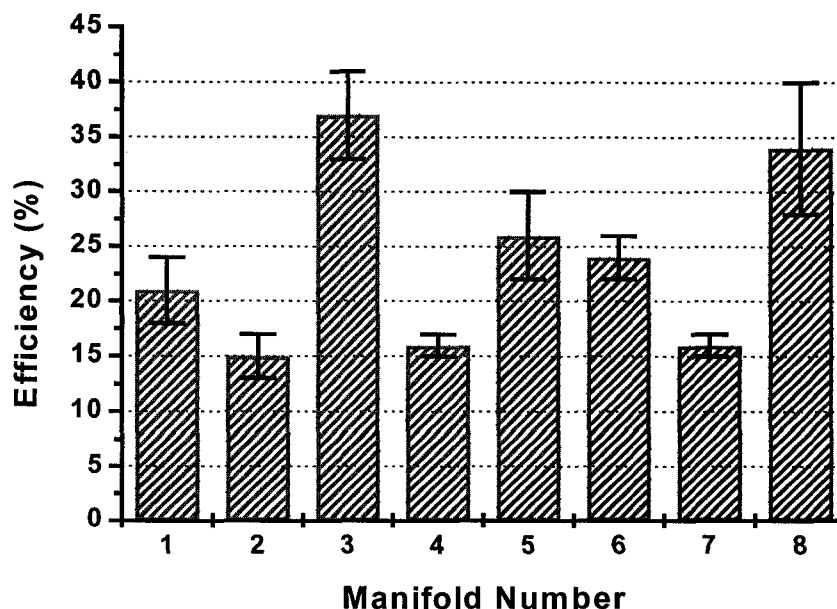


**Figure 3.10:** Capture efficiency determined from simultaneous PCR analysis of samples captured in all eight manifolds of the FAT 3000 device ( 50  $\mu\text{m}$  depth).

The FAT 3000 mask was designed for use with an anisotropic etching process. The intention was to form a master in silicon by anisotropic reactive ion etching, form a nickel relief as a secondary master and stamp parts in plastic using a hot embosser. Difficulties with that process, outlined in Chapter 5, led to our using the mask to isotropically etch patterns in glass. The 1:1 aspect ratio associated with glass etching gave cross-sections between each channel that differed slightly. Also, undercutting of manifold 2 meant that these designs did not give fully separate sealed flow paths. The resulting structures are illustrated by the cartoons in Figure 3.11. These isotropic etching features slightly complicated the interpretation of the results with these devices.

As presented in Table 3.1, there are differences of up to 28% between the cross sectional areas of the eight different channel manifolds. This will create small differences between manifolds in terms of linear flow rates with a magnitude proportional to the area differences when using a constant volumetric flow rate. Comparing the results obtained on manifolds 1, 3 and 7, which have the same cross-sectional area ( $0.181 \text{ mm}^2$ ), it can be concluded that the stepwise bifurcation design of channel 3 gives a higher efficiency than a simple splitter design, because of a more effective distribution of bead and cell flows.

The same trend was observed comparing the efficiencies obtained on manifolds 6 and 8 (cross-sectional area of  $0.166 \text{ mm}^2$ ).

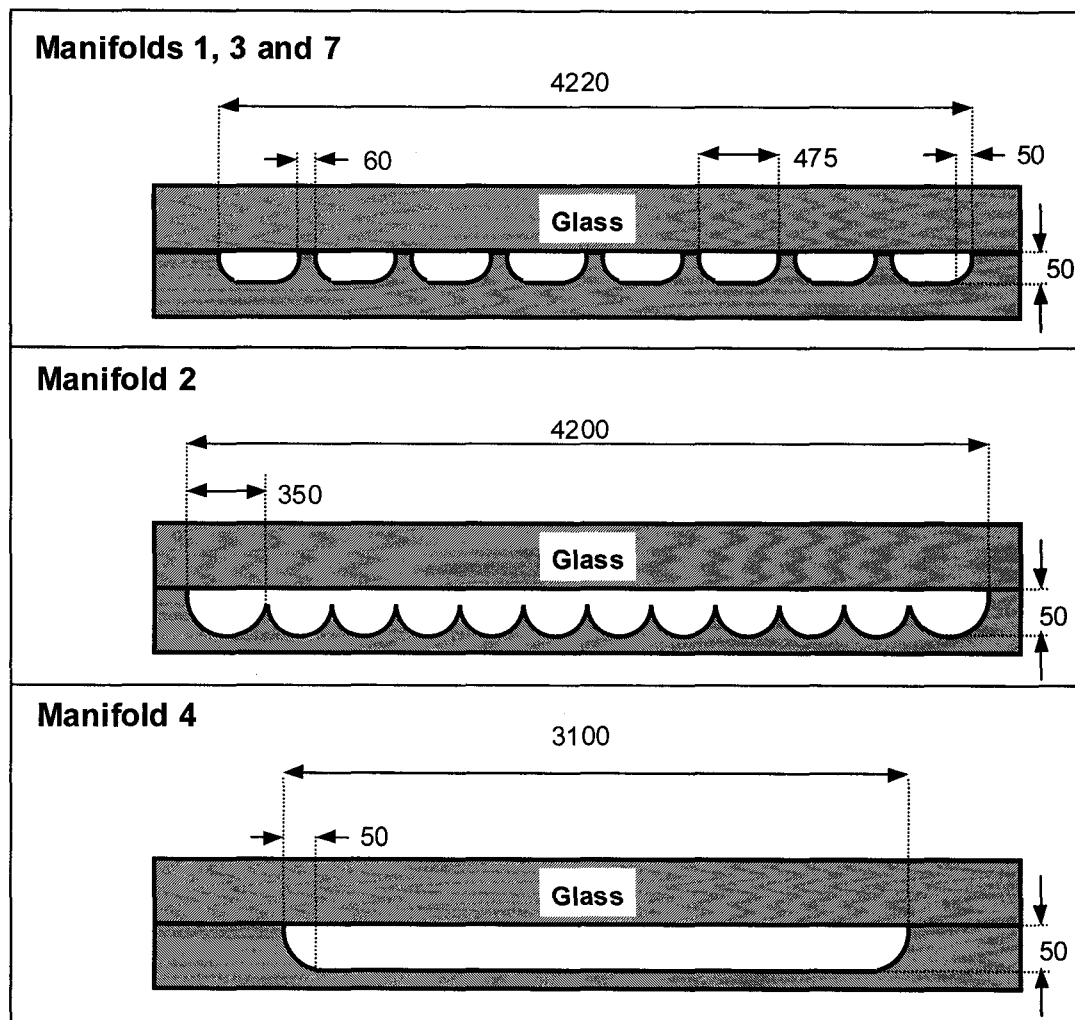


**Figure 3.11:** Cross-section profiles in the capture area of manifolds 1, 2, 3, 4 and 7 of the FAT 3000 device. Manifolds 5, 6 and 8, missing here, have similar profiles to manifolds 1, 3 and 7.

Comparing manifold 3 (cross-section area of  $0.181 \text{ mm}^2$ ) and manifold 8 (cross-section area of  $0.166 \text{ mm}^2$ ), no statistically significant difference was observed in terms of efficiency, even though the cross sectional area and linear flow rate differed by 9 %. The largest difference of 28 % in flow rate for the cross sectional areas of manifolds 2 ( $0.197 \text{ mm}^2$ ) and 4 ( $0.154 \text{ mm}^2$ ) also did not give a statistically distinguishable difference in capture efficiency. Based on the pairs of manifolds contrasted, it can be concluded that the difference in the cross-sections between the eight channels did not produce enough

change in flow rate in the capture zone to influence the capture efficiency. Therefore the differences between the manifold structures arise from the flow path geometry.

The similar values of capture efficiency obtained in manifolds 2 and 4 can be explained by considering the actual cross-section of manifold 2, presented in Figure 3.11, which is more similar after etching to a single wide channel. Because the 12 flow paths are not separated, the beads migrated towards the central region, where the magnetic field was stronger, even if initially the beads were distributed uniformly between channels. In this situation, a larger resistance to flow forced the cells to move predominantly through the side regions, at enhanced flow rates. This type of manifold is thus more similar in behavior to manifold 4, than to manifold 1, explaining the similar low capture efficiencies of both manifolds 2 and 4.

The smaller capture efficiency of manifolds 1 and 7, compared to efficiencies of manifolds 3 and 8, can be explained by there being a less uniform distribution of bead flows between the channels in 1 and 7 versus 3 and 8. Manifolds 1 and 7 have an immediate eight-times split of the flow paths at the entrance, whereas manifolds 3 and 8 use repeated bifurcations to split the flow. The latter design ensures each of the two paths downstream of a split will have the same linear velocity profile at their entrance. In contrast the eight-times split will see a higher flow rate at the center channels than at the sides. This flow rate difference could be expected to lead to a difference in the amount of beads trapped in each channel. Once the beads were introduced into the channels, the cells would flow predominantly through the less filled channels, where the resistance to flow was reduced. The low abundance of beads in those channels may lead to a reduced capture rate. Or it may be that the flow rate through those channels was increased enough to reduce the capture efficiency.

Comparing the efficiencies obtained with manifolds 5, 6 and 7, which have the same eight-times splitting scheme, it can be concluded that splitting in a larger number of channels increased the non-uniformity of the magnetic beds obtained and the non-uniformity of the flow rate between channels, reducing the efficiency. In contrast, for the stepwise flow bifurcation of manifolds 3 and 8, an increased number of bifurcated channels slightly favored the formation of uniform magnetic beds.

### 3.3.3.2 Experiment 2 Performed on Four Manifolds of the FAT 3000 Device

The capture efficiency study was repeated on manifolds 1, 3, 4 and 6 to determine the reproducibility of our results between different runs. Samples of 1  $\mu\text{L}$  containing 890 Jurkat cells were aliquoted from reconstituted blood ( $8.9 \times 10^5$  Jurkat cells/mL and  $8.9 \times 10^9$  horse red blood cells/mL, 1: 10000 ratio). Cells were captured on-chip, then transferred for PCR (method C) as described in section 2.2.3.4. A set of reconstituted blood standards was also analyzed by PCR as described in section 3.2.3.2b. Standards contained between 15 % and 200% of the T cells analyzed on-chip. Peak height values used in calculations are an average of three or four electropherograms. A set of PCR calibrations runs were performed at the same time as the PCR sample runs. Efficiencies were calculated based on one 1  $\mu\text{L}$  sample analyzed on manifold 1 and two 1  $\mu\text{L}$  samples analyzed on manifolds 3, 4 and 6. Figure 3.12 shows the capture efficiencies calculated based on the new calibration curve (experiment 2), plotted with the values obtained previously (experiment 1). Differences between the new and old efficiency values were between 3% on manifold 3 and 7% on manifold 6, but a similar trend was observed.

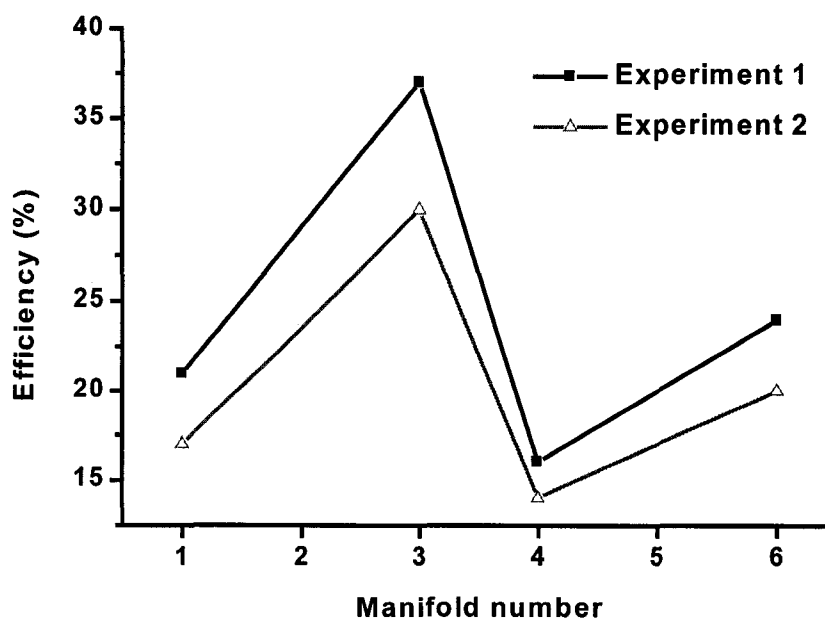


**Figure 3.12:** Capture efficiency determined in different experiments for manifolds 1, 3, 4 and 6 of the FAT 3000 device. The 300 bp PCR product obtained following method C for PCR amplification was separated at 370 V/cm (section 3.2.4.2b).

Figure 3.13 shows the efficiencies obtained simultaneously amplifying 1  $\mu\text{L}$  samples captured sequentially on one manifold. As before, the best efficiency was obtained on manifold 3 and the lowest on manifold 4. Differences in efficiency between samples analyzed on the same channel were between 1% on manifold 4 and 9% on manifold 3.

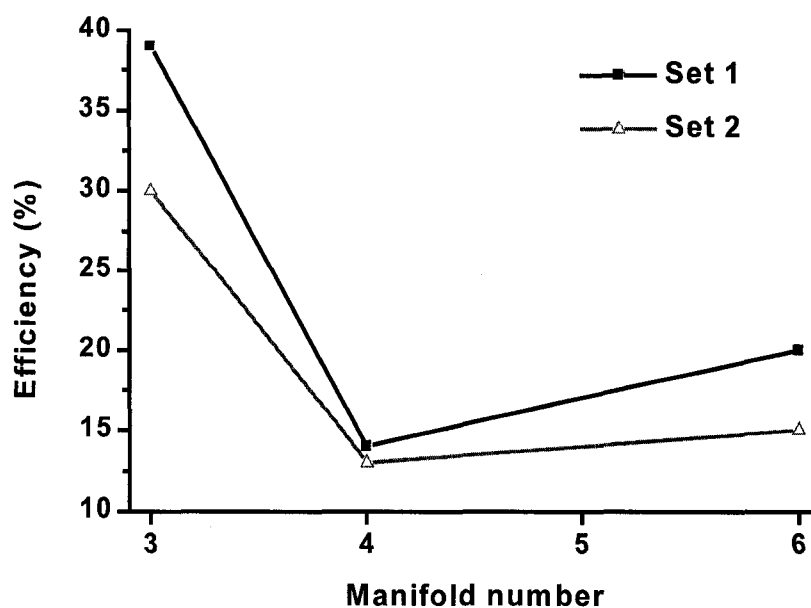


**Figure 3.13:** Capture efficiency determined for different samples processed in the same experiment on manifolds 3, 4 and 6 of the FAT 3000 device. The 300 bp PCR product obtained following method C for PCR amplification was separated at 370 V/cm (section 3.2.4.2b).

The results clearly suggest that the stepwise flow bifurcation design of manifolds 3 and 8 more effectively distributes the flow of cells and beads into each of the channels, than does the simple design of manifolds 1, 6 and 7. The poor performance of a single, wide channel shows that narrower channels are much more useful in structuring dense enough magnetic bead beds to trap the cell streams.

### 3.4. Conclusions

A capture efficiency of 42 % was determined using the Y-intersection device, which had a cross sectional area of  $2.17 \times 10^{-2} \text{ mm}^2$  in the main channel, and used a volume flow rate of 0.25  $\mu\text{L}/\text{min}$ . To reduce the analysis time by 50 % at the same flow rate value, the sample was introduced from both reservoirs, A and B simultaneously, after

first introducing the beads to the device. The simple Y-device offered a first platform for studying on-chip blood sample preparation for genetic analysis and provided guidance for designing of the new FAT 3000 device. The time of 30 min requested for loading 2  $\mu$ L in the Y-device was too long. As a result we recognized a need to make a much larger volume channel. The time required to capture cells from the same volume of sample (2  $\mu$ L) was reduced 10 times to 3 min in the subsequent FAT 3000 design. A single inlet reservoir was designed in an effort to ease the sample introduction and minimize the analysis time. Testing the eight different splitting manifold designs permitted us to establish that the stepwise flow bifurcation of manifolds 3 and 8 was the best option available. The capture efficiency obtained with manifold 3, with eight channels after three bifurcations was 37 %.

Our results indicate that magnetic bead bed can be used on chip to capture cells that are present in a 1:10000 ratio and that the material can be recaptured from the chip for further analysis. Blood samples can be introduced directly into the chips without any prior preparation. Using the presented approach there is no need to include a separate mixing step of the beads with the cells. The beads can be introduced into the channel before obtaining the blood sample, simplifying the process for a user. Since Protein A has a high affinity for many types of IgG, our approach can be adapted to many different types of antigenic determinants by varying the bound antibody. This will allow an easy transfer of this method to separate a different type of human cell or bacterial cell from human blood. However, since the Protein A beads will bind endogenous antibodies in the blood sample there is the possibility other components of the blood could also be captured. Such interfering effect would have to be examined in more detail. Alternatively, the antibody of interest could be immobilized in a less generic manner using standard methods.

### 3.5 References

- [1] Akane, A.; Matsubara, K.; Nakamura, H.; Takahashi, S.; Kimura, K. *Forensic Sci.*, **1994**, *39*, 362-372.
- [2] Al-Soud, W. A.; Radstrom, P. *J. Clin. Microbiol.*, **2001**, *39*, 485-493.



- [3] Singleton, P. *DNA methods in clinical microbiology*, Kluwer Academic Publishers: Dordrecht, The Netherlands **2000**.
- [4] Zeiller, K.; Liebich, H. G.; Hannig, K. *Eur J Immunol*, **1971**, *1*, 315-322.
- [5] Huang, Y.; Joo, S.; Duhon, M.; Heller, M.; Wallace, B.; Xu, X. *Anal Chem*, **2002**, *74*, 3362-3371.
- [6] Vykoukal, J.; Yang, J.; Becker, F. F.; Gascoyne, P. R. C.; Krulevitch, P.; Ackler, H.; Hamilton, J. In *Micro Total Analysis Systems*; A. van den Berg; W. Olthuis; P. Bergveld, eds.; Kluwer Academic Publisher: Enschede, The Netherlands, **2000**, pp. 127-130.
- [7] Gascoyne, P. R. C.; Vykoukal, J.; Weinstein, R.; Gandini, A.; Parks, D.; Sawh, R. In *Micro Total Analysis Systems*; Yoshinobu Baba; Shuichi Shoji; Albert van den Berg, eds.; Kluwer Academic Publisher: Nara, Japan, **2002**; Vol. 2, pp. 323-325.
- [8] Altendorf, E.; Zebert, D.; Holl, M.; Vannelli, A.; Wu, C.; Schulte, T. In *Micro Total Analysis Systems 1998*; D. Jed Harrison; Albert van den Berg, eds.; Kluwer Academic Publisher: Banff, Canada, **1998**, pp. 73-76.
- [9] Wolff, A.; Larsen, U. D.; Blankenstein, G.; Philip, J.; Telleman, P. In *Micro Total Analysis Systems*; D. Jed Harrison; Albert van den Berg, eds.; Kluwer Academic Publisher: Banff, Canada, **1998**, pp. 77-80.
- [10] Telleman, P.; Larsen, U. D.; Philip, J.; Blankenstein, G.; Wolff, A. In *Micro Total Analysis Systems*; D. Jed Harrison; Albert van den Berg, eds.; Kluwer Academic Publisher: Banff, Canada, **1998**, pp. 39-44.
- [11] Gawad, S.; Schild, L.; Renaud, P. *Lab on a Chip*, **2001**, *1*, 76-82.
- [12] Cabuz, C.; Padmanabhan, A.; Fritz, B.; Cabuz, E.; Schwichtenberg, J.; Reutiman, P.; Demers, B.; Rezachek, T.; Satren, E.; Battrell, F. In *Micro Total Analysis Systems*; Yoshinobu Baba; Shuichi Shoji; Albert van den Berg, eds.; Kluwer Academic Publishers: Nara, Japan, **2002**; Vol. 2, pp. 646-648.
- [13] Fu, A. Y.; Spence, C.; Scherer, A.; Arnold, F. H.; Quake, S. R. *Nat Biotechnol*, **1999**, *17*, 1109-1111.
- [14] Krüger, J.; Singh, K.; O'Neill, A.; Jackson, C.; Morrison, A.; O'Brien, P. *J. Micromech. Microeng.*, **2002**, *12*, 486-494.
- [15] Wilding, P.; Kricka, L. J.; Cheng, J.; Hvichia, G.; Shoffner, M. A.; Fortina, P. *Anal Biochem*, **1998**, *257*, 95-100.
- [16] Cheng, J.; Sheldon, E. L.; Wu, L.; Uribe, A.; Gerrue, L. O.; Carrino, J.; Heller, M. J.; O'Connell, J. P. *Nat Biotechnol*, **1998**, *16*, 541-546.
- [17] Huang, Y.; Ewalt, K. L.; Tirado, M.; Haigis, R.; Forster, A.; Ackley, D.; Heller, M. J.;

- O'Connell, J. P.; Krihak, M. *Anal Chem*, **2001**, *73*, 1549-1559.
- [18] Cheng, J.; Shoffner, M. A.; Hvichia, G. E.; Kricka, L. J.; Wilding, P. *Nucleic Acids Res*, **1996**, *24*, 380-385.
- [19] Obeid, P. J.; Christopoulos, T. K.; Crabtree, H. J.; Backhouse, C. J. *Anal Chem*, **2003**, *75*, 288-295.
- [20] Lenigk, R.; Liu, R. H.; Athavale, M.; Chen, Z.; Ganser, D.; Yang, J.; Rauch, C.; Liu, Y.; Chan, B.; Yu, H.; Ray, M.; Marrero, R.; Grodzinski, P. *Anal Biochem*, **2002**, *311*, 40-49.
- [21] Zammateo, N.; Hamels, S.; De Longueville, F.; Alexandre, I.; Gala, J. L.; Bresseur, F.; Remacle, J. *Biotechnol Annu Rev*, **2002**, *8*, 85-101.
- [22] Trau, D.; Lee, T. M.; Lao, A. I.; Lenigk, R.; Hsing, I. M.; Ip, N. Y.; Carles, M. C.; Sucher, N. J. *Anal Chem*, **2002**, *74*, 3168-3173.
- [23] Fortina, P.; Surrey, S.; Kricka, L. J. *Trends Mol Med*, **2002**, *8*, 264-266.
- [24] Schneegass, I.; Kohler, J. M. *J Biotechnol*, **2001**, *82*, 101-121.
- [25] Hong, J. W.; Fujii, T.; Seki, M.; Yamamoto, T.; Endo, I. *Electrophoresis*, **2001**, *22*, 328-333.
- [26] Giordano, B. C.; Ferrance, J.; Swedberg, S.; Huhmer, A. F.; Landers, J. P. *Anal Biochem*, **2001**, *291*, 124-132.
- [27] Kurian, K. M.; Watson, C. J.; Wyllie, A. H. *J Pathol*, **1999**, *187*, 267-271.
- [28] Woolley, A. T.; Lao, K.; Glazer, A. N.; Mathies, R. A. *Anal Chem*, **1998**, *70*, 684-688.
- [29] Tillib, S. V.; Strizhkov, B. N.; Mirzabekov, A. D. *Anal Biochem*, **2001**, *292*, 155-160.
- [30] Tang, T.; Badal, M. Y.; Ocvirk, G.; Lee, W. E.; Bader, D. E.; Bekkaoui, F.; Harrison, D. J. *Anal Chem*, **2002**, *74*, 725-733.
- [31] Strizhkov, B. N.; Drobyshv, A. L.; Mikhailovich, V. M.; Mirzabekov, A. D. *Biotechniques*, **2000**, *29*, 844-854.
- [32] Effenhauser, C. S.; Bruin, G. J.; Paulus, A. *Electrophoresis*, **1997**, *18*, 2203-2213.
- [33] Jiang, G.; Harrison, D. J. *Analyst*, **2000**, *125*, 2176-2179.
- [34] Weigl, B. H.; Bardell, R. L.; Kesler, N.; Morris, C. J. *Fresenius J Anal Chem*, **2001**, *371*, 97-105.
- [35] Kopp, M. U.; Mello, A. J. n. d.; Manz, A. *Science*, **1998**, *280*, 1046-1048.
- [36] Lagally, E. T.; Simpson, P. C.; Mathies, R. A. *Sens. Actuators B*, **2000**, *63*, 138-146.
- [37] Liu, Y.; Ganser, D.; Schneider, A.; Liu, R.; Grodzinski, P.; Kroutchinina, N. *Anal Chem*, **2001**, *73*, 4196-4201.
- [38] Woolley, A. T.; Hadley, D.; Landre, P.; deMello, A. J.; Mathies, R. A.; Northrup, M. A. *Anal Chem*, **1996**, *68*, 4081-4086.

- [39] Khandurina, J.; McKnight, T. E.; Jacobson, S. C.; Waters, L. C.; Foote, R. S.; Ramsey, J. M. *Anal Chem*, **2000**, *72*, 2995-3000.
- [40] Fan, Z. H.; Mangru, S.; Granzow, R.; Heaney, P.; Ho, W.; Dong, Q.; Kumar, R. *Anal. Chem.*, **1999**, *71*, 4851-4859.
- [41] Heller, M. J. *Annu Rev Biomed Eng*, **2002**, *4*, 129-153.
- [42] Goubault, C.; Viovy, J.-L.; Bibette, J. In *Micro Total Analysis Systems*; Yoshinobu Baba; Shuichi Shoji; Albert van den Berg, eds.; Kluwer Academic Publisher: Nara, Japan, **2002**; Vol. 2, pp. 844-846.
- [43] Ahn, C. H.; Allen, M. G.; Trimmer, W.; Jun, Y.-N.; Erramilli, S. *J. Microelectromech. Syst.*, **1996**, *5*, 151-158.
- [44] Choi, J.-W.; Ahn, C. H.; Bhansali, S.; Henderson, H. T. *Sens. Actuators B*, **2000**, *68*, 34-39.
- [45] Choi, J. W.; Liakopoulos, T. M.; Ahn, C. H. *Biosens. Bioelectron.*, **2001**, *16*, 409-416.
- [46] Choi, J.-W.; Oh, K. W.; Han, A.; Wijayawardhana, C. A.; Lannes, C.; Bhansali, S.; Schlueter, K. T.; Heineman, W. R.; Halsall, H. B.; Nevin, J. H.; Helmicki, A. J.; Henderson, H. T.; Ahn, C. H. *Biomed. Microdevices*, **2001**, *3*, 191-200.
- [47] Salimi-Moosavi, H.; Szarka, R.; Andersson, P.; Smith, R.; Harrison, D. J. In *Micro Total Analysis Systems*; D. Jed Harrison; Albert van den Berg, eds.; Kluwer Academic Publisher: Banff, AB, Canada, **1998**, pp. 69-72.

## CHAPTER 4: Microfabricated Electrolysis Pump System for Isolating Rare Cells in Blood \*♦

### 4.1 Introduction

The preparation of biological samples for analyses such as immunoassays or genetic assays within microfluidic devices would greatly contribute to the automation of analytical procedures, yet remains a significant challenge. The relatively large volumes of sample that are required to minimize sampling error for low concentrations of a pathogen mean that electrokinetic pumping methods do not have the required capacity. While a variety of designs of mechanical micropumps with higher capacity have been tested [1-3], the most widespread approach uses a diaphragm actuated by means of electrostatic, piezoelectric, or thermal expansion mechanisms. The fabrication of membrane or diaphragm based pumps is often complex, involving many photolithographic steps. The complexity makes the cost high for use with biological sample preparation, which often requires single use, disposable components. Further, very few of those pumps have been tested with biological fluids, and we have found no reports of blood samples being mobilized with a micropump. Since pumping blood is much more challenging than most fluids, this remains a significant test for a micropump.

Electrochemical production of gas bubbles by electrolyzing water provides an actuation mechanism that can deliver high displacement volumes relative to the size of the device. The electrolysis of water to actuate a diaphragm has been described and used in several applications [4, 5]. For example, a wrist-worn infusion pump has been developed for a drug delivery system [6], and electrolysis was used to provide a H<sub>2</sub>/O<sub>2</sub> gas mixture to feed a flame ionization detector [7]. Recently, a group at the University of Twente [8, 9] described a microfabricated electrochemical pump, in which gas formed by

---

\* A version of this chapter was published:

V. I. Furdui, J. K. Kariuki and D. J. Harrison, *J. Micromech. Microeng.* **2003**, 13, S164-S170

♦ The experimental data, acquired in this study and described in this chapter, would not have been obtained without the participation of James K. Kariuki. He designed the electrodes mask, sputtered the electrodes on glass substrates and anodically bonded some Si-glass devices. James K. Kariuki fabricated the Si wafers using my optimized Bosch procedure and helped me to test the devices.

electrolysis directly displaced solvent to form a bubble pump. Low voltages were applied to a sample electrolyte solution located in the pump chamber in order to pump sample loaded in a meander attached to the pump chamber. Flow rates up to 2  $\mu\text{L}/\text{min}$  were achieved [8]. The device fabrication process required only two mask steps, and could ultimately be adapted to low cost fabrication in plastic.

Here we describe the adaptation of the Twente electrolysis micropump to the manipulation and initial processing of a blood sample. Our goal was a device that would deliver blood to a processing zone on chip where rare cells could be captured, and purified by washing away the remaining blood components, followed by delivery of the isolated cells from the chip for analysis. Immunomagnetic cell separation methods [10-12] were used to trap cells inside the micro flow channels [13]. Rare cells were captured on antibody coated magnetic beads [14, 15], which were then trapped by a magnetic field in a region within the chip. A pair of electrolysis chambers was designed to work in a stepwise fashion to first deliver blood, and then the wash buffer needed to purify the rare cells. As described in this report, to accomplish these goals we increased the electrolysis chamber and the sample meander capacity from 1.5 to 7.5  $\mu\text{L}$ . The initial Twente design was difficult to fill, allowing the introduction of only one liquid, and so we also developed a system of access holes for the device along with a procedure that greatly eases filling. Successful testing of the design with reconstituted blood samples has shown that it could ultimately serve as the first stage of a more complex analytical system, providing the initial sample cleanup stage required by a micro total analysis system ( $\mu\text{-TAS}$ ) for clinical diagnostic applications.

## **4.2 Experimental Section**

### **4.2.1 Fabrication**

The reservoirs, channels and chevrons of the design shown in Figure 4.1a and Figure 4.2 were etched on a silicon wafer (100 mm diam, 500-550  $\mu\text{m}$  thick, 1-20  $\Omega\text{ cm}$  resistivity, p type; Silicon Valley Microelectronics, San Jose, CA, USA) to a nominal depth of 100  $\mu\text{m}$  using deep reactive ion etching (DRIE). An Oxford Instruments Series 100 DRIE (Bristol, UK) operating the Bosch process with an ICP power of 450 W was used. Etching was done at 25 W for 25 s ( $\text{SF}_6$  flow rate 75 sccm), followed by 10 W for

8 s ( $C_4F_8$  flow rate 50 sccm) during the polymer deposition step. Between 70-80 cycles were needed to etch a depth of 100  $\mu\text{m}$ . Nominal channel widths were 300  $\mu\text{m}$  for the sample and buffer meander reservoirs and 600  $\mu\text{m}$  for the main channel. Typical depths of 103 – 105  $\mu\text{m}$  were measured with an Alphastep profilometer (KLA-Tencor, San Jose, CA, USA), and widths of 600 – 640  $\mu\text{m}$  were determined by profilometry and by optical microscopy. The filling holes (800  $\mu\text{m}$  diam.) were drilled in the silicon wafer, using a jewelers drill and diamond coated drill bits (Lee Valley, Ottawa, ON, Canada), giving about 0.2  $\mu\text{L}$  volumes in these ports. To isolate the electrodes from the Si substrate, a 200 nm thermal oxide was grown in a quartz tube furnace at 900°C in water vapor saturated flowing nitrogen for 2 h.

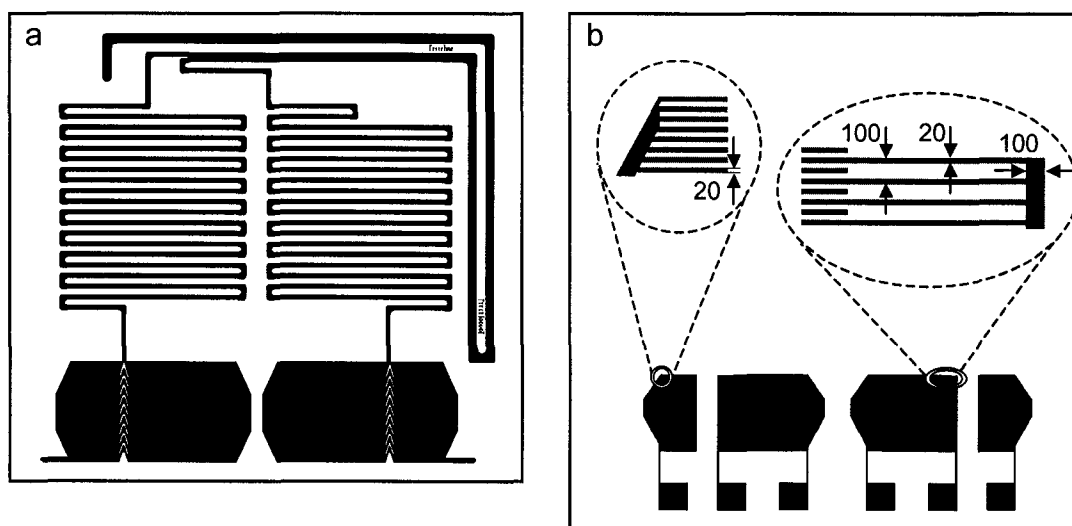


**Figure 4.1:** Mask design for the Si die (a) and the glass cover plate (b).  
 a) Channels were either 300 or 600  $\mu\text{m}$  wide, as illustrated by two different line widths;  
 b) Design of the interdigitated electrodes with details showing dimensions in  $\mu\text{m}$ .

A 25 nm thick titanium adhesion layer was sputtered (Leskar, magnetron system) on a Schott borofloat glass wafer, followed by a 150 nm thick platinum layer. The glass was cleaned in piranha (3:1 mixture of  $H_2SO_4:H_2O_2$ ) for 15 min, then rinsed in nanopure water. The electrodes drawn in Figure 4.1b were patterned by photolithography using positive HPR 504 photoresist (Arch Chem., Norwalk, CT, USA) and a lift-off process. The wafer was sonicated in acetone for 6-8 h to obtain lift-off. Annealing the glass cover plates after patterning the Ti/Pt electrodes was required to prevent electrode delamination in the first 30 min of use. Each electrode area was 9.83  $\text{mm}^2$ .

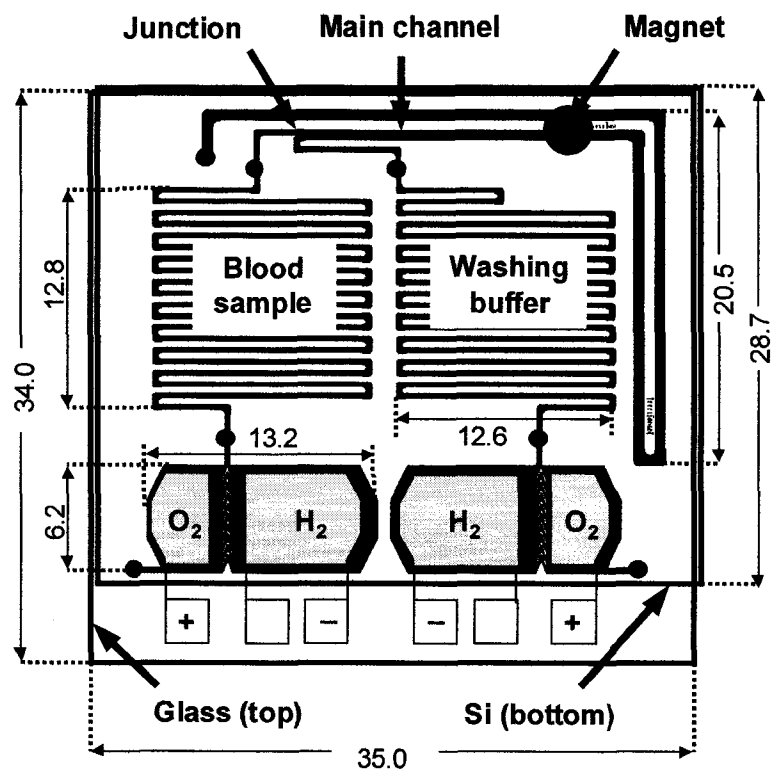


**Figure 4.2:** Drawing of the Si die and the larger glass cover plate, showing dimensions of various flow channels in mm. Channels were  $\sim 103 \mu\text{m}$  deep, and either  $300$  or  $600 \mu\text{m}$  wide, as illustrated by two different line widths. Analyte and catholyte compartments are illustrated with labels showing the gases generated.

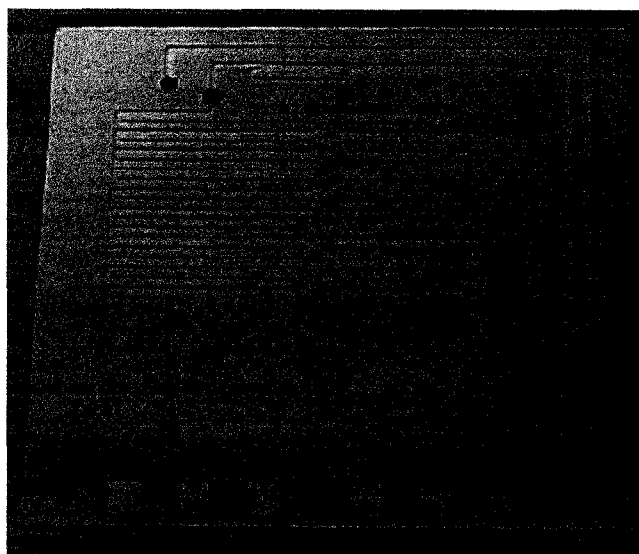


**Figure 4.3:** Image of the integrated device obtained by anodic bonding of the silicon die to the glass cover plate.

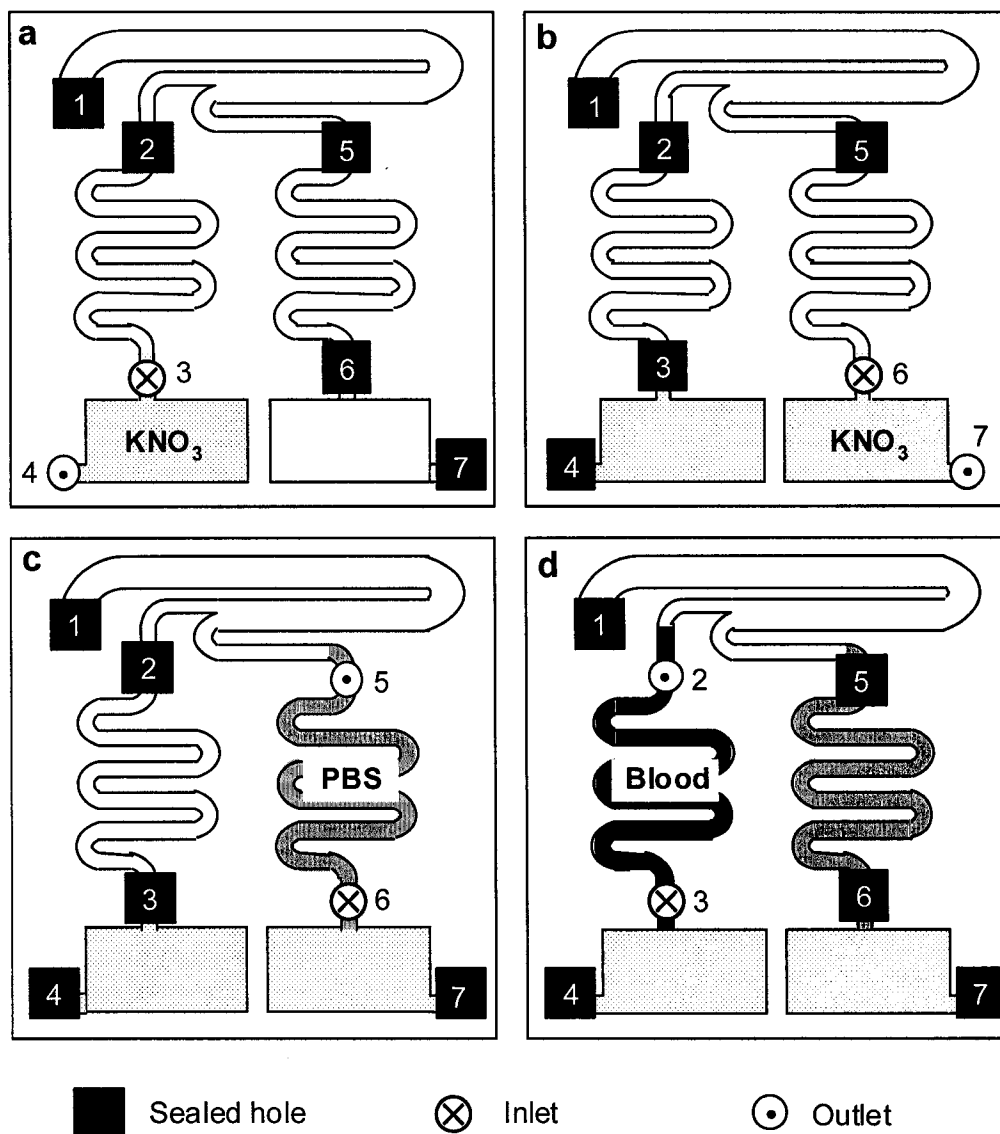


**Figure 4.4:** Scheme for filling the various chambers within the chip, showing which access holes were blocked at each stage. Access holes are marked by numbers for reference in the text. Sealed holes are shown with black squares, flow inlet is marked by a cross, and flow outlet by a dot. Step (a) and (b), filling the electrolysis chambers; step (c), filling the wash buffer meander; step (d), filling the blood sample meander. Tape was used to cover the holes, with one piece placed over several holes to reduce handling effort.

Anodic bonding of glass to Si was performed on diced dies using 1000 to 1500 V, at 300 to 400°C [9]. Complete bonding required 10 to 15 minutes. Contact wires were glued onto the bonding pads using a conductive epoxy (Chemtronics, Kennesaw, GA,



USA). Epoxy glue was applied where the metal leads passed out of the electrolysis chambers, to prevent any leakage due to poor bonding over top of the electrodes.

#### 4.2.2 Operation and Measurement Procedures

Devices were filled with three different liquids in sequence using a syringe pump or a 10  $\mu\text{L}$ -micropipet with a “gel-loading” micro-capillary tip (O.D. = 0.61 mm, cat. no. F103-10, Rose Scientific Ltd., Edmonton, AB, Canada). The numbering of the access holes and the filling sequence is shown in Figure 4.4. Insulating tape (Scotch Super 33 vinyl electrical tape, 3M, USA) was used to temporarily seal various holes during filling. When using a syringe pump, the electrolysis pump chambers were filled with 0.5 M  $\text{KNO}_3$  infused at 100  $\mu\text{L}/\text{min}$  into the first chamber through access hole 3, with holes 1, 2, 5, 6 and 7 sealed, and then through hole 6, with holes 1, 2, 3, 4 and 5 sealed. Hole 7 was then sealed and hole 5 was opened to infuse 40  $\mu\text{L}$  of Dulbecco’s PBS 14190 (1x) buffer (Life Tech., Rockville, Maryland, USA) through hole 6 at 50  $\mu\text{L}/\text{min}$ . Holes 5 and 6 were then sealed and holes 2 and 3 were opened to allow delivery of reconstituted horse blood through hole 3 at 50  $\mu\text{L}/\text{min}$ . All the holes were then kept sealed until access hole 1 was opened at the start of the experiment. When using a micropipet the same filling sequence was employed, but 10  $\mu\text{L}$  was delivered at each step.

Reconstituted horse blood samples were prepared, containing  $5.5 \times 10^5$  Jurkat cells/mL and  $1.0 \times 10^{10}$  horse red blood cells/mL (1: 18,200 ratio of Jurkat cells to horse red blood cells) in 1:1 horse plasma to RPMI media 1640. Before mixing, the cells were counted with a hemacytometer (Sigma-Aldrich, Oakville, ON, Canada). (The total cell concentration is similar to a blood sample, so the physical properties of the reconstituted blood, e.g. viscosity, are comparable to those of a blood.) Jurkat cells (ATCC No. TIB 152, an immortalized human T-cell line) were prepared according to the supplier’s (ATCC) instructions. Anti-human CD3 (BD PharMingen Canada, Mississauga, ON) was loaded onto 1-2  $\mu\text{m}$  diam. paramagnetic beads by mixing 100  $\mu\text{L}$  of Protein A paramagnetic particle suspension (13.3 mg solid/mL suspension, with 100  $\mu\text{g}$  Protein A/mL of suspension, Polysciences, Warrington, PA, USA) with 1000  $\mu\text{L}$  of 40  $\mu\text{g}/\text{mL}$  Anti-human CD3 in an Eppendorf tube. Particles were pelleted with a magnetic field and washed three times with PBS to remove unbound anti-CD3. The particles were

resuspended in 99  $\mu\text{L}$  PBS and 1  $\mu\text{L}$  of this suspension was mixed with 500  $\mu\text{L}$  reconstituted blood.

For pump operation a Hewlett Packard power supply (Model 6215A) provided constant voltage, while an RDE4 potentiostat/galvanostat (Pine Instrument, Grove City, PA, USA) was used to apply constant current. A 6 mm diam. NdFeB permanent magnet (Edmund, Ind. Optics, Barrington, NJ, USA) was used to create the magnetic field for bead trapping on the chip. To visualize gas production and pumping, a CCD camera (JVC, Model TK-1280U) attached to a BH-2 Olympus microscope with a 5X power objective was used. Displacement of liquid was viewed on a video monitor. The time for the liquid front to travel a distance of 0.2 – 1.0 mm along the main channel was measured using a stopwatch. The distance was measured using a scale that was prepared on the mask pattern and fabricated on the device beside the channel, as illustrated in a photo (see Figure 4.10). The nominal cross section of the channel and the distance traveled was used to calculate the volumetric flow rate. The absolute volume flow rates in any given device differed by up to +10 % from the nominal values reported, due to variations in dimensions of the channels from chip to chip.

## **4.3 Results and Discussion**

### **4.3.1 Design and Fabrication**

Two electrolysis pumps were integrated side by side, attached to the same flow manifold, to use one for pumping sample, and the other to pump a wash fluid. Figure 4.2 shows the device layout. Interdigitated electrodes are located in the electrolysis chambers, and a chevron of Si barriers separates the anolyte and catholyte compartments, in order to reduce mixing of the gases produced. A long meander is present downstream of the pumps to provide sample or buffer reservoirs. While similar to the Twente design [8], the device differs in a number of aspects. It is about three times larger in width and length, and holds about 7.5  $\mu\text{L}$  of electrolyte in the pumping chambers. A number of additional inlet and outlet holes were added to ease the filling of these devices. Additionally, the pump chambers were rounded at the corners to reduce the tendency to trap air bubbles during filling. As shown in Figure 4.5, the chevron structure at the entrance to the electrolysis chambers was positioned to partition 2/3 of the liquid towards

the larger H<sub>2</sub> chamber and 1/3 through the smaller O<sub>2</sub> chamber, to reduce the tendency to trap bubbles during filling.

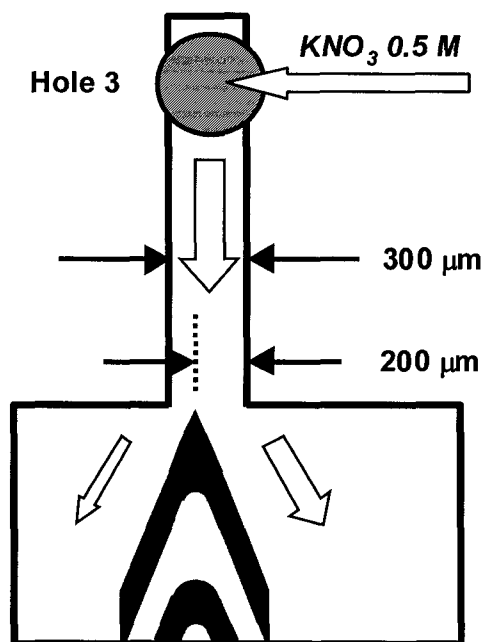


**Figure 4.5:** Detail of the layout of the chevron barrier used to reduce gas mixing between the anolyte and catholyte compartments, and the inlet to the electrolysis chamber from access hole 3.

The original Twente design, with a single access port, was filled by placing the device in an evacuated chamber, with liquid over the port, and then returning the chamber to atmospheric pressure. This procedure is inconvenient, does not allow for flushing if bubbles form in the device, and means the sample liquid is the only one that can be introduced. The access hole pattern we have introduced readily allows the ingress of separate background electrolyte, sample and wash buffers. Figure 4.4 and the experimental section give the filling procedure, which is simple to perform. The device can be filled manually with a pipet in less than 4 minutes, or with a syringe pump. Steps 1-3 in Figure 4.4 can be performed in advance, the device may then be sealed and stored for several days before the blood sample is introduced at the time of use. Adding the blood sample from a pipet and re-sealing the device requires less than 1 minute. These changes in inlet design created a device that could be filled in a flexible fashion, allowing the pump fluid to be different than the sample fluid. Further, the ability to introduce a

separate wash fluid in one of the meanders is a crucial element in creating a system for sample processing that can perform both a capture and a subsequent wash step.

### 4.3.2 Pump Performance

The pump rate in the device was proportional to the applied current, as expected [8]. A sequence of flow rates as a function of current could be easily measured for a single charge of buffer solution when the current was kept below 90  $\mu\text{A}$ . Figure 4.6 shows this dependence for a pump filled with 0.5 M  $\text{KNO}_3$ . The response of flow rate to current density was  $0.078 \mu\text{L}/\text{min}$  per  $\mu\text{A}/\text{mm}^2$  for the current range shown in Figure 4.6, compared to  $0.049 \mu\text{L}/\text{min}$  per  $\mu\text{A}/\text{mm}^2$  in the smaller Twente device [8]. The maximum flow rate obtained was  $1.4 \pm 0.1 \mu\text{L}/\text{min}$  at a current of 180  $\mu\text{A}$ , but this rate consumed the electrolyte solution too rapidly to obtain a series of flow rate values at different (high) currents. Figure 4.6 shows that not all the current was used to produce  $\text{H}_2$  and  $\text{O}_2$  gases, since flow was achieved only after applying more than 20  $\mu\text{A}$ .

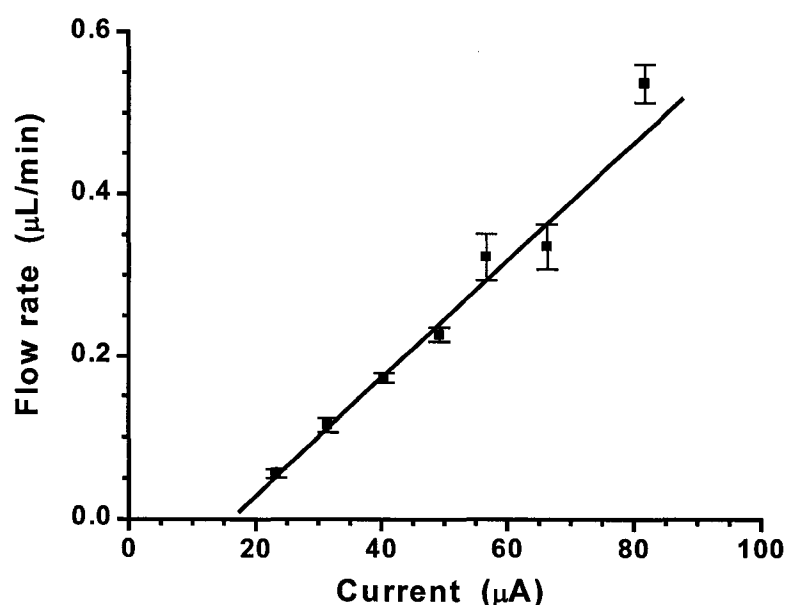


**Figure 4.6:** Flow rate as a function of applied current for a device filled with 0.5 M  $\text{KNO}_3$ . Error bars are the standard deviation of 3 to 6 measurements. All data was obtained in one device, with one charge of electrolyte.

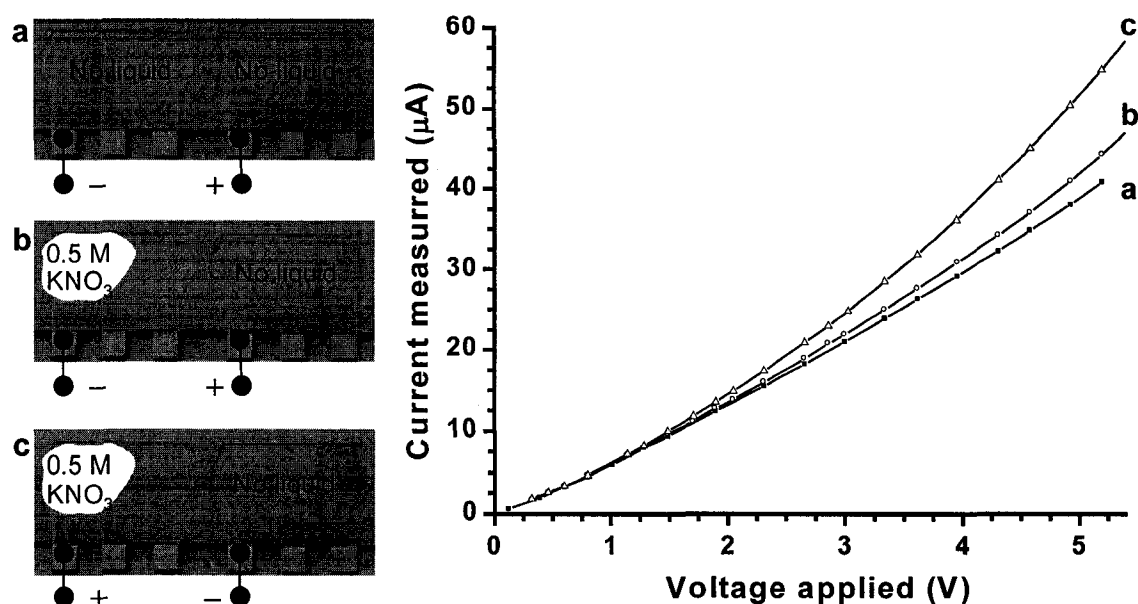


**Figure 4.7:** Current leakage through one device, determined by applying constant voltages at electrodes of different pump units in:

- new dry device;
- one unit filled with 0.5 M  $\text{KNO}_3$  at the cathode;
- one unit filled with 0.5 M  $\text{KNO}_3$  at the anode.

The offset current was also observed in a dry device, by applying constant voltages at the electrodes of two different pumps from the same device, as presented in Figure 4.7a. This corresponds to direct contact-to-contact leakage through the silicon. The measured offset current was even higher if an aqueous 0.5 M  $\text{KNO}_3$  solution was present in one of the two pump chambers. We tentatively assign this to leakage from the silicon to the electrolyte and then through the electrode array. This is consistent with the leakage being higher with solvent in the anode chamber, as Si is oxidized with low overpotential, and the Si/oxide/ electrolyte junction is under forward bias. The wet thermal oxide grown to passivate the silicon surface was clearly not sufficiently effective. The Twente device used a 250 nm thick oxide, vs. the 200 nm thick layer used here, indicating the wet oxidation process used in this study did not produce an oxide of sufficient quality.

The flow rate was also evaluated using various constant applied voltages, in order to evaluate the compliance voltage required to achieve a given pump rate. The pumping performance of the device was tested with reconstituted blood samples and with PBS.

Reconstituted horse blood was spiked with a known amount of Jurkat cells, a human derived T-cell line, to provide a target that could be captured [16] by the anti-CD3 coated magnetic bead particles. Reconstituted blood was free of endogenous leukocytes, which attack the Jurkat cells and change their concentration over time. Figure 4.8 shows that voltages of 2.7 to 3.7 V were required for pump rates of 0.2 to 1.4  $\mu\text{L}/\text{min}$ . Corresponding currents ranged from 30 to 200  $\mu\text{A}$ .

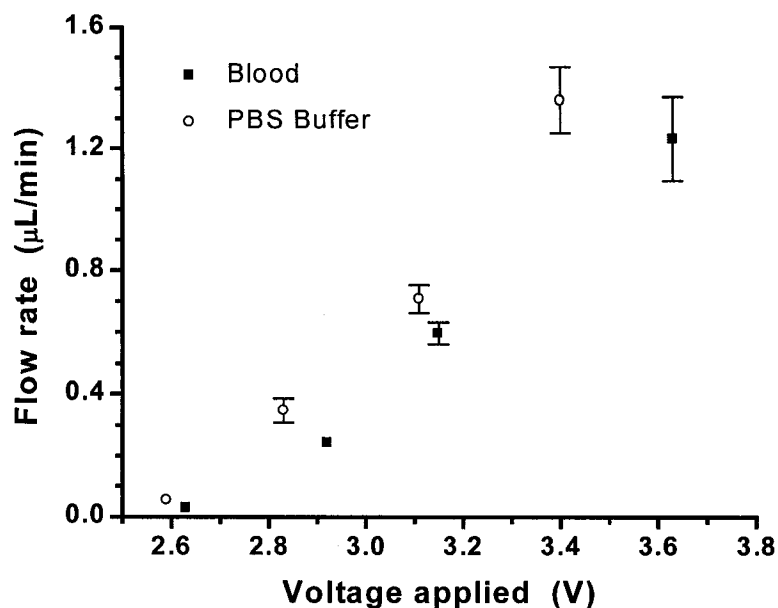


**Figure 4.8:** Flow rate as a function of applied potential comparing the pumping of reconstituted horse blood or phosphate buffered saline. Error bars are shown when larger than the point plotted, and are the average of 4 to 6 measurements.

The flow rate obtained for pumping blood was slightly lower than that for pumping PBS buffer, at the same applied potential. This is consistent with the much greater viscosity of blood ( $51 \pm 13 \text{ mPa} \cdot \text{s}$ ) [17] compared to PBS buffer ( $1.3 \text{ mPa} \cdot \text{s}$ ) [18], requiring a higher backpressure be developed in the pump chamber. Flow rates were determined for periods of 2.5 to 15 s, depending on the rate, and currents were stable for each measurement period. A maximum of 6.5 – 7  $\mu\text{L}$  of blood could be delivered from the sample meander reservoir. However, once the gas bubbles in the electrolysis chamber exceeded 60 % of the volume, large fluctuations in the current and the flow were observed. Care was taken not to exceed 60 % for the data reported. The variation in

current between measurements was  $\pm 3\text{-}5\%$  (RSD,  $n = 3$  to  $6$ ) for PBS and  $\pm 10\%$  for reconstituted blood. While the errors in current did not increase with voltage, Figure 5 shows that there was some increased variation in the pump rate from run to run at higher voltages.

The results established that blood could be pumped reliably by the electrolysis pump at flow rates  $\leq 0.5\ \mu\text{L}/\text{min}$ . For a batch processing system such as this the fluctuations in flow rate at  $> 1.2\ \mu\text{L}/\text{min}$  would not create any difficulties in an analysis. Thus the pump works for its intended batch delivery purpose at all flow rates tested. While a small amount of mixing of blood and electrolysis buffer occurred at access holes 3 and 6, the ingress of some blood constituents into the electrolysis chamber did not significantly affect the pumping ability. Blood samples are known to be challenging to pump [19]. The few reports of cells pumped with a micropump are performed at  $\sim 10^6$  cells/mL or less [20], much below the value of  $5 \times 10^9$  cells/mL in whole blood, or  $1 \times 10^{10}$  cells/mL in our reconstituted blood sample. Thus, our result is an important milestone along the road to creating a  $\mu\text{-TAS}$  for clinical samples.

### 4.3.3 Rare Cell Capture System

The ability of the design to deliver a sample, trap magnetic beads in the main flow path, and then deliver a wash buffer to remove the blood constituents not trapped by the beads was then tested. Samples of reconstituted blood were mixed with magnetic, anti-CD3 coated beads and delivered into the sample meander reservoir. The electrolysis pump was then used to pump blood through the magnetic bead-trapping zone in the main channel at various flow rates between  $0.05$  and  $0.5\ \mu\text{L}/\text{min}$ . After delivering  $2\text{-}3\ \mu\text{L}$  of blood from the sample meander, the sample pump was turned off and the same voltage was applied to the wash buffer pump. Visual observation showed the blood was washed away, leaving Jurkat cells bound to magnetic particles trapped within the main flow path. Figure 4.9 shows a sequence of video images of the region where the two flows, blood and PBS, merge into the main channel. Displacement of the blood by the buffer is clearly seen. (The dark lines along the edges are the walls, not remaining blood.)

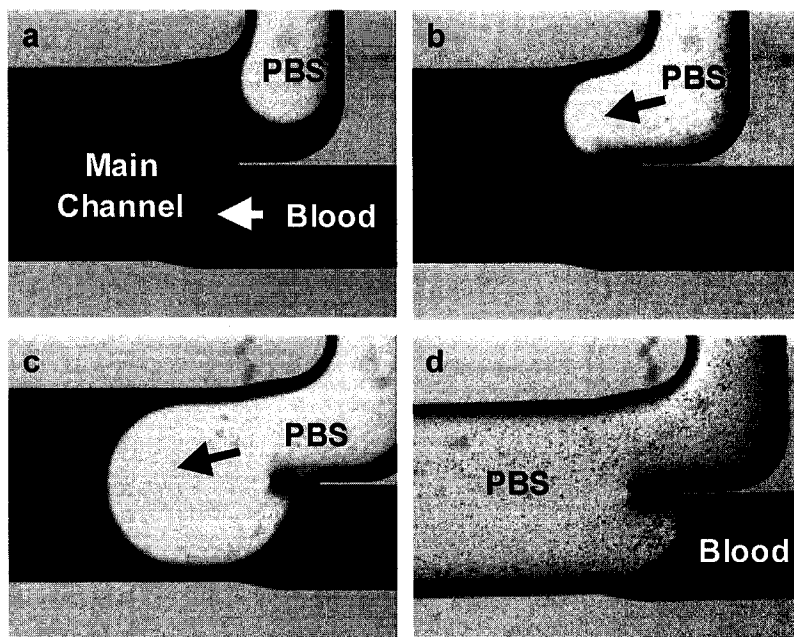


**Figure 4.9:** Video frames showing a) the flow of blood pumped by the sample pump, and b-d) the flow of phosphate buffered saline (PBS) delivered by the wash pump to flush the blood sample downstream. The main channel was  $600\ \mu\text{m}$  wide and each feed channel before the junction was  $300\ \mu\text{m}$  wide.

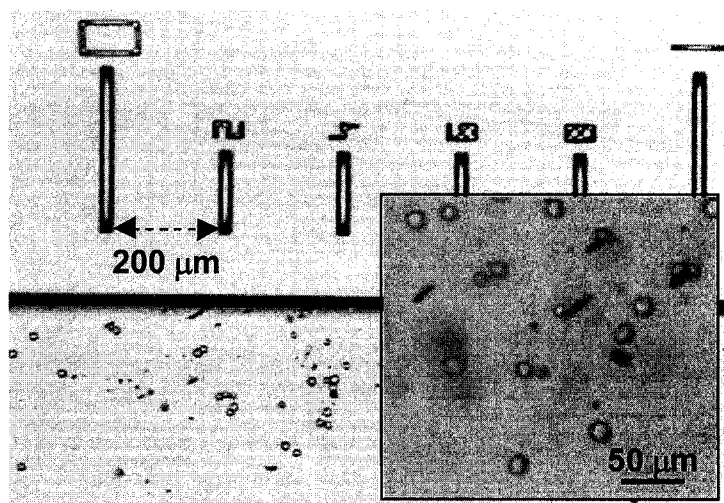


**Figure 4.10:** Photomicrographs at two magnifications, showing Jurkat cells trapped within the main flow channel by anti-CD3 coated immunomagnetic beads and an applied magnetic field. The dark lines in the inset are chains of magnetic beads, and the open circular objects are  $15\ \mu\text{m}$  diam. Jurkat cells. The scale fabricated in the device to measure flow can be seen as well.

Figure 4.10 shows the cells and strands of magnetic beads retained by the field after the washing step. The  $15\ \mu\text{m}$  diam. size identifies the cells as Jurkat, assuming no WBC



contamination in the horse RBC fraction. Counting the captured cells indicated 450-540 cells were typically captured, corresponding to 40-49 % cell capture efficiency for a 2  $\mu$ L sample delivery, given the loading of Jurkat cells in the reconstituted blood samples. This result is comparable to those we have reported previously for on-chip, magnetic bead capture, where an external syringe pump [15] was used for pumping.

We found the devices could be used 2- 6 times before they were plugged by components of the blood samples. Devices exposed to buffers alone could be used until the electrodes delaminated from the glass, which required longer than 30 min at 5 V or 180  $\mu$ A applied. These devices would probably be used with a single clinical sample and then disposed, so their current durability is more than adequate.

#### **4.4. Conclusions**

Our results show that the Twente micro-electrolysis pumps are readily adapted to use with clinically relevant volumes of blood samples, and can be used as part of a sample clean up procedure. The fluid introduction ports we added to the Twente design provide a very simple way to load solvents into each zone of the device, and are a useful advance. The results illustrate the pumps can be used as part of a system, each pump providing the actuation for one element of a number of sample processing steps. Further improvements in device design are made clear by the current study; our Si passivation procedure needs to be improved, the volume of the electrolysis chamber should be made at least twice as large as the volume of the sample meander to improve pump flow rate stability, and the overall volumes could be increased further to process larger samples. Should the device be manufactured for commercial use, the design could be fabricated in a plastic substrate, eliminating the electrical passivation issue and reducing the cost per device. We anticipate such devices would be interfaced to downstream immunoassay or genetic assay stages, which might be used multiple times, but that these chips could serve as a front end sample preparation stage. Chips could be preloaded with buffers, allowing the user to simply open a port, inject a sample with a pipet, seal the device and turn it on, as we have demonstrated. Automation of the magnetic field changes could clearly be achieved using electromagnets instead of permanent magnets.

#### 4.5 References

- [1] Gravesen, P.; Branbjerg, J.; Jensen, O. S. *J. Micromech. Microeng.*, 1993, 3, 168-182.
- [2] Elwenspoek, M.; Lammerink, T. S. J.; Miyake, R.; Fluitman, J. H. J. *J. Micromech. Microeng.*, 1994, 4, 227-245.
- [3] Reyes, D. R.; Iossifidis, D.; Auroux, P.-A.; Manz, A. *Anal. Chem.*, 2002, 74, 2623-36.
- [4] Volanschi, A.; Olthuis, W.; Bergveld, P. *Sensors and Actuators A: Physical*, 1996, 52, 18-22.
- [5] Neagu, C. R.; Gardeniers, J. G. E.; Elwenspoek, M.; Kelly, J. J. *J. Micromech. Microeng.*, 1996, 5, 2-9.
- [6] O'Keefe, D.; O'Herlihy, C.; Gross, Y.; Kelly, J. G. *Br. J. Anaesth.*, 1994, 73, 843-6.
- [7] Amirav, A.; Tzanani, N. *Anal. Chem.*, 1997, 69, 1248-55.
- [8] Böhm, S.; Olthuis, W.; Bergveld, P. *Journal of Biomedical Microdevices*, 1999, 1, 121-130.
- [9] Böhm, S.; Timmer, B.; Olthuis, W.; Bergveld, P. *J. Micromech. Microeng.*, 2000, 10, 498-504.
- [10] Rembaum, A.; Dreyer, W. J. *Science*, 1980, 208, 364-8.
- [11] Safarik, I.; Safarikova, M. *J. Chromatogr. B Biomed. Sci. Appl.*, 1999, 722, 33-53.
- [12] Trippler, M.; Meyer zum Buschenfelde, K. H.; Gerken, G. *J. Virol. Methods.*, 1999, 78, 129-47.
- [13] Choi, J. W.; Liakopoulos, T. M.; Ahn, C. H. *Biosens. Bioelectron.*, 2001, 16, 409-16.
- [14] Furdui, V. I.; Harrison, D. J. In *Micro Total Analysis Systems 2001*; J. M. Ramsey; Albert van den Berg, eds.; Kluwer Academic Publisher: Monterey, CA, USA, 2001, pp. 289-290.
- [15] Furdui, V. I.; Harrison, D. J. In *Micro Total Analysis Systems 2002*; Yoshinobu Baba; Shuichi Shoji; Albert van den Berg, eds.; Kluwer Academic Publisher: Nara, Japan, 2002; Vol. 2, pp. 700-703.
- [16] Beverley, P. C.; Callard, R. E. *Eur. J. Immunol.*, 1981, 11, 329-34.
- [17] Philippe, F.; Lacombe, C.; Bucherer, C.; Drobinski, G.; Montalescot, G.; Thomas, D. *J Mal Vasc*, 2001, 26, 243-7.
- [18] Lide, D. R. ed. *CRC Handbook of Chemistry and Physics*, CRC Press: Boca Raton, Florida, USA, 2002.
- [19] Vidakovic, S.; Ayre, P.; Woodard, J.; Lingard, N.; Tansley, G.; Reizes, J. *Artif Organs*, 2000, 24, 478-82.
- [20] Andersson, H.; van der Wijngaart, W.; Nilsson, P.; Enoksson, P.; Stemme, G. *Sensors and Actuators B: Chemical*, 2001, 72, 259-265.

## CHAPTER 5: Fabrication of Embossed Microfluidic Devices<sup>♦</sup>

### 5.1 Introduction

Interest in plastic or polymer-based microfluidic systems has arisen rapidly mainly because of the demand for low-cost, disposable products for medical and genetic applications of  $\mu$ TAS devices. Producing plastic devices has advantages over glass and/or silicon technology, such as mass fabrication and rapid production at lower manufacturing cost. Plastic materials exhibit a large variety of properties, some of them complementary to glass and silicon properties. An extensive set of techniques for fabrication of microfluidic systems in plastic has been developed. The most common materials and the relevant techniques are discussed briefly in this introduction.

The plastic materials considered for fabrication offer particular properties such as easy machining, optical transparency for easy monitoring, inertness to the specific conditions of the assay, adequate thermal and electrical properties, the ability to be thermally bonded and if required, the ability to chemically modify the surface [1]. The choice of a material for polymer fabrication is based on its properties, which have a major influence on the fabrication process and the application of the devices. Plastics are often preferred to pure polymers, mainly because plastics contain additives that impact on their processing and shelf life. These additives include fillers (e.g. mica, talc, calcium carbonate), plasticizers (e.g. dioctyl phthalate in polyvinyl chloride), heat stabilizers (e.g. organo-tin compounds in polyvinyl chloride), antioxidants (e.g. phenols, amines), and UV stabilizers (e.g. benzophenones, salicylates) [2]. The glass transition temperature ( $T_g$ ) represents the temperature at which the polymer substrate changes from a rigid glassy material to a softer, but not melted, material.

Polymers can be classified as thermoplastic, duroplastic and elastomeric. The thermoplastic polymers are the most important group used in microfabrication. They are characterized as unlinked or weakly linked polymer chains, which become plastic above  $T_g$ , so they can be molded into specific shapes and maintain their shape after cooling below  $T_g$ . Duroplastic or thermoset polymers are strongly crosslinked.

---

<sup>♦</sup> Results obtained by Dean Nair (summer undergraduate student) for thermal bonding of plastic devices performed on a Carver hydraulic press are included in this chapter.

They have to be cast directly into their final shape, since thermal reshaping is not possible. Elastomeric polymers have very weakly crosslinked polymer chains, which allow elastic stretching under external forces. Duroplastic and elastomeric polymers do not melt before reaching decomposition temperature [3, 4].

The standard thermoplastic polymers suitable for microfabrication are presented in Table 5.1 with some of their physical and chemical properties. The polymers included are polyamide 6 (PA6), polyamide 66 (PA66), polycarbonate (PC), polymethyl-methacrylate (PMMA), polystyrene (PS), polyethylene (PE), polyethylene-terephthalate (PET), polypropylene (PP), polybutene (PB), polytetrafluoroethylene (PTFE) and polyimide (PI). The most used elastomeric polymer is polydimethylsiloxane (PDMS) Sylgard 184, which offers good optical properties above 230 nm [1, 2, 4-6].

**Table 5.1:** Standard thermoplastic polymers used in microfabrication

Micro-molding material	T <sub>g</sub> (°C)	Heat distortion temp. (°C)	Linear expansion coefficient (10 <sup>-5</sup> K <sup>-1</sup> )	Thermal conductivity (W m <sup>-1</sup> K <sup>-1</sup> )	Strong acid/base (*)	Solvent	Clarity UV/Vis (**)
PA6	60	180	8	0.29		soluble	
PA66	70	200	8	0.23		soluble	
PC	150	148-150	6.5	0.21	+/+	soluble	+/+
PMMA	106	80-110	7-9	0.186	+/-	soluble	-/+
PS	80-100	78-90	7	0.18	+/-	soluble	+/+
PET	81	-	-	-	+/-	soluble	
PE	10	40-65	14-20	0.35-0.46		soluble	
PP	0-10	90-100	10-20	0.22		soluble	
PB	-	-	-	0.13	+/-	resistant	-/+
PTFE	>250	-	12	0.24	-/-	resistant	-/+
PI	310-65	388	4.5-5.6	-		-	

\* +/+ attacked by strong acid/base; +/- attacked by strong acids only; -/- resistant

\*\* +/+ UV/Visible transparent; -/+ Visible transparent only

Polymer micromachining techniques can be classified into replication based methods, such as imprinting, hot embossing, injection molding and elastomer casting, or etching based methods, such as laser photoablation and X-ray lithography [2]. While hot embossing and injection molding can be used for high-volume production, casting is largely used for rapid prototyping of low-volume test series. The etching methods are specific to the application and material and may require unique microfabrication steps be developed.

The most widely used replication method to date is hot embossing. After fabrication, the replication tool is mounted in the embossing system together with a planar plastic substrate. Both are heated separately in a vacuum chamber, which prevents trapping of air in small cavities and corrosion of the metal masters, and controls emission of water or solvent vapor from the plastic. A temperature above  $T_g$  of the polymer is used. The master contacts the substrate and then embosses it with a controlled pressure, typically  $0.5\text{--}2\text{ kN/cm}^2$ . While continuing to apply the embossing force, the master-substrate system is cooled below  $T_g$ , then the master is mechanically removed from the substrate [4, 5, 7].

The master has been fabricated from different materials such as silicon [5], nickel [8, 9], nickel alloys [4, 10], other metals and quartz [11]. Si masters were obtained by KOH etching or by dry etching methods such as reactive ion etching or the Bosch process (deep reactive ion etching) [4, 10]. A quartz master was obtained by wet etching [11]. The metal masters have been obtained by electroplating methods. The simplest approach employs a photolithographic method on a substrate to define the areas that should be electroplated. Another method involves the lithography of photoresist for Si dry etching, followed by electroplating of the Si substrate [8, 10, 12]. A more elaborate method is the LIGA process (German acronym for lithography electroplating molding). Exposing the substrate to X-ray's degrades the features defined by photolithography. Usually PMMA substrates are used since PMMA is highly X-ray absorbent and sensitive to X-ray degradation. The exposed, degraded polymer is dissolved, yielding microstructures with high aspect ratio and straight, smooth walls. After seeding a conductive layer by thermal evaporation or sputtering, the substrate is electroplated with the metal of choice [2, 4, 13].

A simpler version of the hot embossing process is imprinting, in which thin chromel wires or a silicon micromachined master is used to replicate simple structures [14, 15]. So far PS, polyethylenetetrathalate glycol (PETG), PMMA, polyvinylchloride (PVC) and PC have been successfully imprinted or hot embossed [1, 2, 5, 7, 16].

McCormick et al. first applied injection molding to the fabrication of microstructures [8]. The technique consists of introducing a melted polymer under high pressure into an evacuated molding cavity containing the mold insert as the master structure. The masters are fabricated using the same methods described previously for

master fabrication for hot embossing. Injection molding of microstructures has been successfully applied to PMMA [8, 17-19], PC [18, 20, 21] olefin copolymers [18, 19, 22, 23].

Casting or soft lithography uses a relief master usually fabricated in silicon. An elastomeric polymer, most often PDMS, is cast onto the silicon master and allowed to cure, then the elastomeric polymer is peeled off the master. Whitesides et al. first introduced the use of crosslinked PDMS, a durable hydrophobic elastomer [24-26] for this purpose.

The etching based methods, namely laser photoablation, optical lithography in deep photoresist and X-ray lithography, do not require the fabrication of a master, but have limited fabrication throughput because patterning must be done for each device produced. In laser photoablation, the energy of a laser pulse is used to fragment the polymer molecules and to remove the decomposed polymer fragments from the ablated regions. The excimer lasers used to micromachine specific polymers deliver light pulses at 193 nm (for PS, PC, PE, PP, cellulose acetate, polyethyleneterephthalate) [27, 28], 248 nm (polyimide, PC, PMMA) [29-33] and 308 nm (polyesters, polyester-PC blend, PC) [34]. Certain modifications are induced in the surface chemistry in comparison to the untreated material. A modification of this procedure involves completely cutting through a thin polymer foil. To obtain a microfluidic device, this foil is placed between two polymer or glass plates [35].

In the deep photoresist technique a thick layer of photoresist, usually the epoxy polymer SU-8, is deposited and lithographically processed. A second sacrificial polymer is used to fill the SU-8 network, followed by deposition and access hole patterning of SU-8, then by dissolution of the sacrificial polymer [36, 37].

X-ray lithography is involved in the LIGA process, presented earlier, without performing the final electrochemical deposition. Exposing the substrate to X-ray degrades the features defined by photolithography. The exposed, degraded polymer is dissolved, yielding microstructures with high aspect ratio and straight, smooth walls. Synchrotron radiation was used directly to fabricate PMMA devices [38].

To obtain a microfluidic device with enclosed features, the substrate bearing the micromachined features has to be bonded to a coverplate. Different methods have been

reported, including thermal bonding [39-41], lamination [8, 39, 42, 43], gluing [44, 45] and laser welding [46]. A combination of thermal bonding and adhesive tape bonding was reported [47]. Bonding was also performed using a sacrificial channel and adhesive printing [48].

Thermal bonding has normally been characterized by relatively low bond strength, since the possible channel collapse limits the bonding temperature and the force applied [41]. Very good bond strength, comparable with the anodic bonding strength of the silicon-glass systems, was obtained using cyclic olefin copolymer substrates with hydrophilic surfaces modified by argon plasma [49]. The bond strength also increased when an oxygen plasma treatment of PC substrates was used prior to bonding [9]. In lamination, the layers are held together by an adhesive, most commonly pressure-sensitive or thermally activated adhesive. The substrates (laser cut or stamped) are characterized by significantly worse dimensional tolerances as compared with other techniques, such as hot embossing. Although good bonding can be obtained using glues, the challenge of properly bonding around the features without destroying them is significant.

This chapter presents a method for fabrication of polycarbonate (PC) microfluidic devices. Polycarbonate has different reported T<sub>g</sub> values, such as 143-150 °C [50], 149 °C [3], 150 °C [4] and 157 °C [1]. PC is soluble in ethanolamine, dioxane, chlorinated hydrocarbons and cyclohexanone, but insoluble in alcohols, aliphatic hydrocarbons and water [6]. Since a PCR platform requires thermal cycling between room temperature and 95 °C, clarity for detection of the separated products, and does not require handling of corrosive compounds or organic solvents, PC would be a good polymeric candidate for the fabrication of such a device. While the use of PC has been reported for microfluidic devices there are no truly well characterized processes described in the open literature. Each fabrication facility must invest effort in developing their own functioning process in-house. This is the goal of this thesis study. (The challenge can be likened to developing a synthesis of a compound that is known, but for which no complete scheme has been published.) A Si substrate was etched by deep reactive ion etching (DRIE) and used as the master to create a secondary master of electrochemical deposited Ni as a tool. After machining, the resulting Ni master was used to emboss PC substrates. The

embossed substrate was thermally bonded to a coverplate to obtain the plastic device. The method used for master fabrication, first proposed by Elders et al. for molding, was named DEEMO (dry etching, electroplating, molding) [10]. A silicon master was etched using deep reactive ion etching (DRIE), a nickel master was electroplated and plastic substrates were molded using the Ni master. The method is a less costly version of the LIGA process and can fabricate features with high aspect ratio. The challenges related to this approach are the Ni electroplating step, high accuracy in the plastic stamping step and the device bonding.

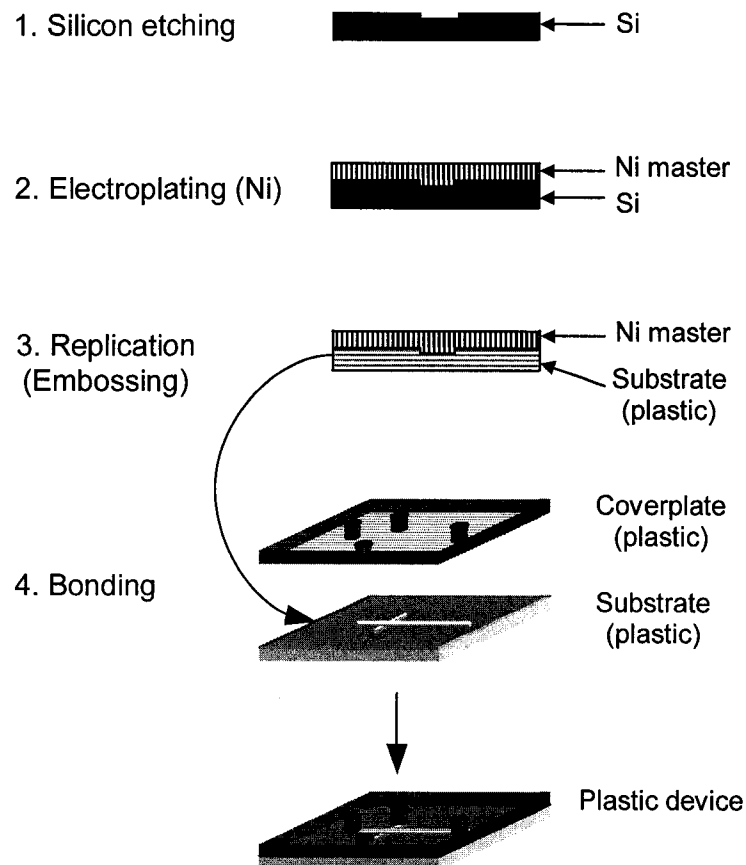


**Figure 5.1:** Schematic of the plastic device fabrication procedure employed in this study

## 5.2 Fabrication

A master in silicon was anisotropically etched using DRIE and used to form a nickel relief as a secondary master. The Ni master was used to stamp features in plastic



substrates (PC) using a hot embosser. After drilling the access holes, the substrates were thermally bonded to the coverplates to obtain plastic devices. The process is shown in Figure 5.1.

### 5.2.1 Anisotropical Etching on Silicon Wafer

The manifolds of the FAT 3000 device with nominal channel widths presented in Figure 3.2 were etched on a silicon wafer (100 mm diam., 500-550  $\mu\text{m}$  thick, 1-20  $\Omega\text{ cm}$  resistivity, p type; Silicon Valley Microelectronics, San Jose, CA, USA) using deep reactive ion etching (DRIE). An Oxford Instruments Series 100 DRIE (Bristol, UK) with an ICP power of 450 W was used to operate the Bosch process.

Preliminary tests were done on one Si wafer using 15, 20 or 25 s etching time for sets of 21 cycles, while keeping constant the other variables. Every cycle consisted of etching at 50 W ( $\text{SF}_6$  flow rate 75 sccm), followed by the polymer deposition step at 20 W for 10 s ( $\text{C}_4\text{F}_8$  flow rate 50 sccm). The 21<sup>st</sup> cycle had no deposition step. It was followed by an intermediate depth measurement using an Alphastep profilometer (KLA-Tencor, San Jose, CA, USA). The wafer was then returned to the DRIE for further etching. The etched structures were inspected by scanning electron microscopy (SEM). Gold sputtering on 1 $\times$ 1 cm Si pieces (excised from the etched Si wafer) was performed on a Desk II (Denton Vacuum, Cherry Hill, NJ, USA) and SEM on LEO 1430 system (LEO Electron Microscopy, Cambridge, England).

The data obtained from the preliminary studies determined the optimal conditions to be used for etching 70  $\mu\text{m}$  deep structures. The Si wafer required for Ni master fabrication was etched using 62 cycles, the last cycle without the polymer deposition step. Etching was done at 50 W for 20 s ( $\text{SF}_6$  flow rate 75 sccm) and polymer deposition at 20 W for 10 s ( $\text{C}_4\text{F}_8$  flow rate 50 sccm). The etched structures were inspected by SEM. Depths were measured with the Alphastep profilometer and ranged between 67 and 76  $\mu\text{m}$ .

### 5.2.2 Master Fabrication by Ni Electroplating onto the Etched Silicon Wafer

Ni electroplating onto the surface of the etched silicon wafer was performed at Optical Electro Forming (Clearwater, Florida, USA). The Ni master was delivered

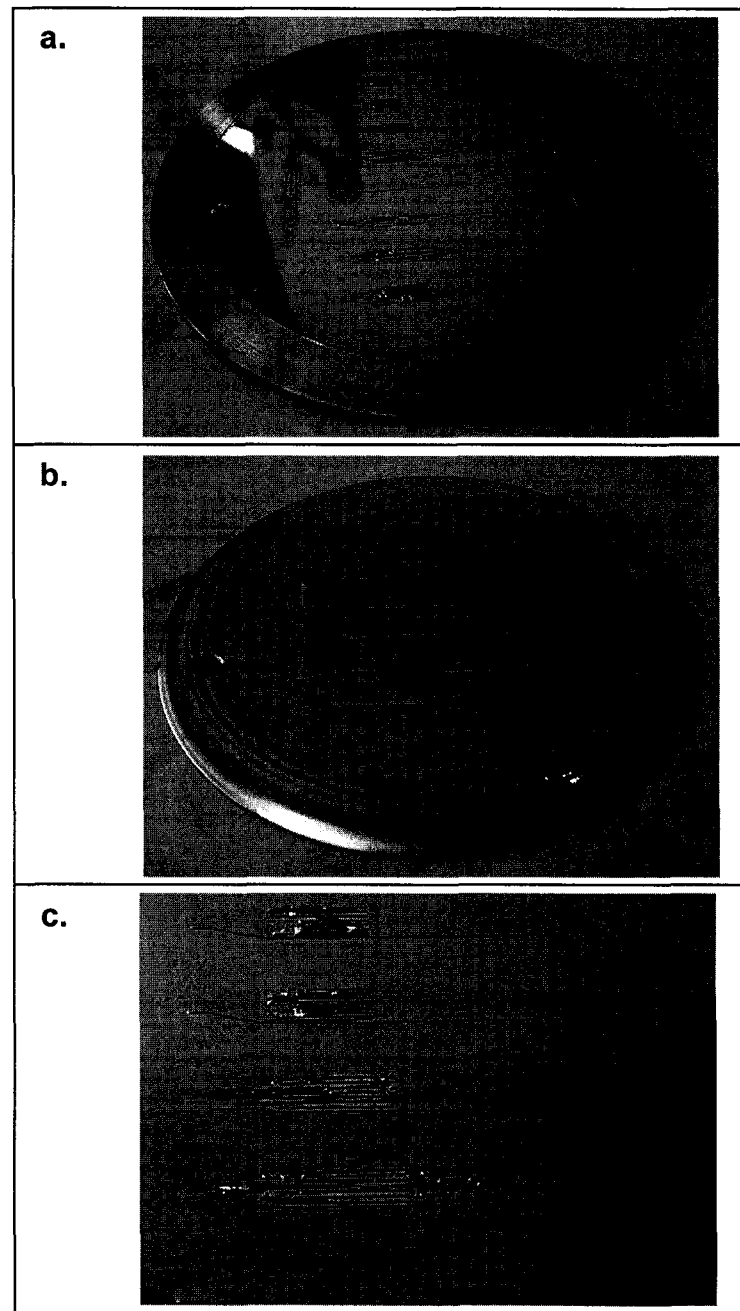


**Figure 5.2:** Images of the Ni master fabricated by electrochemical deposition onto a Si wafer with features of the FAT 3000 device etched at  $70\ \mu\text{m}$ :

- a. front side image;
- b. backside image;
- c. detail presenting the small fragments of Si fixed inside some channels.

without successfully removing the silicon from the Ni surface. As shown in Figure 5.2, the features were transferred from the Si surface, but some Si clumps remained mechanically trapped. Different attempts were performed to remove the Si parts,

including the following. The Ni tool was immersed for 2 h in 10% KOH, after etching the SiO<sub>2</sub> layer with buffered oxide etch (BOE: NH<sub>4</sub>F, HF). The Ni tool was plasma etched with SF<sub>6</sub>. An EDP bath (ethylenediamine, pyrocatechol, 115 °C) was also used.

The Ni tool was machined in the Machine Shop (Department of Chemistry, University of Alberta) to flatten the backside and fit into the opening of the ring type fixture from the hot embosser. The machined Ni master had a 102 mm diameter and 2.84 mm thickness. A stainless steel disc (2.50 mm thick) and graphite sheets (0.14 mm thick, Graphite Machined Products, Downey, CA, USA) with the same diameter as the master were machined and used to fix the tool in the hot embosser. Two graphite sheets were added between the master-stainless steel disc and the stainless steel-embosser fixture to compensate for surface irregularities and to allow good heat transfer.

### 5.2.3 Feature Embossing on Polycarbonate Surface

A commercial hot embossing system (HEX 01) manufactured by Jenoptik Mikrotechnik (Germany) was used for replication. Just before embossing, the 10×12 cm planar clear PC substrates were cleaned with isopropyl alcohol using clean room paper and dried with N<sub>2</sub>. The Ni master was mounted in the upper section of the hot embosser chamber and a PC substrate (Lexan, 12.5×10 cm, 2.14 mm thick, GE Polymershapes, Edmonton, AB, Canada) was clamped at the lower section of the chamber, on top of a glass substrate. The chamber was closed, placed under vacuum and the Ni master and the plastic substrates were heated separately to the embossing temperature (between 160 °C and 195 °C) above T<sub>g</sub> of the polycarbonate (149 °C). The tool was brought into contact with the substrate and embossed with a 15 kN controlled force for 120 s. With the embossing force still applied, the tool-substrate was cooled for separation from the mold, below T<sub>g</sub>, to 138 °C. After cooling, the Ni master was mechanically separated from the PC substrate with the embossed features. The cycle time of the embossing process was related to the embossing temperature used and ranged from 10 to 15 min.

The embossed structures were inspected by SEM after cutting 1×1 cm pieces from the same manifold and details are shown later in Figures 5.7 and 5.8. A gold layer was sputtered to obtain the conductive layer required for SEM. The surface of the Ni master and the embossed substrates were also characterized by scanning white light

interferometry performed on a Zygo optical profilometer (New View 5000, Middlefield, CT, USA).

**Table 5.2:**

Conditions used for bonding of 8×7 cm embossed substrates on a Carver hydraulic press

Bonding temp (°C)	Force (kN)	Bonding times (min)	Annealing temp (°C)	Annealing time (min)
* 135	40	10, 15, 20, 25, 30	145, 150	10
135	41	10	145, 150	8, 10
140	3	10, 12.5	-	-
140	14	15	-	-
140	15	15	-	-
140	20	5, 7, 8	-	-
140	29	8, 10, 12	-	-
141	12	10	145	10, 15
141	14	10, 15	145	10, 15
141	18	10	145	10
142	3	5, 10	-	-
142	14	15	-	-
143	3	13, 14, 15, 16	-	-
144	3	5	135	10
144	3	6, 8, 10, 12	-	-
145	12	15	-	-
145	13	15	-	-
145	14	15	-	-
145	16	12, 15, 17, 18.5, 20	-	-
146	3	5, 6, 8, 10, 15	-	-
148	3	4, 5, 12, 15	-	-
150	3	4,5,6,7,8,9,10,15	-	-

\* Trials were also performed on 4×5, 5×6 and 6×7 cm substrates

#### 5.2.4 Bonding of Microfluidic Devices

The first bonding tests were performed with the hot embossing system (HEX 01, Jenoptik), after removing the master with its fixture ring and the substrate clamping system. Two blank pieces, sandwiched between glass substrates (10×10 cm, 2.2 mm thick) were embossed at temperatures between 145 °C and 175 °C. A qualitative evaluation of bond strength was made by attempting to pry the pieces apart. Rectangular pieces were bonded at a 45° offset so that the corners could be easily grabbed. Bond strength was judged on a qualitative scale. Poor bond strength means the wafers came apart with little if any force applied. Median bond strength took noticeable effort applied

by hand. Good bond strength means the wafers would not come apart without breaking the plastic.

A set of trials was performed on a Carver hydraulic press (model 3889 1DI1A00, Wabash, Indiana, USA) by Dean Nair, a summer undergraduate student. Correlation between bonding time, force applied and bonding temperature was investigated. The bonding temperature, force applied and bonding times used are summarized in Table 5.2. For easy comparison of the force applied for bonding with the two different systems, the mass units set on the Carver hydraulic press were multiplied by  $g=9.8 \text{ m/s}^2$  and are reported in force units (kN). Annealing of some bonded devices was performed at  $145 \text{ }^\circ\text{C}$  for 10 min under minimal force of 1.8 kN (180 kg). For easy alignment with the coverplate, the access holes (1.5 mm diam) were drilled in the embossed substrate using a jewelers drill. One embossed substrate (trimmed at  $8 \text{ cm} \times 7 \text{ cm}$ ) and a coverplate were cleaned at a time with isopropyl alcohol and placed between two glass substrates and introduced into the hydraulic press, which was maintained at the bonding temperature.

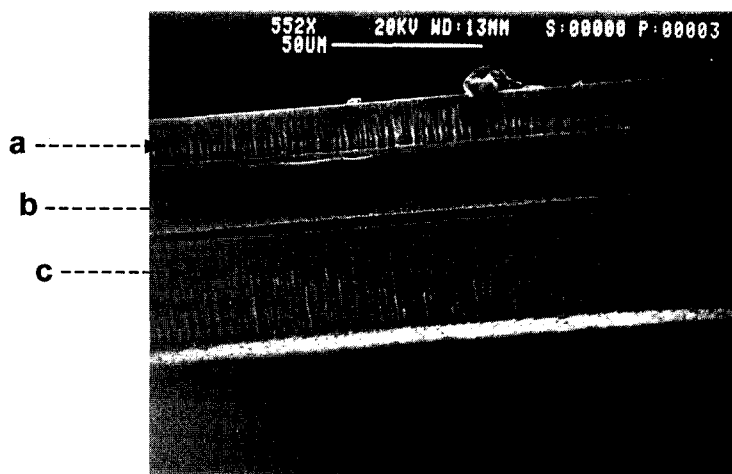


**Figure 5.3:** SEM images presenting the sidewall of a channel etched with DRIE on a Si substrate. The standard Bosch procedure was used with modified etching times (see experimental section 5.2.1 for details) that gave different etching rates as follows:

- a. 15 sec /cycle (etching rate of  $0.68 \text{ } \mu\text{m/ cycle}$ );
- b. 20 sec /cycle (etching rate of  $1.18 \text{ } \mu\text{m/ cycle}$ );
- c. 25 sec /cycle (etching rate of  $1.75 \text{ } \mu\text{m/ cycle}$ ).

## 5.3 Results and Discussions

### 5.3.1 Master Fabrication

An anisotropically etched (DRIE) master in silicon was used to form a nickel relief as a secondary master and stamp parts in plastic using a hot embosser. The challenge associated with etching the FAT 3000 device was caused by the presence of relatively large features to be etched (about 12 % of the surface) and the targeted depth (70  $\mu\text{m}$ ). Preliminary tests were performed to determine the optimal conditions for etching 70  $\mu\text{m}$  deep structures. The 15, 20 and 25 s etching times produced etching rates of 0.68  $\mu\text{m}/\text{cycle}$  (1.66  $\mu\text{m}/\text{min}$ ), 1.18  $\mu\text{m}/\text{cycle}$  (2.39  $\mu\text{m}/\text{min}$ ) and 1.75  $\mu\text{m}/\text{cycle}$  (3.04  $\mu\text{m}/\text{min}$ ), respectively. The SEM image presented in Figure 5.3 shows the differences in sidewall roughness obtained for the tested etching times. Since the goal was to achieve a deep etch with minimal sidewall roughness, an etching time of 20 s/cycle was selected. The SEM image presented in Figure 5.4 shows the quality of the etch obtained on a wafer etched using the same conditions as for the Si master produced.

As expected for the Bosch process [51], the depth obtained was determined by the aspect ratio of the features and the position on the wafer. For a 1500  $\mu\text{m}$  wide feature the depth obtained increased for features positioned further from the center of the wafer (Figure 5.5a). The depth obtained at a central position (72.78  $\mu\text{m}$ ) was 95% of the value obtained on the most lateral features (76.45  $\mu\text{m}$ ). For trenches up to 15  $\mu\text{m}$  wide positioned close together, the depth achieved was reported to increase with the width of the feature [51]. For the large features studied here a clear trend was not observed (Figure 5.5b), although the 250  $\mu\text{m}$  wide feature was etched at 91 % of the depth achieved for a 1500  $\mu\text{m}$  wide feature.

The difficulties associated with mechanically removing Si from the Ni surface were caused by the nature of the Bosch etching process. Every cycle consists of an etching and a deposition step. Etching is performed by  $\cdot\text{F}$  radicals (from  $\text{SF}_{6(\text{g})}$ ) reacting with Si on the unprotected surface, producing  $\text{SiF}_4$  gas. After a short time the etching is stopped, to limit possible lateral etching. The sidewalls are then protected by polymerization of  $\text{CF}_2$  radicals (from  $\text{C}_4\text{F}_8(\text{g})$ ). As a result of this stepwise procedure, the sidewalls are not etched perfectly smooth, as shown in Figures 5.3 and 5.4c. The electrochemically deposited Ni became locked into the Si wafer, as a result of the scalloping on the walls of the Si

features. When Ni was removed from the Si mold, some of the silicon remained trapped, as shown in Figure 5.2a and c.

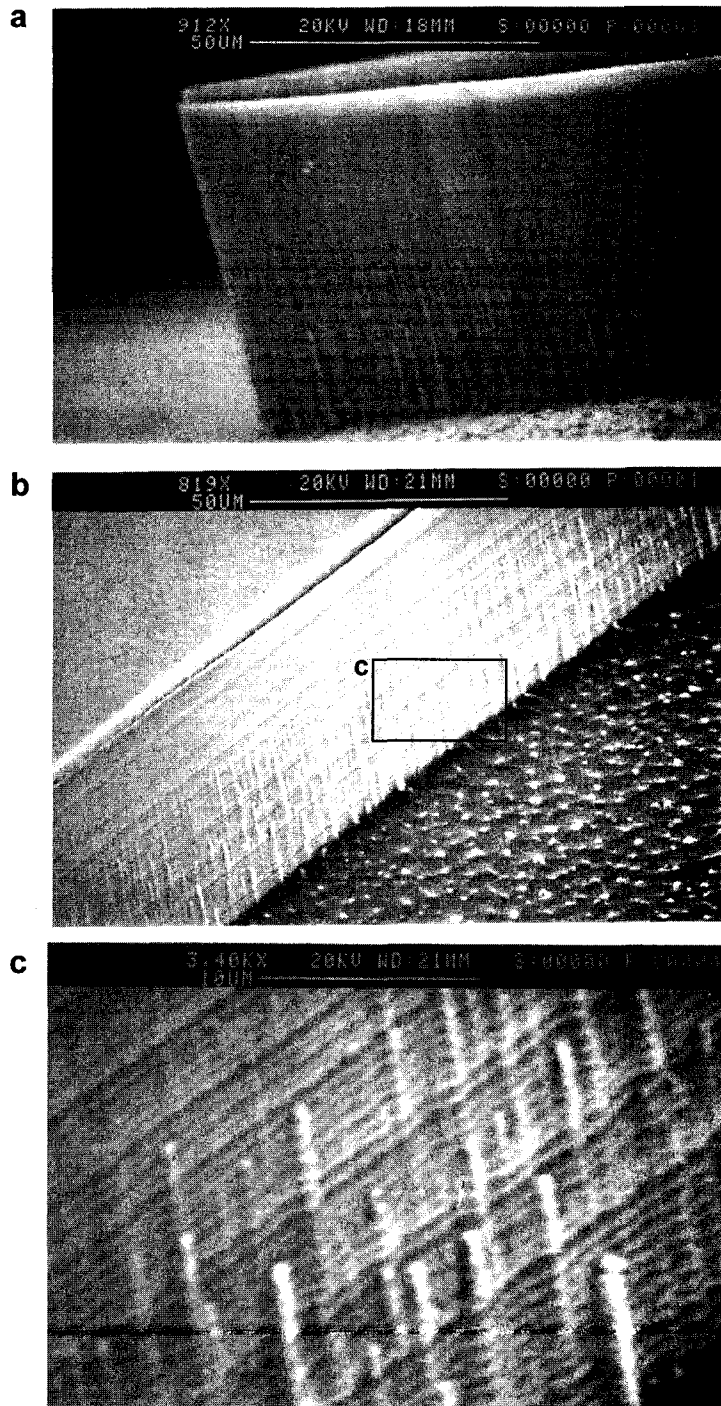


**Figure 5.4:** SEM images presenting details of the features etched to a 70 μm depth on silicon wafer, using the optimised conditions for the Bosch process, with an average etch rate of 1.18 μm/cycle.

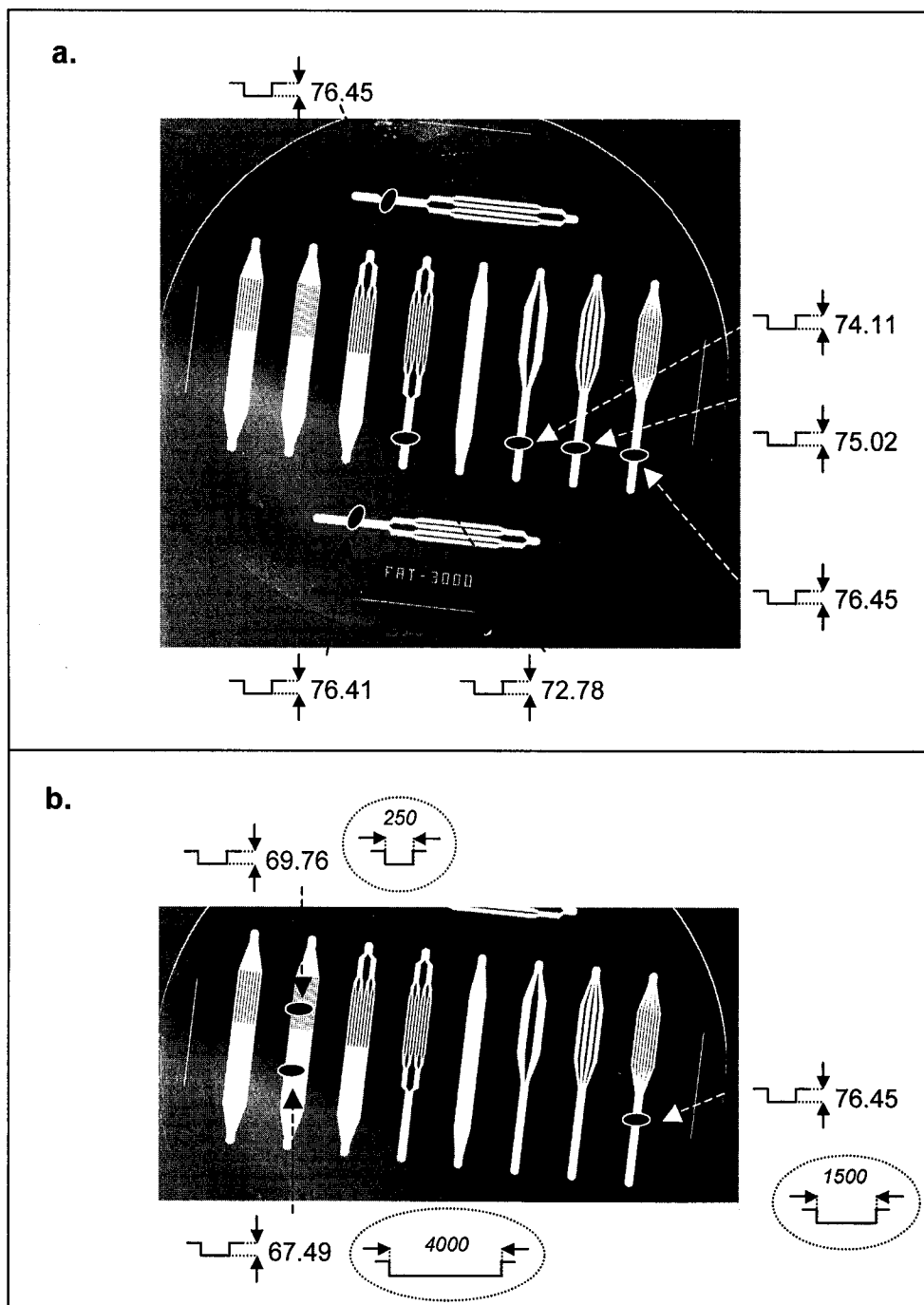


**Figure 5.5:** Images of the FAT 3000 device etched on silicon. Differences in depth with position on the wafer were determined for 1500  $\mu\text{m}$  wide channels (a) and for channels with different widths (b). All dimensions are in  $\mu\text{m}$ .

As it was mechanically impossible to remove the Si clumps remaining on the Ni master without damaging the surface, the Ni tool was immersed in 10% KOH, after



etching the SiO<sub>2</sub> layer with buffered oxide etch (BOE: NH<sub>4</sub>F, HF). No significant amount of Si was removed, so the Ni tool was instead plasma etched with SF<sub>6</sub>. The Ni tool was removed from the Oxford Instruments DRIE system with less than 10% of the Si removed after 15 min of etching. There was no visible negative effect on the Ni surface. Since the DRIE instrument is provided with a Si wafer loading system, the instrument required special handling to manually load the Ni tool. The operation would have needed to be repeated more than 10 times (the strong heating of the tool limits the length of one cycle) for complete Si removal, due to the significant heating of the tool during each cycle. This was regarded as too slow and inefficient for a procedure. As a result, an EDP bath was used to etch the silicon in less than 4 h. But due to an unidentified process, a deposit was formed on the Ni surface.

Relatively high and similar melting points for both Si (1410 °C) and Ni (1455 °C) [52] excluded the possibility of removing the Si by melting. Electrochemical removal of Si is not practical, since the lower potential associated with Ni oxidation would affect the Ni surface (oxidation potentials are 0.257 V for Ni/Ni<sup>2+</sup> (acidic solution), 0.72 V for Ni/Ni(OH)<sub>2</sub> (basic solution), 0.909 V for Si/SiO<sub>2</sub> (acidic solution) and 1.69 V for Si/SiO<sub>2</sub> (basic solution) [53]). The Si-Ni system required specific chemical methods able to remove the Si debris without interfering with the Ni surface. When KOH was used, its concentration was lowered from 30% (as in normal Si etchants) to 10 % to prevent a possible corrosion of the Ni surface (Ni(OH)<sub>2</sub>). The KOH failed to give a productive etching of Si. The SF<sub>6</sub> plasma etching procedure worked, but with an extremely low etching rate. The extensive heating quickly generated by the DRIE process suggested that we find a more efficient method. The EDP etchant offered the required rapid and efficient method to remove the Si debris, but it was also the cause of a deposition, probably a silicate, formed on the Ni surface. Improper handling during machining also added some circular scratches on the master's surface. The somewhat damaged Ni master obtained after Si removal and machining is shown in Figure 5.6. The Ni master was quite expensive to produce and was only one step in developing the overall process. It was decided that the master could still be used to begin developing the other steps in the procedure, despite its flaws. However, the master limited the quality of the embossed structures.

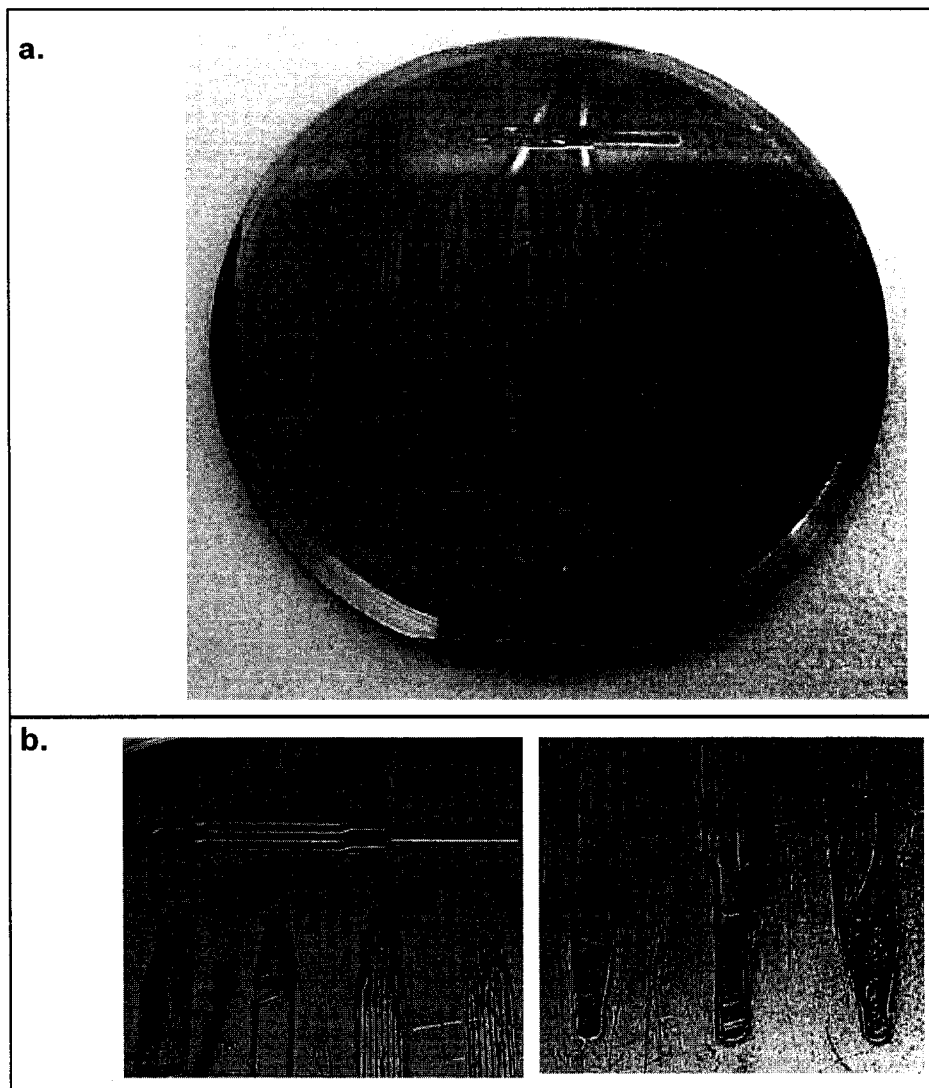


**Figure 5.6:** Image of the Ni master after chemical treatment for removing Si fragments and machining (a). Details presented show the chemical and mechanical deterioration of the Ni master (b).

### 5.3.2 Embossing on Polycarbonate Substrates

Embossing polycarbonate was performed as described in section 5.2.3 at temperatures between 160 °C and 195 °C. The SEM images obtained from structures embossed at 165 °C and 170 °C are shown in Figure 5.7 and from structures embossed at 175 °C and 195 °C in Figure 5.8. Although no significant difference was observed in channel depth embossed at the temperatures tested ( $67.90 \pm 2.38 \mu\text{m}$ , 22 measurements), the sidewalls were distorted when the temperature was 160 °C and 165 °C (Figure 5.7a).

The height of the embossed pillars (100  $\mu\text{m}$  wide, Figures 5.7 and 5.8) was influenced by the embossing temperature. Their height represented 70-72 % of the height obtained for

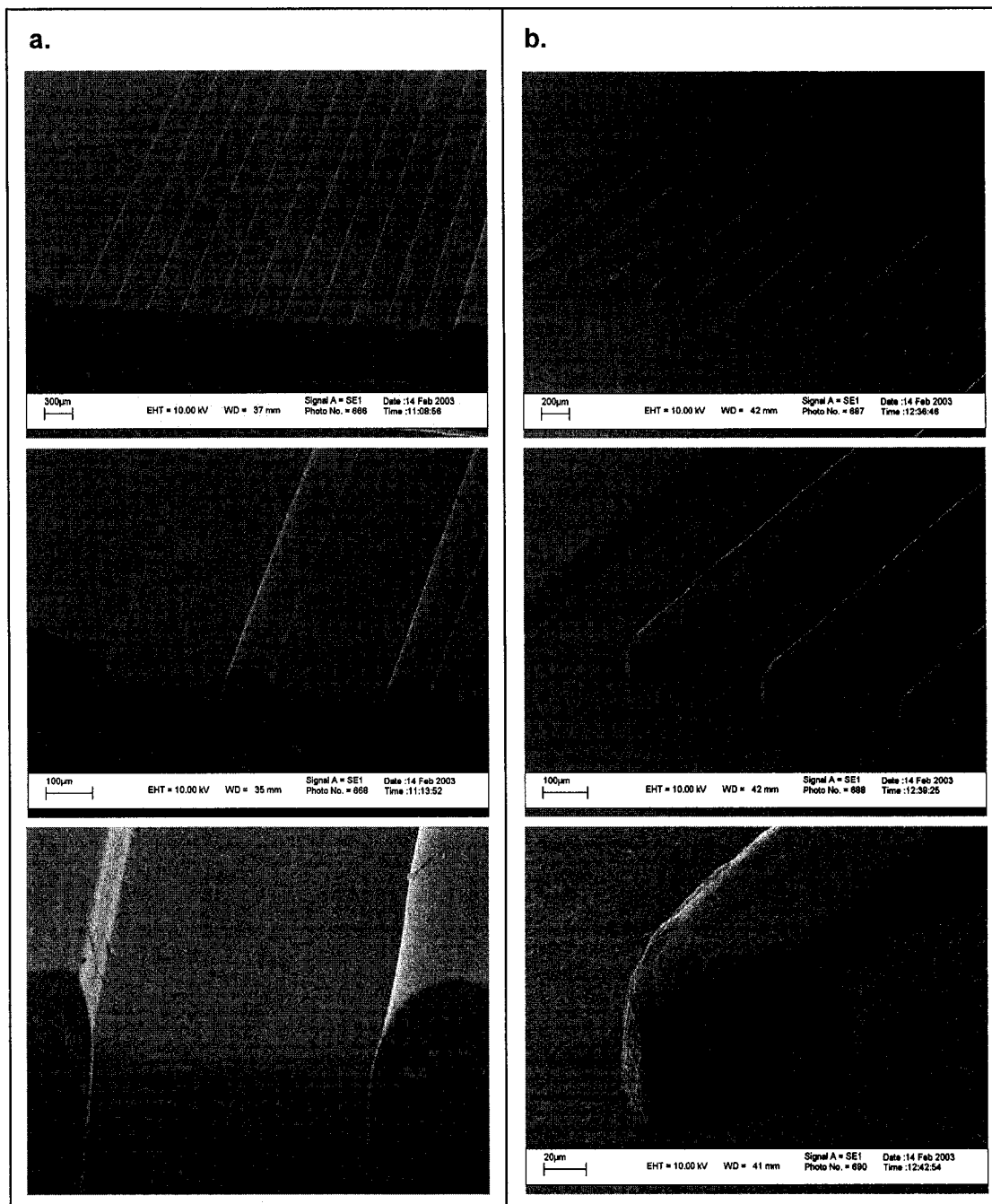


**Figure 5.7:** Scanning electron microscopy images presenting details of the same features of the FAT 3000 device, embossed on PC at 165 °C (a) and 170 °C (b).

the sidewalls defining the large channel (4100  $\mu\text{m}$  wide) when embossing at 160  $^{\circ}\text{C}$ , 90-92 % at 165  $^{\circ}\text{C}$  and 100 % at 170-195  $^{\circ}\text{C}$ . A minimum temperature of 170  $^{\circ}\text{C}$  was determined to be optimal when using a 15 kN force applied for a 120 s embossing time.

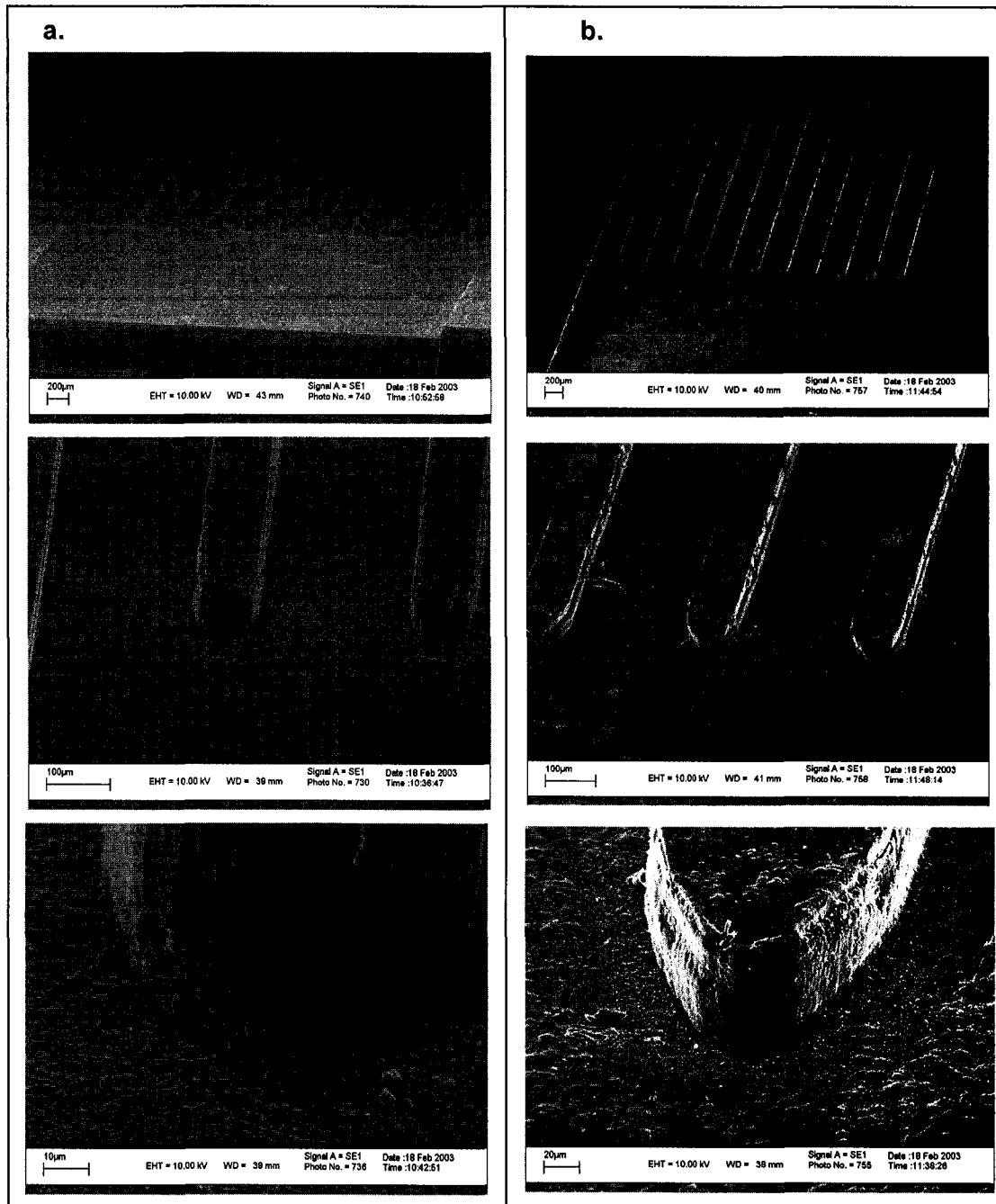


**Figure 5.8:** Scanning electron microscopy images presenting details of the same features of the FAT 3000 device, embossed on PC at 175  $^{\circ}\text{C}$  (a) and 195  $^{\circ}\text{C}$  (b).

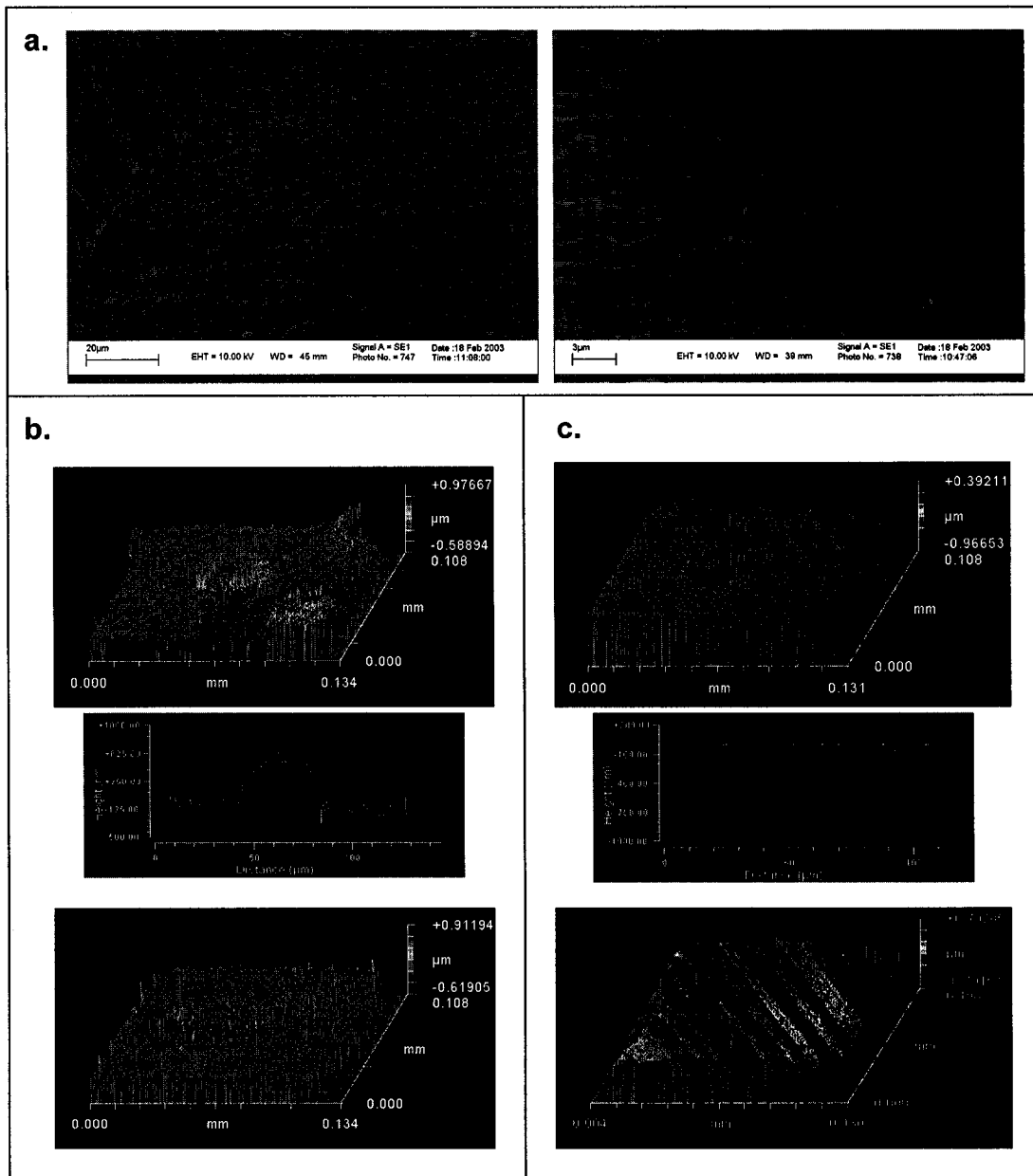


**Figure 5.9:** Characterization of channel surface:

- Images of embossed channels on polycarbonate obtained by scanning electron microscopy;
- Details of the embossed structures on polycarbonate obtained by optical profilometry;
- Details of the Ni tool used for embossing obtained by optical profilometry.

The surface roughness was investigated by SEM on substrates embossed at 175 °C (Figure 5.9a). For a realistic conclusion, the surface roughness obtained must be compared with the surface roughness of the Ni master used for embossing. Since the relatively large Ni master could not be loaded for SEM inspection, optical profilometry was used. As shown in Figure 5.9c, the largest defects on the Ni master consisted of holes

0.800  $\mu\text{m}$  deep with a diameter of 40  $\mu\text{m}$ . The scratches mechanically generated during machining were 0.150-0.600  $\mu\text{m}$  deep, forming 5-10  $\mu\text{m}$  wide circular lines. The defects on the embossed structures consisted of 0.600-0.800  $\mu\text{m}$  deep and 25-40  $\mu\text{m}$  wide peaks. As the defects observed on the master were reproduced on the embossed structures, the surface roughness of the master was the critical factor in influencing the surface roughness of the embossed PC substrates. No deterioration in the quality of the embossed structure was observed even after embossing more than 100 substrates, clearly showing the better efficiency of the Ni master compared with other materials such as silicon [50].

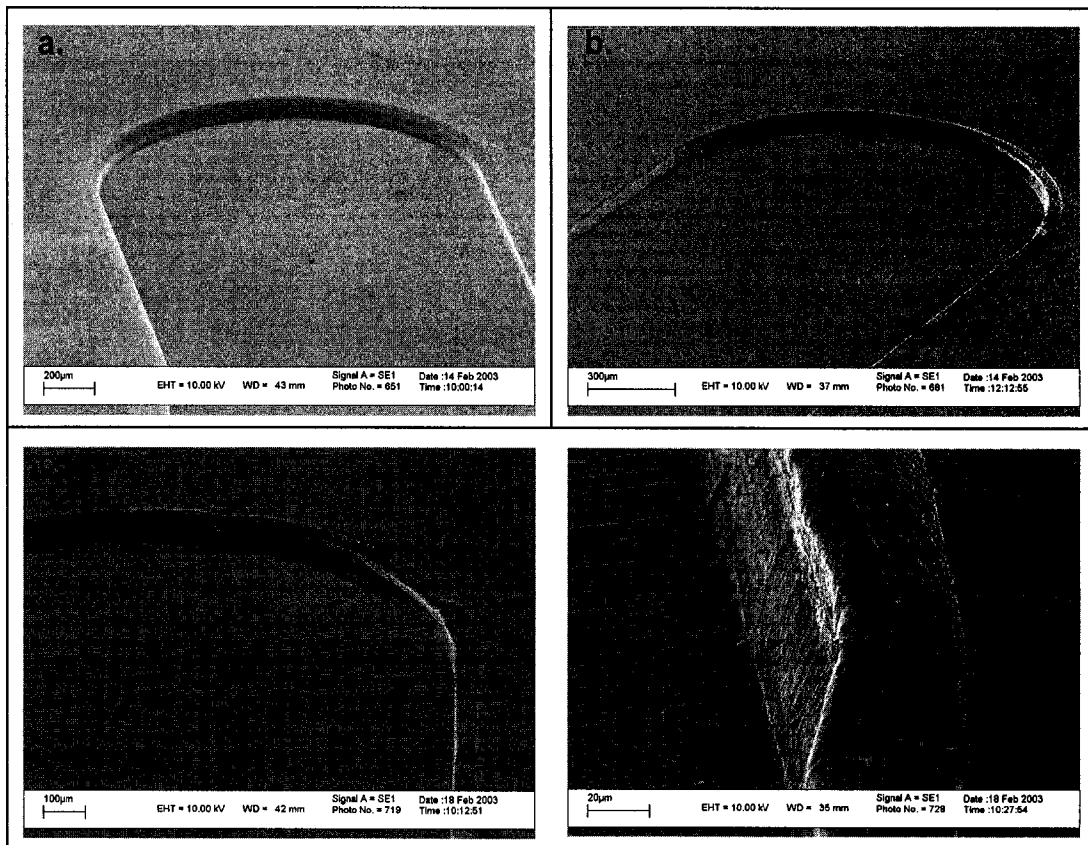


**Figure 5.10:** SEM images presenting a defect on the right side of a 1500  $\mu\text{m}$  wide feature embossed on PC at 165 °C (a), 170 °C (b) and 175 °C (c). De-molding temperature was 138 °C. The detail (d) shows a structure embossed at 175 °C.

A common embossing problem was the accumulation of the substrate material on the upper part of a sidewall on one side of the large manifolds (Figure 5.10d). The problem was not related to the embossing temperature (Figure 5.10a-c), although the extent of the defect was less evident for the manifold embossed at 165 °C, when, as

mentioned before, the sidewalls were not properly reproduced. Esch et al. [50] attributed this defect to the difference in thermal expansion coefficients of the Si master used in their study and the plastic substrate. Typical thermal expansion coefficients are two times smaller for metals ( $1-4 \times 10^{-5} (\text{°C})^{-1}$ ) than for plastic ( $5-7 \times 10^{-5} (\text{°C})^{-1}$ ) [3]. However, another factor affecting this process may be the combination of lower thermal conductivity (up to 500 times) and larger heat capacity (2-3 times) of the plastic substrate compared with the Ni, resulting in a permanent temperature gradient between the middle and outside of the substrate during embossing. At de-molding, as the Ni master is removed from the plastic surface the heat transferred from the inside of the substrate can cause local expansion. As the master is removed, the pulling force acts on the clamping units located on the two sides of the substrate. It is possible that this force caused a light lifting from one side, based on slightly different elasticity properties of the clamping units, which makes the resulting pulling force to act on one side of the channel, creating the observed accumulation. This explanation is sustained by the location of the defect on the same side of all features on any substrate. The defect was similar on all embossed substrates. To minimize these defects, the separation between the master and the substrate should occur at the minimal temperature at which the plastic is no longer soft and deformable. In our study the optimal de-molding temperature was 138 °C, 2 °C lower than the temperature used by Esch et al. [50]. However the defect was still observed.

### 5.3.3 Thermal Bonding of Plastic Devices

Blank PC substrates were used in the preliminary bonding tests performed with the hot embosser. Strong bonding was obtained at 160 °C with a force of 15 kN applied. As the temperature was increased, a lower force could be used without affecting the bond strength. At 155 °C the bond strength was reduced even when applying the maximum force (20 kN), but was still strong enough to hold the two pieces together. Bonding at such high temperature is not practical, since at temperatures over 149 °C ( $T_g$  of the PC), the embossed features from the substrate would be greatly affected. When the temperature was lowered to 155 °C, the bonding was weak and only fractions of the surface bonded. A strong bond (even at 130 °C) was obtained when acetone was sprayed on the surface, but since such a solvent could affect the embossed features, the solvent-

assisted bonding method was not investigated in further detail. (Acetone softens the surface.) However, adding a few drops of acetone along the edges of the device, after thermal bonding, conferred good mechanical stability on the devices.

A more detailed study was performed using the Carver hydraulic press, when an embossed substrate with access holes was bonded to a coverplate using different bonding times and temperatures, at forces up to 40 kN.

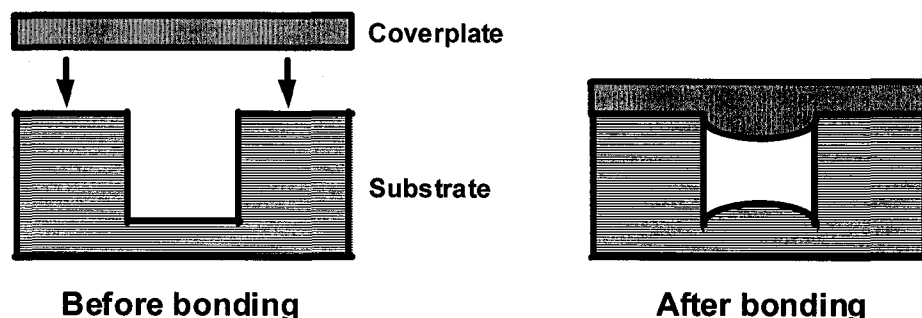


**Figure 5.11:** Schematic of the channel deformation observed after bonding.

**Table 5.3:** Characteristics of the PC bonding at 135 °C and 40 kN. Annealing was performed at 145 °C for 10 min. (8×7 cm embossed substrates were bonded on 12.5×10 cm coverplates)

Bonding Time (min)	Substrate Deformation (μm) *	Coverplate Deformation (μm) *	Total Depth (μm)	Achieved depth (%)	Bond ** strength
10	2.60	4.34	56.88	89	4
10	4.30	18.78	38.61	63	3
10	5.86	15.62	42.30	66	3
15	3.95	15.04	48.49	72	3
20	5.09	15.44	45.38	69	3
25	4.40	16.49	43.59	68	3
30	4.51	15.79	45.20	69	2
30	5.50	17.28	41.58	65	2

\* Values measured in the middle of the channel (maximal values)

\*\* Bond strength scale: 1(weak) < 2 < 3 < 4(strong); see section 5.2.4 for definition of weak and strong

A substantial drawback of thermal bonding has been the deformation and collapse of the embossed features due to the force applied at such high temperatures. Excellent bond strength between the embossed piece and a cover plate was easily obtained at



temperatures higher than 150 °C, but with significant channel collapse. Channel integrity was maintained at a lower bonding temperature and force, but insufficient bond strength was produced. Due to the heat and force applied during the bonding process, plastic from the cover plate would flow into the channel and the bottom of the channel would migrate upwards (Figure 5.11). A uniform bond on the total contact surface was rarely obtained. A reason for this could be the possible non-planarity of the embossed structures, which prevents a good contact between the substrate and coverplate.

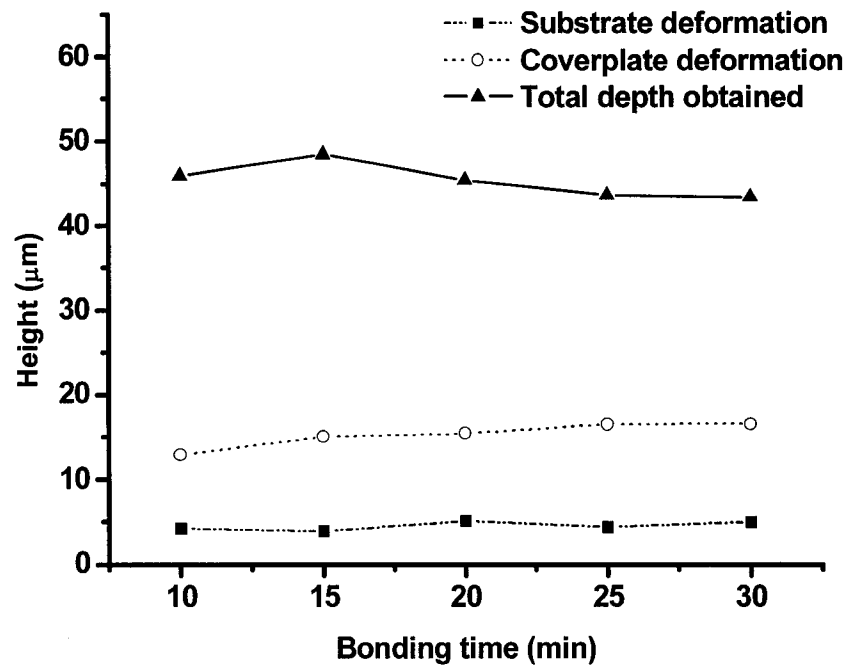


**Figure 5.12:** Dependence of the depth obtained, substrate and coverplate deformation on bonding time. The deformation values represent the maximum deformation measured in the middle of the channel, when bonding was performed at 135 °C and 40 kN, followed by annealing for 10 min at 145 °C and 1.8 kN.

Annealing of the bonded devices was also adopted to increase the bond strength [41]. The best results were obtained using a force of 40 kN (4100 kg) and a bonding temperature of 135 °C, followed by cooling at room temperature for 10 min and annealing at 145 °C for 10 min with minimal force of 1.8 kN (180 kg), then cooling to room temperature. To characterize the channel deformability, the devices were pulled apart, profiled and compared with the profiles observed before the bonding. Table 5.3 presents the maximal deformability observed in the middle of a 1500 μm channel, the

height of the peak created on the coverplate (Figure 5.11) and the calculated minimal depth in the embossed channel after bonding. The optimal bonding time was 15 min as shown in Figure 5.12, when 70 % of the normal channel depth was obtained. Average values were plotted for the multiple measurements performed.

#### 5.4 Conclusions

The DRIE process used to etch the silicon master did not produce the required smooth sidewalls required for easy removal of electroplated Ni from the Si master. The removal of the Si debris without affecting the Ni surface turned out to be a challenge. Although some qualitative improvements are possible for the DRIE etching of Si (particularly reducing the number of features on the wafer and also targeting a smaller depth) the process limitations in producing smooth sidewalls still remains. The reduced life of the Si wafer as a master, described in other studies [2, 50], could be partially caused by the imperfections in sidewall smoothness of the features, which can cause the master to break.

A more promising method to etch features with smooth sidewalls in silicon is the cryogenic DRIE process. In this process  $\text{SF}_6$  is also used for silicon etching, but passivation is obtained continuously by the formation of a blocking layer of silicon oxide/fluoride on the sidewalls as the system is cooled with liquid  $\text{N}_2$ . This non-stepwise process can be performed in the same equipment used for the Bosch process and allows a smoother sidewall etching [51]. While this ability has been added to the Nanofab equipment, it was not available during the research period of this dissertation.

As reported elsewhere [50], the problem of side ridges formed during embossing was also encountered in this effort. The accumulation of substrate material on the upper sidewalls was found to be unrelated to the embossing temperature. It appeared to be related to the substrate clamping system and is minimized but not completely avoided by optimizing the de-molding temperature.

Although conceptually simple, thermal bonding of plastic wafers was a challenge, which is only partially solved in this lab. Good bonding was obtained on areas smaller than the substrates used, suggesting that smaller devices up to  $5 \text{ cm} \times 5 \text{ cm}$  would be easier to bond. Other methods should also be considered, including the lamination of the

embossed substrates with plastic materials such as PET that are designed for thermal lamination.

## 5.5 References

- [1] Soper, S. A.; Ford, S. M.; Qi, S.; McCarley, R. L.; Kelly, K.; Murphy, M. C. *Anal Chem*, **2000**, 72, 643A-651A.
- [2] Becker, H.; Locascio, L. E. *Talanta*, **2002**, 56, 267-287.
- [3] Strong, A. B. *Plastics Materials and Processing*, Prentice-Hall: New Jersey, USA **2000**.
- [4] Becker, H. In *Biochip Technology*, J. Cheng; L. J. Kricka, eds.; Harwood Academic Publishers: Philadelphia, PA, USA, **2001**, pp. 63-96.
- [5] Becker, H.; Dietz, W.; Dannberg, P. In *Micro Total Analysis Systems*; D. Jed Harrison; Albert van den Berg, eds.; Kluwer Academic Publishers: Banff, Canada, **1998**, pp. 253-256.
- [6] Mark, F. H.; Bikales, N. M.; Overberger, C. G.; Menges, G. eds. *Encyclopedia of polymer science and engineering*, John Wiley & Sons: New York\ **1985-1989**.
- [7] Becker, H.; Heim, U. *Sens. Actuators A*, **2000**, 83, 130-135.
- [8] McCormick, R. M.; Nelson, R. J.; Alonso-Amigo, M. G.; Benvegna, D. J.; Hooper, H. H. *Anal. Chem.*, **1997**, 69, 2626-2630.
- [9] Klintberg, L.; Svedberg, M.; Nikolajeff, F.; Thornell, G. *Sens. Actuators A*, **2003**, 103, 307-316.
- [10] Elders, J.; Jansen, H. V.; Elwenspoek, M.; Ehrfeld, W. In *MEMS '95*: Amsterdam, The Netherlands, **1995**, pp. 238-243.
- [11] Lee, G.-B.; Chen, S.-H.; Huang, G.-R.; Sung, W.-C.; Lin, Y.-H. *Sens. Actuators B*, **2001**, 75, 142-148.
- [12] Fintschenko, Y.; van den Berg, A. *J. Chromatogr. A*, **1998**, 819, 3-12.
- [13] Becker, E. W.; Ehrfeld, W.; Hagemann, P.; Maner, A.; Munchmeyer, D. *Microelectronic Engineering*, **1986**, 4, 35-56.
- [14] Martynova, L.; Locascio, L. E.; Gaitan, M.; Kramer, G. W.; Christensen, R. G.; MacCrehan, W. A. *Anal. Chem.*, **1997**, 69, 4783-4789.
- [15] Locascio, L. E.; Gaitan, M.; Hong, J.; Eldefrawi, M. In *Micro Total Analysis Systems*; D. Jed Harrison; Albert van den Berg, eds.; Kluwer Academic Publishers: Banff, Canada, **1998**, pp. 367-370.

- [16] Ueno, K.; Kitagawa, F.; Kim, H.-B.; Tokunaga, T.; Matsuo, S.; Misawa, H.; Kitamura, N. *Chem. Lett.*, **2000**, 858-859.
- [17] Ogura, M.; Agata, Y.; Watanabe, K.; McCormick, R. M.; Hamaguchi, Y.; Aso, Y.; Mitsuhashi, M. *Clin. Chem.*, **1998**, *44*, 2249-2255.
- [18] Choi, J.-W.; Kim, S.; Trichur, R.; Cho, H. J.; Puntambekar, A.; Cole, R. L.; Simkins, J. R.; Murugesan, S.; Kim, K.; Lee, J.-B.; Beaucage, G.; Nevin, J. H.; Ahn, C. H. In *Micro Total Analysis Systems*; J. Michael Ramsey; Albert van den Berg, eds.; Kluwer Academic Publishers: Monterey, CA, USA, **2001**, pp. 411-412.
- [19] Trichur, R.; Kim, S.; Zhu, X.; Suk, J. W.; Hong, C.-C.; Choi, J.-W.; Ahn, C. H. In *Micro Total Analysis Systems*; Yoshinobu Baba; Shuichi Shoji; Albert van den Berg, eds.; Kluwer Academic Publishers: Nara, Japan, **2002**; Vol. 1, pp. 395-397.
- [20] Thomas, N.; Ocklind, A.; Blikstad, I.; Griffiths, S.; Kenrick, M.; Derand, H.; Ekstrand, G.; Ellstrom, C.; Larsson, A.; Andersson, P. In *Micro Total Analysis Systems*; Albert van den Berg; W. Olthuis and P. Bergveld, eds.; Kluwer Academic Publishers: Enschede, The Netherlands, **2000**, pp. 249-252.
- [21] Kellogg, G. J.; Arnold, T. E.; Carvalho, B. L.; Duffy, D. C.; Sheppard, N. F. In *Micro Total Analysis Systems*; Albert van den Berg; W. Olthuis; P. Bergveld, eds.; Kluwer Academic Publishers: Enschede, The Netherlands, **2000**, pp. 239-242.
- [22] Ahn, C. H.; Choi, J.-W.; Puntambekar, A.; Hong, C.-C.; Zhu, X.; Gao, C.; Trichur, R.; Chilukuru, S.; Dutta, M.; Murugesan, S.; Kim, S.; Sohn, Y.-S.; Nevin, J. H.; Beaucage, G.; Lee, J.-B.; Lee, J. Y.; Bissell, M. G. In *Micro Total Analysis Systems*; Yoshinobu Baba; Shuichi Shoji; Albert van den Berg, eds.; Kluwer Academic Publishers: Nara, Japan, **2002**; Vol. 1, pp. 187-189.
- [23] Trichur, R.; Kim, S.; Lee, S. H.; Abdelaziez, Y. A.; Starkey, D. E.; Halsall, H. B.; Heineman, W. R.; Ahn, C. H. In *Micro Total Analysis Systems*; Yoshinobu Baba; Shuichi Shoji; Albert van den Berg, eds.; Kluwer Academic Publishers: Nara, Japan, **2002**; Vol. 1, pp. 560-562.
- [24] Kumar, A.; Biebuyck, H. A.; Whitesides, G. M. *Langmuir*, **1994**, *10*, 1498-1511.
- [25] Kumar, A.; Whitesides, G. M. *Appl. Phys. Lett.*, **1993**, *63*, 2002-2004.
- [26] Wilbur, J. L.; Kumar, A.; Kim, E.; Whitesides, G. M. *Adv. Mater.*, **1994**, *7*, 600-604.
- [27] Srinivasan, R.; Mayne-Banton, V. *Appl. Phys. Lett.*, **1982**, *41*, 576-579.
- [28] Roberts, M. A.; Rossier, J. S.; Bercier, P.; Girault, H. *Anal Chem*, **1997**, *60*, 2035-2042.
- [29] Preuss, S.; Langowski, H. C.; Damm, T.; Stuke, M. *Appl. Phys. A*, **1992**, *54*, 360-362.

- [30] Lin, Y.; Xu, N.; Wen, J.; Matson, D. W.; Smith, D. R. In *Micro Total Analysis Systems*; D. Jed Harrison; Albert van den Berg, eds.; Kluwer Academic Publishers: Banff, Canada, **1998**, pp. 343-346.
- [31] Lazare, S.; Granier, V. *J. Appl. Phys.*, **1988**, *63*, 2110-2115.
- [32] Mensinger, H.; Richter, T.; Hessel, V.; Doepper, J.; Ehrfeld, W. In *Micro Total Analysis Systems*; Albert van den Berg; Piet Bergveld, eds.; Kluwer Academic Publishers, **1995**, pp. 237-242.
- [33] Matson, D. W.; Martin, P. M.; Bennett, W. D.; Kurath, D. E.; Lin, Y.; Hammerstrom, D. J. In *Micro Total Analysis Systems*; D. Jed Harrison; Albert van den Berg, eds.; Kluwer Academic Publishers: Banff, Canada, **1998**, pp. 371-374.
- [34] Stebani, J.; Wokaun, A.; Lippert, T.; Kunz, T. In *EPO 770924*, **1997**.
- [35] Weigl, B. H.; Kriebel, J.; Mayes, K.; Yager, P.; Wu, C. C.; Holl, M.; Kenny, M.; Zebert, D. In *Micro Total Analysis Systems*; D. Jed Harrison; Albert van den Berg, eds.; Kluwer Academic Publishers: Banff, Canada, **1998**, pp. 81-84.
- [36] Webster, J. R.; Burns, M. A.; Burke, D. T.; Mastrangelo, C. H. In *Micro Total Analysis Systems*; D. Jed Harrison; Albert van den Berg, eds.; Kluwer Academic Publishers: Banff, Canada, **1998**, pp. 249-252.
- [37] Renaud, P.; van Lintel, H.; Heuschkel, M.; Guerin, L. In *Micro Total Analysis Systems*; D. Jed Harrison; Albert van den Berg, eds.; Kluwer Academic Publishers: Banff, Canada, **1998**, pp. 17-22.
- [38] Baba, Y.; Tabata, O. In *Micro Total Analysis Systems*; D. Jed Harrison; Albert van den Berg, eds.; Kluwer Academic Publishers: Banff, Canada, **1998**, pp. 331-334.
- [39] Paulus, A.; Williams, S. J.; Sassi, A. P.; Pin Kao, H. T.; Hooper, H. H. *Proc. SPIE Microfluid. Devices Syst.*, **1998**, *3515*, 94-103.
- [40] Liu, Y.; Ganser, D.; Schneider, A.; Liu, R.; Grodzinski, P.; Krutchinina, N. *Anal Chem*, **2001**, *73*, 4196-201.
- [41] Rosenberger, F.; Jones, E.; Lee, C.; DeVoe, D. In *Micro Total Analysis Systems*; Yoshinobu Baba; Shuichi Shoji; Albert van den Berg, eds.; Kluwer Academic Publishers: Nara, Japan, **2002**; Vol. 1, pp. 404-406.
- [42] Weigl, B. H.; Bardell, R. L.; Cabrera, C. R. *Advanced Drug Delivery Reviews*, **2003**, *55*, 349-377.
- [43] Sassi, A. P.; Paulus, A.; Cruzado, I. D.; Bjornson, T.; Hooper, H. H. *J. Chromatogr. A*, **2000**, *894*, 203-217.

- [44] Soane, D. S.; Soane, Z. M.; Hooper, H. H.; Alonso-Amigo, M. G. In *International Patent WO 98/45693*, **1998**.
- [45] Ekstrom, B.; Jacobsen, G.; Ohman, O.; Sjodin, H. In *International Patent WO 91/16966*, **1990**.
- [46] Kamper, K. P.; Dopfer, J.; Ehrfeld, W.; Oberbeck, S. *Proc. IEEE MEMS*, **1998**, 432-437.
- [47] Liu, Y.; Rauch, C. B.; Stevens, R. L.; Lenigk, R.; Yang, J.; Rhine, D. B.; Grodzinski, P. *Anal Chem*, **2002**, *74*, 3063-3070.
- [48] Sugimoto, M.; Saika, H.; Shibata, S.; Shinohara, S.; Tabata, O. In *Micro Total Analysis Systems*; Yoshinobu Baba; Shuichi Shoji; Albert van den Berg, eds.; Kluwer Academic Publishers: Nara, Japan, **2002**; Vol. *1*, pp. 398-400.
- [49] Puntambekar, A.; Murugesan, S.; Trichur, R.; Cho, H. J.; Kim, S.; Choi, J.-W.; Beaucage, G.; Ahn, C. H. In *Micro Total Analysis Systems*; Yoshinobu Baba; Shuichi Shoji; Albert van den Berg, eds.; Kluwer Academic Publishers: Nara, Japan, **2002**; Vol. *1*, pp. 425-427.
- [50] Esch, M. B.; Kapur, S.; Irizarry, G.; Genova, V. *Lab on a Chip*, **2003**, *3*, 121-127.
- [51] Walker, M. J. *Proceedings of SPIE*, **2001**, *4407*, 89-99.
- [52] Petrucci, R. H.; Harwood, W. S. *General Chemistry Principles and Modern Applications*, Prentice Hall: New Jersey, USA **1997**.
- [53] Bard, A. J.; Parsons, R.; Jordan, J. *Standard Potentials in Aqueous Solutions*, IUPAC, Marcel Dekker: New York, USA **1985**.

## CHAPTER 6: Summary and Future Suggestions

This chapter summarizes the results presented in the previous chapters and suggests further directions for the work presented. The thesis work focuses on integrating rare cell capture from blood on a disposable sample-preparation device for a portable platform. Such a module is the interface between a macroscopic world sample and any PCR-based microfluidic system. Immunomagnetic separation of T cells from human blood and Jurkat cells from reconstituted horse blood was performed and characterized. Although more rare cells are ultimately contemplated, the T cells or Jurkat cells considered in this study offered a good initial model of rare cells in blood.

In Chapter 2, a PCR procedure was optimized and adapted for the characterization of the capture efficiencies obtained with devices tested in Chapter 3. The method uses direct PCR amplification of a T cell receptor (TCR)  $\gamma$  gene junctional region and is to be used to determine the on-chip T cell capture efficiency of different microfluidic devices. The method was required since a simple cell counting method was impractical for the magnetic bead-bed method considered in this thesis.

In Chapter 3, we described the use of paramagnetic beads for cell capture within microfluidic channels. After preliminary tests performed on a simple Y microfluidic device, eight different devices were designed and tested in an effort to reduce the analysis time, while maintaining the capture efficiency. A simple increase of the channel size for a quick processing of larger volumes of sample did not work for the immunomagnetic bead-bed method used in this study. It was necessary to split the flow into several smaller channels to get satisfactory capture efficiency. Testing the eight different splitting manifold designs, presented in Figure 3.2, permitted us to establish the stepwise flow bifurcation of manifolds 3 and 8 as the best option available. The capture efficiency obtained with manifold 3, with eight channels after three bifurcations was 37 %.

In Chapter 4, we presented the first integration of micro-electrolysis pumps for the manipulation and initial processing of a blood sample. Jurkat cells were captured from a 7.5  $\mu\text{L}$  reconstituted horse blood sample using a pair of electrolysis chambers, which were designed to work in a stepwise fashion. First the blood sample was delivered when the pre-labeled cells were captured, and then a buffer was used to wash the captured cells.

Annealing the glass coverplates solved a problem in the fabrication with Ti/Pt electrode delamination. Since the digits of the electrodes were only 20  $\mu\text{m}$  wide, increasing their width would probably positively influence their lifetime and further reduce delamination. Another problem with leakage current observed through the silicon of the devices would be totally eliminated for a device fabricated on plastic, or by improved oxide growth. Difficulties associated with bead introduction into the main channel were caused by the close location of access holes 1, 2 and 5 (Figure 4.4). The temporary solution we employed was to pre-label the cells. This approach used a reduced number of beads per cell and allowed counting of the captured cells. The beads could be introduced on-chip by providing increased hole distances in a future design. The blood sample was pumped reliably by the electrolysis pump at flow rates up to 0.5  $\mu\text{L}/\text{min}$ . Earlier reports of cells pumped with a micropump were performed using suspensions containing up to  $10^6$  cells/mL [1], which is far lower than the typical concentration in blood.

In Chapter 5, we presented preliminary results obtained for the fabrication of plastic devices. Polycarbonate (PC) was used, since this material suited the thermal requirements of a PCR system. A master fabricated in silicon was etched using DRIE and used to electroform a nickel relief as a secondary master. The difficulties in removing the Si wafer from the Ni surface were associated with the roughness of the sidewalls obtained by DRIE. One solution would be to use a Si etching technique which generates smooth sidewalls. The cryogenic DRIE process is a promising choice [2]. Since etching and passivation are performed simultaneously, the sidewalls of the etched features should be smoother than the sidewalls obtained with the stepwise Bosch DRIE process. A Ni master possessing the reverse features of the Si surface was used to stamp features into PC substrates by hot embossing. The resulting substrates had the same pattern as the original Si master. After drilling the access holes, substrates could be thermally bonded to a coverplate using a hydraulic press with optimized bonding parameters.

This initial demonstration of an immunomagnetic cell separation from whole human blood on a microchip shows the potential for successfully developing, completely integrated and automated PCR-based microfluidic devices in the future. The system can be easily adapted to other types of antigenic determinants by varying the bound antibody on the Protein A paramagnetic beads. If the possibility of binding endogenous antibodies



from blood onto the Protein A beads is a concern, other standard methods could be used for antibody immobilization. For example, paramagnetic beads covered with immobilized antibodies are available from Dynal Biotech (Lake Success, NY, USA) as 4.5  $\mu\text{m}$  diam particles. Their kits can be used for separation of T cells, B cells, haematopoietic progenitor cells, dendritic cells, myeloid cells, monocytes and NK cells from human blood. The CELlection™ Biotin Binder kit from the same company can be used to bind any biotinylated antibody for the positive isolation of a cell population. The paramagnetic beads are coated with recombinant streptavidin via a DNA linker. The biotinylated antibody is captured via streptavidin on the bead surface and after cell capture the DNA linker provides the cleavable site for cell detachment (<http://www.dynalbiotech.com>). A large variety of biotinylated human, mouse and rat antibodies are available from BD Pharmingen (Mississauga, ON, Canada).

Further studies are needed to determine if the integration of a mixing unit to enhance cell capture by the beads would provide a substantial reduction of analysis time, over the flow capture method used here. The experiments performed in this thesis showed that the beads themselves could be captured efficiently using a flow rate at least 15 times higher than the flow rate used to capture the blood cells on the beads. Thus sample processing could possibly be reduced if a mixing chamber were to precede the magnetic capture step. The capture efficiency of the magnetically labeled cells would need to be investigated for a clear characterization and comparison with the results obtained with our flow-through bead-bed approach. If the use of a mixing unit followed by capturing the labeled cells would offer better or similar capture efficiency in a considerably shorter analysis time, then a simple fabrication process would need to be adopted for the mixer in order to maintain low cost production.

Based on the results presented in this thesis we propose as future work an optimized system which would be able to separate rare cells from a blood sample, lyse the cells and capture the DNA. Such a system can be coupled with the existing on-chip PCR systems and provide a platform for genetic analysis. The system is presented in Figure 6.1. The reservoirs of the pumps need to have a larger capacity than the corresponding meander filled with sample/buffer, to allow complete pumping of the liquid into the main channel

before saturation with gases occurs in the pump reservoir. The main channel would be 3-5 mm wide and should adopt the stepwise flow bifurcation of manifold 3 (Figure 3.2).

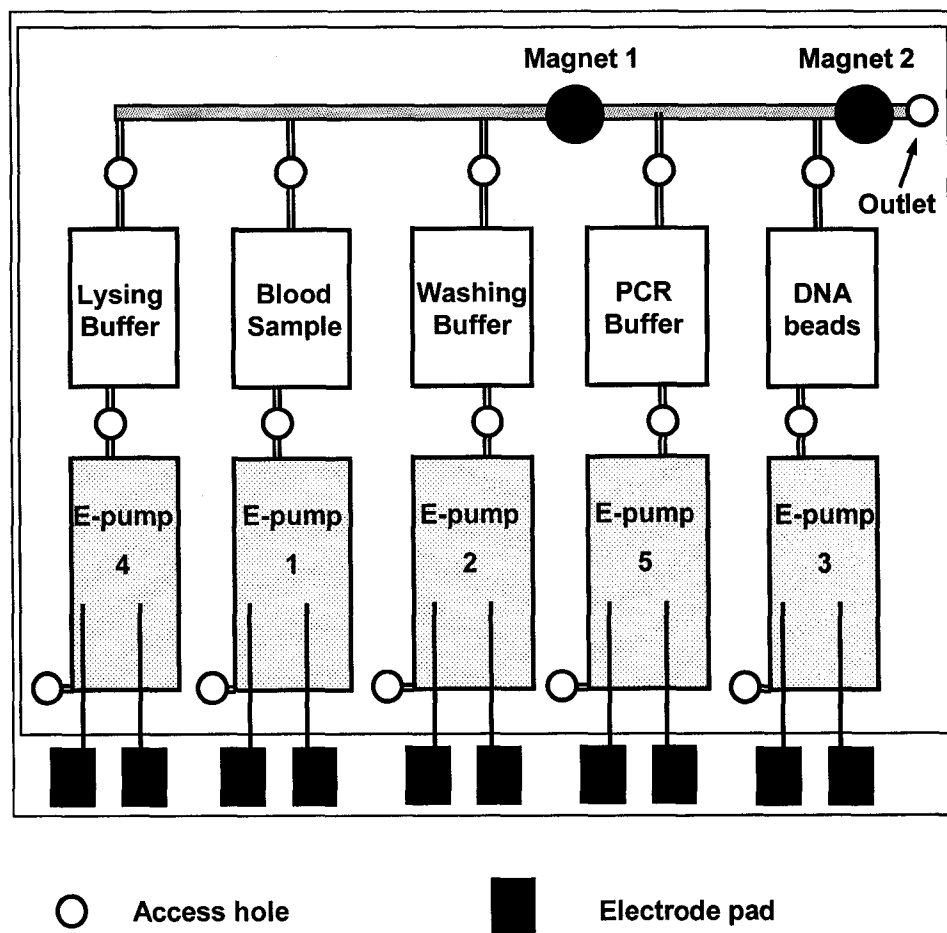


**Figure 6.1:** Proposed integrated system for rare cells separation from a blood sample, cells lysing and DNA capture. The electrochemical pumps are numbered in the order of use.

The Dynabeads used in Chapter 3 to capture DNA from cell suspensions can be introduced into the device as a bead suspension. The paramagnetic beads used to capture specific cells would be introduced in the main channel and captured by Magnet 1. The second pair of magnets (Magnet 2) will be added at a later stage of the process. The meanders will be filled with a blood sample, washing buffer, lysing buffer, PCR buffer, DNA beads (Dynabeads) and all five pump reservoirs with 0.5 M  $\text{KNO}_3$ , as indicated in Figure 6.1. First the blood sample is pumped into the main channel by actuating the electrochemical pump E-pump 1. The cells of interest would be captured at the bead-bed formed at the magnet pair located at Magnet 1. After stopping E-pump 1, E-pump 2 will

start to pump the buffer to wash the captured cells. After stopping E-pump 2, the second pair of magnets will be placed at Magnet 2, as shown in Figure 6.2, while keeping in place the first pair of magnets. Then the Dynabeads (DNA capture beads) will be pumped (E-pump 3) into the main channel and captured by the second pair of magnets (Magnet 2). Once the beads are completely introduced into the main channel, E-pump 3 is stopped and the lysing buffer is pumped using E-pump 4. The captured cells are lysed and the DNA is captured by the Dynabead bed formed at the second pair of magnets (Magnet 1). Finally the PCR buffer is pumped from E-pump 5 to wash the DNA of impurities. Such a system integrated on a plastic platform would offer a good totally integrated sample preparation unit for PCR analysis. The magnets can be replaced by electromagnets on the platform required by this device, or even incorporated on every device using the methods developed by Ahn et al. [3-5].

## 6.1 References

- [1] Andersson, H.; van der Wijngaart, W.; Nilsson, P.; Enoksson, P.; Stemme, G. *Sensors and Actuators B: Chemical*, **2001**, *72*, 259-265.
- [2] Walker, M. J. *Proceedings of SPIE*, **2001**, *4407*, 89-99.
- [3] Choi, J.-W.; Ahn, C. H.; Bhansali, S.; Henderson, H. T. *Sensors and Actuators B: Chemical*, **2000**, *68*, 34-39.
- [4] Choi, J. W.; Liakopoulos, T. M.; Ahn, C. H. *Biosens. Bioelectron.*, **2001**, *16*, 409-16.
- [5] Choi, J.-W.; Oh, K. W.; Han, A.; Wijayawardhana, C. A.; Lannes, C.; Bhansali, S.; Schlueter, K. T.; Heineman, W. R.; Halsall, H. B.; Nevin, J. H.; Helmicki, A. J.; Henderson, H. T.; Ahn, C. H. *Biomedical Microdevices*, **2001**, *3*, 191-200.